# Covalent Functionalization of Metal-Oxide Surfaces with Non-Traditional Ligands

Thesis by

Carl Michael Blumenfeld

In Partial Fulfillment of the Requirements for

the degree of

Doctorate of Philosophy, Chemistry


CALIFORNIA INSTITUTE OF TECHNOLOGY

Pasadena, California

2017

(Defended May 26, 2017)

# ACKNOWLEDGEMENTS

The hardest part of preparing a thesis, other than the formatting, is looking back and realizing how many hands went into the work. My time in the lab was shaped enormously by members of the Caltech community, but also by so many off campus. Here, I hope to pay thanks to the many whom played a role in my life during my PhD, and those who helped get me here. I could not have done it without them!

I assume the logical place to start with my many thanks is with my wonderful and patient advisors, Professor Harry B. Gray and Professor Robert H. Grubbs. Bob and Harry have given me intellectual freedom I never could have imagined. I sought after my own projects and acted as my own manager. I was never alone, however. Harry and Bob proved to be incredible safety nets when I needed them…and they never made it difficult or shameful to ask for help. They also allowed me to fail at times…I needed to. It was essential to my learning experience. I came to Caltech thinking independently but left Caltech as a truly independent thinker. I gained an incredible amount of confidence because of my advisors. In the beginning, every step I took felt like a mistake. Imposters syndrome was a regular issue for me. I thought I needed their permission and blessing for anything. Harry and Bob shot that down quick. The most important lesson I took from them is that a PhD is a degree in problem solving. I happen to specialize in problems regarding surface chemistry. Nonetheless, the challenges they helped me face went well beyond this. By analyzing a problem and doing sufficient background research, most challenges can be mitigated. Beyond their roles as scientific advisors, Harry and Bob have also been great people to get to know. Their lives have been fascinating and they have been so generous in sharing their stories. Bob's stories about agriculture science, for example, have brought a totally different view on the field…I'm grateful to be a chemist! Harry and I can talk for hours about skiing and travel. Life in the Grubbs and Gray groups is great. I couldn't imagine doing grad school any differently.

The faculty at Caltech are absolutely wonderful, and incredibly receptive to meetings and scientific conversations. Nonetheless, one of the biggest challenges to overcome during

my time at Caltech has been scheduling committee meetings. A PhD is difficult but pales in comparison to trying to balance the schedules of Caltech faculty members for meetings. Nonetheless, I wish to thank Professors Mark Davis (my chair), Nate Lewis, and George Rossman for sitting on my committee along with Bob and Harry. It is very rewarding to have meetings and exams where my work, even if only for an hour at a time, is the center of attention for some of the brightest individuals I have ever had the pleasure of getting to know. While not on my committee, Professor John Bercaw has been a fairly large actor in my graduate career. On a number of occasions John has been a sounding board and voice of reason. Even quick conversations with him have saved me hours of suffering and toil. I also wish to acknowledge Professor Brian Stoltz for his helpful conversation with regard to corrole synthesis.

I thank Joshua Palmer for his assistance in guiding me to the Gray and Grubbs groups. He helped me get acquainted at Caltech and introduced me to corrole chemistry, which ended up being a majority of my thesis work. Keith Keitz was an excellent bay mate, especially as a first year graduate student. I am indebted to both Keith and Zach Wickens for taking the time to teach me how to use a schlenk line properly. None of the synthesis I had done at Caltech would have been possible without these wonderful coworkers. Mel Pribisko-Yen was a later bay mate as well as fellow corrole chemist. Our discussions were very helpful toward advancing my work.

Karn Sorasaenee, a former member of the Gray group, and current researcher at Children's Hospital Los Angeles, was a wonderful collaborator on the corrole surface functionalization work. Karn's hands played a major role in two chapters of this thesis. He freely shared his wealth of corrole chemistry and joined me on some challenging synthetic work. Karn helped me published my first paper at Caltech. I thank him for all of his assistance and friendship.

Professor George Rossman, in addition to being on my committee, has really been like a third advisor to me. For a long period of time in fact, I spent more of my days in his lab space, then in either Harry or Bob's. Much like Harry and Bob, he has been nothing short

of an amazing cheerleader and scientific advisor. He challenges me to think for myself, open my eyes to new realms of information, and enjoy small scientific steps. George's labs are constantly seeing influx from other groups. I now know why. More than just running an amazing facility, George knows something about everything. At least it seems that way. Conversations with George have catalyzed some of the most important work I did during my thesis. I could not imagine my time at Caltech without him.

Scott Virgil was a major contributor and influencer in my chemical education. I met Scott when he taught the NMR course offered my first year, however, I did not get to really know him, or his kind wife Silva, until my second or third year of graduate school when I attempted to scale up the corrole synthesis. Despite the fact that I had very limited true synthetic training, Scott challenged me to think in many ways like an organic process chemist. Instead of settling with scaling a dangerous, poorly understood reaction, we sought after a higher yielding, safer, scalable type of synthesis. To most readers this seems to be a fairly small detail. To me, I realized I made a lifetime supply of the parent ligand I would study during my PhD and my fingers remained intact during the process!

Within the lab, I have had the privilege to work with a fair number of people. I'd like to thank Katie Fisher, an undergraduate student I mentored for several years. It was exciting to watch her progress as a student and a researcher. She is now a graduate student at Yale and I wish her the best. Peter Dornan and Lennon Luo gave me a glimpse of catalysis work. Despite my shortcomings, Peter and Lennon were incredibly supportive and helpful. I'm especially grateful for their patience. Chris Marotta and Michael Schulz have been great collaborators during work on upconverting nanoparticles. Our regular discussions, Michael's quickness with a TEM, and Chris's ability to produce limitless numbers of samples have really advanced this work. I have also had the privilege to work with and co-author papers with Astrid Muller, Brad Brennan, and Brendon McNicholas. Collaborating with you all has been a truly rewarding experience.

The most recent project I worked on was one regarding chemotherapeutic filtration. I won't provide too much detail here, however, it would be a mistake to not write thanks to

the many collaborators here. The Hetts lab at UCSF, especially Steve Hetts and Mariam Aboian, have been phenomenal to work with and learn from. Dr. Michael Schulz, mentioned above, has been a fantastic partner in crime on this work. I don't know anyone else who would go out on a limb and try such a crazy and oddball project. We have tried tons of stuff together. Most of it hasn't worked…and the stuff that has, well, that has been a wonderful surprise. Nonetheless, with some choice music (the title of a song we cannot name here in this thesis for decency sake), we can accomplish anything…or at least try.

The Grubbs and Gray groups were incredibly supportive during my time at Caltech…They were my big, no huge, research families! Over the years I have had the privilege of being coworkers with Bryan Stubbert, Qixi Mi, Hema Karunadasa, Smaranda Marinescu, Mike Rose, Paul Oblad, Paul Bracher, Morgan Cable, Josh Palmer, Alec Durrell, Keiko Yokoyama, Yan Choi Lam, Brad Brennan, Astrid Mueller, Bryan Hunter, Tania Darnton, Mike Lichterman, Sarah Del Ciello, Brendon McNicholas, Josef Schwan, Judy Lattimer, Daniel Konopka, Nicole Bouley-Ford, Heather Williamson, Gretchen Keller, Peter Agbo, Sarah Welhin, Brian Sanders, Oliver Shafaat, Emmanuelle Despagne-Ayoub, Wes Sattler, Aaron Sattler, Chris Roske, James Blakemore, James McKone, Maraia Ener, Kana Takematsu, Jeff Warren, Wes Kramer, Shabnam Hematian, Katie Fisher, Tony Vlcek, and Sam Johnson from the Gray group and Chris Daeffler, Julian Edwards, Myles Herbert, Keith Keitz, Benjamin Sveinbjornsson, Lauren Rosebrugh, Renee Thomas, Brendan Quigley, Nicholas Swisher, Anton Toutov, Matthew Van Wingerden, Ray Weitekamp, Zach Wickens, Hoyong Chong, Sarah Bronner, Jeff Cannon, Alexey Federov, John Hartung, Weibin Li, Vanessa Marx, Niki Millward, Garret Miyake, Bill Morandi, Victoria Piunova, Nanditha Nair, Josh Palmer, Pinky Patel, Peili Teo, Hiroshi Miyazaki, Choonwoo Lee, Michael Lerch, Keary Engle, Rob MacFarlane, Shane Mangold, Mel Pribisko-Yen, Daniel O'Leary, Tonia Ahmed, Alice Chang, Chris Bates, Pablo Guzman, Mike Haibach, Brendon McNicholas, Patrick Montgomery, Noah Fine Nathel, Juneyoung Lee, Michael Schulz, Jiaming Li, Zainab Al Saihati, Allegra Liberman-Martin, Tzu-Pin Lin, Dan Ziegler, Willie Wolf, Aidan Fenwick, Karthish Manthiram, Lennon Luo, Nebojša Momčilović, Jordan Theriot, Stanley Manatt, Chris Marotta, Peter Dornan, and Felix Rivas from the Grubbs group. I hope I hit everyone and I'm sorry if I missed anyone. In some way or stage, all of these people had a

valuable influence on my career. Church 217 was my home away from home during my time at Caltech. I'd like to thank my officemates for the company support. This large and constantly in flux group over the years has included Brendan, Nick, Zach, Victoria, Hoyoung, Weibin, Tonia, Chris, June, Mel, Willie, Nebo, Tori, and Noah.

I'd like to thank the Northwestern chemistry community for fostering my love of science and specifically chemistry. When I arrived at Northwestern, the promise I made to myself was that I would never take another chemistry course. Dumbest, most short lived promise of my life. Dr. Fred Northrup, the departmental undergraduate chemistry advisor helped assemble an incredible curriculum that drew my interest. Professor Brian Hoffman took me into his lab when I was a naïve freshman and facilitated the beginning of what has been a very long but fascinating academic career. Professor E-Money (Evan) Trivedi was my graduate mentor who patiently took me under his wing when I was a freshman. He taught me to think for myself and struggle through challenges. He along with his wife Dr. Staci Wegener guided me as I grew up in college and learned what research based science was about. Evan and Staci, I wouldn't have gone after a PhD if it weren't for you both. Two classes in college truly stood out to me. Professor J. Fraser Stoddart's course on nanomechanostereochemistry shook the foundation of what I thought chemistry was and changed the way in which I think about molecules in three dimensional space. Professor Sonbinh Nguyen's organometallics course helped me fall in love with metals—he too was one of Bob's graduate students. I really think it was his course that got me interested in applying to Caltech.

In terms of getting my work done or simply just existing at Caltech, I am incredibly indebted to the members of the staff and the general community. Thank you to Rick and Brian (more recently) in the glass shop and Mike and Steve in the machine shop. These gentlemen are capable of making dreams come true in terms of lab equipment. I say dreams because even when I tried to sketch some of these ideas out, they appeared nonsensical. Nonetheless, careful assistance, guidance, and experience in the shop brought some truly wonderful pieces of equipment to life. Jeff in the electronics shop has helped me create some really useful pieces of equipment including pseudo-disposable mechanical stirrers. None of

the ChemoFilter work discussed in the thesis would have been possible had it not been for his ingenuity. Cora, Denise, Carlos, and Corey have kept stockrooms on campus full and ready to go so that at any point I can have exactly what I need to get my work done. Elisa and Steve in the purchasing office have saved me on more occasions than I can count. All of my work was possible because of the speed in which I could get my hands on reagents and equipment to take into the lab. Joe Drew has kept our actual labs alive, coming to the rescue when it appears to rain above our fume hoods or the temperature in the room drops to nearly 50 degrees. Over the years, the members of the stockroom have changed, however, Memo, Art, Greg, and Armando have ensured that I receive any materials when they arrive on campus. The custodial staff is amazing at Caltech. They work tirelessly to keep the campus in shape and for that I'd like to say thank you. During the majority of my Caltech life, Agnes Tong was a mainstay in our division. I don't think I would have made it to graduation without her guidance and patience for times when I would forget to do things like register for class or if I just needed a friendly face. Mona Shahgholi, David Vander Velde, and Chi Ma have helped me more times than I can count with mass-spec, NMR, and SEM, respectively. I am indebted to both Bruce Brunschwig and Jay Winkler for helpful discussions and for keeping the MMRC and BILRC accessible to students like me. These facilities were invaluable in a lot of the work presented in this thesis. Larry, Mike, and the late Dr. Marsh were incredible resources for assistance with crystallography but also during afternoon word jumble sessions. Siddharth Dasgupta has been available for countless helpful discussions for which I am grateful for. Linda and Rick…the only way of really describing what you have done for me is making day to day life possible from organizing Bob's schedule to providing 408 reservations at the drop of a hat. Thank you both for keeping everything organized and on schedule, and everything else you do! The graphics resources department has saved me on many occasions with rush jobs when I was nothing short of desperate. Thank you all for your help. The Caltech community is much larger than this. I know I have missed some people. For that I'm sorry but I am really and truly grateful for Caltech as a whole for providing such a warm and inviting community.

Eating and cooking have been primary fixtures of my Caltech life outside of the lab. Many of my friendships have centered around constant culinary adventures. Miguel (Mike)

Post was one of my first friends at Caltech. Within a few weeks of our first term, we celebrated the Jewish holidays together. We broke fast with cans of Budweiser during Yom Kippur. From this moment on, I knew we would be friends. We eventually ended up roommates and destroyed our kitchen on more occasions than I can count but every time was great. Brandon Carroll has been a very good friend. He introduced me to craft beer and star gazing, two great interests of mine. Crystal and Captain Fluffy Pants (Yali) have been wonderful friends, willing to try any restaurant at the drop of a hat or learn to ski even as far away as Utah. Alice has been a good friend who can commiserate in our mutual feelings over the state of Florida and our love for tofu soup. Noah has been my wise postdoc friend, always available to join me for dinner especially when I'm stressed about something and need some company to vent to. Elle is a friend I met while climbing. I can always count on her for finding amazing beer from all over the country and bringing it back to share. I'd also like to thank Ernie and the rest of Ernie's Al Fresco for providing amazing, spicy sustenance (always order painful red—there is no better!) on countless occasions.

Outside of the Caltech community, I have a number of close friends that have kept me (relatively) sane during my graduate career. EricWolfKirchMasterFlexicles, an amazing friend from college, moved to Los Angeles a few months before me. As soon as I got here, we hit the ground running going off on our adventures into the mountains. More than that, he taught me how to drive a stick shift car and didn't ban me from lessons after I spilled a burrito all over the front seat when I stalled out. Thanks buddy! Katherine of Marovitch has been a great friend ensuring I always have a good laugh. Porpsicle, Kitt, and Sydney (the Kidney) have always been around for late night adventures. Eran, Crabby Abby, and Agler are friends I met in Israel, the few weeks before I moved to Pasadena. We don't see each other too often but whenever we are together it is as if time has never passed. Mike Arutunian and I met at the gym within my first few weeks at Caltech. We lifted, climbed, and ate together throughout my career in Pasadena. John Facendola is a chemist at USC I met a few years back at a conference. Chemistry made us friends but we always seem to have a great time, no matter the occasion. Jake and MVPaul, I met more recently, on a 4$^{th}$ of July camping trip. Despite having known them for only about a year, it seems like I've known them most of my life. Besides, no one else will really drink Coors Banquet with me. Reiter, a close

friend from college, moved out to the San Diego area during my time in grad school. He was called the Mad Scientist for a reason—his stories never get old and we usually have to fight to not do something stupid together. What better friend could I ask for. Simone is always there for me, whether it's providing an apartment to hang out at near the airport, or just around to go grab super late night food. She has been a great friend!

I learned to ski during my tenure at Caltech. I was originally very hesitant to learn but skiing has become an incredible source of activity and entertainment. I have gone on a number of trips but two trips with some friends really stand out—Whistler Blackcomb, Canada and Alta, Utah. Some new people have joined the trip and I hope it continues to grow but my constants on what now seems to be an annual ski trip include my girlfriend Ilana and my friends Reidawg (Andrew) Reiter, Enrique (Eric) Magda, Simone Slykhous, and Dan Davis. These trips have been some of the best of my life and have helped me keep my cool (at least the little bit I have) throughout grad school. We travel from all over the country for these trips but I'm glad I can count on my friends to keep it going. It has always been something I look forward to.

Southern California has been a wonderful place to live for the last 6 years. I have really started to enjoy hiking, sledding, and rock climbing. The Grubbs group has very much been a catalyst for this and other activities. Bob, Mike, Alice, Felix, Karthish, Zainab, Crystal, Chris, Patrick, Julian, Lauren, Willie, Vanessa, Nebo, Michael, Aidan, Noah, Allegra, Jiaming, and of course the puppies Togofloof, Captain Fluffy Pants (Yali), and Sadie have been great group adventure companions, even when we get lost and hike an extra four or five miles (without enough water). Also, there is nothing quite like seeing a dog go sledding (actually riding on the sled)…trust me.

I'm incredibly grateful to for my family. They have been incredibly supportive. I don't get to see my grandma and Marvin as often as I would like but they are only a phone call away. Grandma is a highlight of my trips home for Thanksgiving and is always there for me when I need a laugh. Paul and Bill, my older brothers, and their families, despite living in Maryland are always there for me when I need a pick me, a good laugh, or to blow

off steam. I don't get to see them as often as I would like but every time I see them, it's as if time hasn't passed. They have been nothing but supportive and for that I am grateful.

My younger brother, Maxwell, is my best friend. Despite being a few years younger, he is a constant voice of reason and full of tough love. No matter time of day or what part of the world he is off adventuring in, Max is only a phone call away. I don't know if anyone really gets why we laugh together constantly, but we do. When we are together, I think people question if we aren't really big elementary school aged children. Trust me when I say that it is hard to find two adults, that when together, could be so immature. We always have a great time. I couldn't have made it this far without him.

My parents, Marcy and Bob, mean everything to me. They never forced a track for me or said I had to do something—they just wanted me to be happy. I left high school expecting to go to law school. I entered grad school expecting to go to academia. About halfway through grad school I realized I was more interested in small start-ups. At no point did my family discourage me—they have instead been my cheerleaders. Going home to see my family and the critters is always perfect. There is no more comfortable feeling knowing that they are always there for me and that I can just be myself. It has been hard for me and my parents, being on opposite coasts of the country, but I can always count on them being there for me, no matter the time of day. Thank you both again for everything—the love, both soft and tough, the laughter, and the encouragement. Thank you for everything.

I'd like to thank my girlfriend Ilana for the blood, sweat, and tears she put into my PhD. We were great friends in college but started out dating in a long distance relationship. There was a lot of flying, weird talking schedules, and skype cooking dates. After some time, she was able to move out to California so we could actually be together rather. She has been there for my best and worst. Grad school wasn't easy. It shouldn't be. But she made it a hell of a lot easier. She patiently taught me to ski and has been my constant partner in new adventures. We've learned to thrown together pasta from scratch in under an hour, driven down the PCH in a day, gone on a four-hour trip for fish tacos. This all scratches the surface. Suffice it to say, thanks to Ilana, outside of the lab, my time at Caltech has been a

constant source of adventure and education. I could not have gotten through this without here support.

Lastly, I'd like to thank you all for reading this. The rambling is near over. There have been a lot of repeated names listed above. I know this has been a pretty long section. Honestly, it's probably not long enough. I'm sure I've missed some people. Sorry! There have been so many important people influencing my daily life, especially during my time in Pasadena. Thank you all again. Now on to the "sciency" stuff.

# ABSTRACT

Herein detailed are the syntheses, properties, and applications of metal-oxide nanosubstrates covalently functionalized with two classes of materials, inorganic macrocycles called corroles, and genomic deoxyribonucleic acid (DNA). These products have found biomedical applications in tumor imaging and chemotherapeutic sequestration, respectively. Both classes of prepared materials are the first of their kind.

Corroles are tetrapyrrolic macrocycles, which have found applications in tumor imaging and treatment, catalysis, solar fuels, and energy conversion. The direct functionalization of metal-oxides with inorganic macrocycles, including corroles, has largely revolved around the formation of hydrogen bonding type interactions between the substrate and the ligand. Hydrogen bonding motifs result in materials with only moderate stability due to solvent dissolution. In the first three chapters of this thesis, the scalable preparation of 5,10,15-(trispentafluorophenyl) corrole and its subsequent covalent functionalization of metal-oxide surfaces are discussed.

**Chapter 1** details mechanistic elements of the oligomerization and oxidative cyclization of 5,10,15-(trispentafluorophenyl) corrole from pentafluorobenzaldehyde and pyrrole. Prior to this work the synthesis of triperfluoroaryl corroles was dangerously exothermic and could only be carried out on milligram scale. Mechanistic insights led to a safe and scalable synthesis of the desired corrole species, achieving a 17.0 % yield (4.58 g). A detailed discussion of the covalent functionalization of the surface of $TiO_2$ with chlorosulfonated derivatives of 5,10,15-tris(pentafluorophenyl) corrole is presented in **Chapter 2**. The chlorosulfonated species investigated include the freebase, gallium, and aluminum corroles. Hydroxyl groups on the metal-oxide react with the chlorosulfonyl groups of the corrole ring *via* nucleophilic attack, resulting in the formation of sulfonic ester linkages. The aluminum species was further investigated as a potential near-infrared optical contrast agent. The details of this study, described in **Chapter 3**, include imaging experiments with immortalized human cancer lines and harvested mouse hepatocytes. This nanoconjugate exhibited low toxicity and efficient cellular uptake.

Conventional chemotherapy agents that target DNA are notorious for producing severe side-effects. Sequestering chemotherapeutics that enters systemic circulation, in a process deemed "ChemoFiltration," is a strategy for reducing off-target toxicity. Materials capable of such activity have yet to be fully realized. Reported in **Chapter 4** are the first methods covalent attachments of genomic DNA to surfaces, namely magnetite ($Fe_3O_4$) nanoparticles, *via* two separate strategies. These materials show efficacy in removing doxorubicin, cisplatin, and epirubicin from biologically relevant solutions. A device coated with this material demonstrated i*n vivo* activity in a porcine model.

# PUBLISHED CONTENT AND CONTRIBUTIONS

Carl M. Blumenfeld, Katherine J. Fisher, Lawrence M. Henling, Robert H. Grubbs, Harry B. Gray, and Scott C. Virgil. **Control of Oligomerization and Oxidation Steps in the Synthesis of Tris(pentafluorophenyl)corrole.** European Journal of Organic Chemistry, **2015**, 3022-3025. doi: 10.1002/ejoc.201500276

C. M. B. participated in the design, performance, as well as analysis of experiments and the preparation of the manuscript.

Carl M. Blumenfeld, Robert H. Grubbs, Rex A. Moats, Harry B. Gray, and Karn Sorasaenee. **Decorating Metal Oxide Surfaces with Fluorescent Chlorosulfonated Corroles.** Inorganic Chemistry, **2013**, 4774-4776. doi: 10.1021/ic400410k

C. M. B. participated in the synthesis of materials, the design, performance, as well as analysis of experiments, and the preparation of the manuscript.

Carl M. Blumenfeld, Bryce F. Sadtler, G. Esteban Fernandez, Lily Dara, Cathie Nguyen, Felix Alonso-Valenteen, Lali Medina-Kauwe, Rex A. Moats, Nathan S. Lewis, Robert H. Grubbs, Harry B. Gray, and Karn Sorasaenee. **Cellular uptake and cytotoxicity of a near-IR fluorescent corrole-$TiO_2$ nanoconjugate.** Journal of Inorganic Biochemistry, **2014,** 39-44. doi: 10.1016/j.jinorgbio.2014.06.015

C. M. B. participated in the synthesis of materials, the design, performance, as well as analysis of experiments, and the preparation of the manuscript.

# TABLE OF CONTENTS

Acknowledgements……...iii
Abstract ……..xiii
Published Content and Contributions…….....xv
Table of Contents……..… xvi
Introductory Remarks.....1
Chapter 1.....2
Chapter 2.....34
Chapter 3.....49
Chapter 4.....71

# *Introductory Remarks*

I came to Caltech to study inorganic chemistry. I thought this implied that I would be making complexes and analyzing them. For better or for worse, my initial chemistry did not work and I took what I thought would be a brief break to investigate surface functionalization with inorganic ligands. This "brief break" wound up turning into nearly my whole Caltech career.

My advisors, Harry and Bob, suggested that rather than rewrite my work, I reformat three published works into discreet chapters for my thesis. I tell this story in reverse order as the first chapter of the thesis is the most recent corrole paper published. This chapter describes the synthesis of the parent corrole, 5,10,15-tris(pentafluorophenyl) corrole, which will be the star of this thesis. The second and third chapters describe the functionalization of this corrole, its covalent coupling to surfaces, and potential applications. Despite the publication years being jumbled, this seems like a fairly logical path to trace.

The final chapter of my thesis is an unpublished manuscript on surface functionalization of metal-oxides with genomic DNA. This work, while not traditionally inorganic as I had expected to do through my career, highlights my interest in surface chemistry of all varieties. As this work has not yet been seen by the world, I hope you find it enjoyable!

*Chapter 1*

# CONTROL OF OLIGOMERIZATION AND OXIDATION STEPS IN THE SYNTHESIS OF TRIS(PENTAFLUOROPHENYL)CORROLE

Although this work was the last published corrole paper in this dissertation, herein discussed is the work that would make corrole use both scaleable and industrially applicable. At the point in which Katie, my undergraduate student, and I approached Scott Virgil about synthetic corrole scale-up, we had already covalently functionalized $TiO_2$ surfaces with chlorosulfonated metalo- and freebase-derivatives of 5,10,15-tris(pentafluorophenyl)corrole.

The initial corrole syntheses were dangerous and low yielding. The traditional workhorse reaction was run solvent free; upon introduction of dilute catalyst to the reaction mixture, the contents of the reaction would start to boil vigorously. This uncontrollable exothermic reaction would then spew a black almost tar-like material all over the fumehood. Whatever material remained was sonicated with large quantities of solvent to promote dissolution, at which point it was chemically oxidized. To improve safety and somewhat temper the exotherm, no large scale reactions were run. Instead, fifteen to twenty microscale reactions were run at which point the tar like material was collected in bulk for oxidation.

Nonetheless, with materials in hand we carried out the chlorosulfonation and subsequent metalation procedures of the parent corrole. These steps were quite low yielding (and are discussed in subsequent chapters) but we were able to access the surface functionalized materials. *In vitro* optical imaging of these materials were studied in collaboration with researchers at Children's Hospital Los Angeles. We observed that these materials were in fact strong candidates as tissue imaging agents.

We hoped to prepare more materials on scale so I approached Scott Virgil in the Caltech Catalysis Center. We believed that by using robotic methods, we could scale up the microreactions and keep our hands away from the violent exotherm. Thankfully, Scott had a different idea! We would develop methods for scaling the reaction, whilst controlling the

exotherm. At the same time, we would also improve the yield of the reaction itself. During the process of developing this reaction, we nearly doubled the yield of the traditional pentafluorophenyl corrole synthesis but at the same time could work on scales more than an order of magnitude larger!

In addition to all of this synthetic work, Katie, my undergrad, while washing out fritted funnels contaminated with tris(pentafluorophenyl) corrole, unintentionally (and very luckily) started the growth of x-ray grade crystals that were essential for the assignment of the positions of the pyrrole protons in the core of the corrole ring.

Described below are our efforts to understand the fundamental steps in the corrole forming reaction. We no longer considered the corrole synthesis to be a single two-step reaction; instead, we observed that each stage of the reaction could be carefully controlled and optimized. In the process of this work, we produced over fifty grams of pure corrole. This is a supply for several graduate lifetimes!

# CONTROL OF OLIGOMERIZATION AND OXIDATION STEPS IN THE SYNTHESIS OF TRIS(PENTAFLUOROPHENYL)CORROLE



## Introduction

The field of corrole synthesis, including its applications, has burgeoned over the last fifteen years. As late as 1998, corroles and their metal complexes found no application.[1] Owing to fundamental work on the original syntheses of corroles from Gross and co-workers, the field has grown enormously.[1, 2] Corroles have found applications in molecular tumor imaging and treatment,[3] solar fuels chemistry,[4] chemical catalysis,[5] and nanomaterial development.[6]

The first synthesis of a corrole dates to 1965 in which Kay and Johnson prepared corrole and corrolato species from a deoxybiladiene intermediate (7). It was not until 1993, however, that a *meso*-aryl-substituted corrole was prepared that led to applications in catalysis (8). In seminal work in the late 1990s, Gross and co-workers discovered a synthesis of tris(pentafluorophenyl)corrole (**1**) from readily available starting materials, pentafluorobenzaldehyde (**2**) and pyrrole (**3**) (1, 2). This discovery changed the course of corrole chemistry, as now investigation could explore both the fundamental properties as well as practical applications of these macrocyclic compounds.

Fully 15 years after the Technion work, we still do not have a clear understanding of the individual steps leading to the corrole formation. Indeed, the situation is much like the state of porphyrin synthesis before the impressive contributions by Lindsey (9). We set as a goal the elucidation of each step in the corrole-forming sequence (Scheme 1).

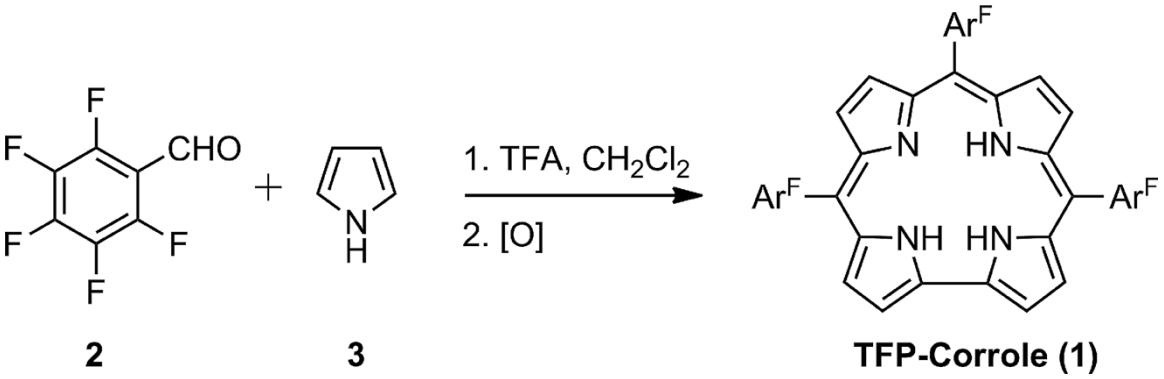


Scheme 1. Synthesis of corrole (TFA = trifluoroacetic acid).

**Results and Discussion**

Our initial experiments were aimed at isolating the pyrrole-aldehyde oligomerization reaction from the subsequence oxidation steps of corrole synthesis. A series of screens was conducted to assess the influence of reaction concentration, temperature, pyrrole to aldehyde ratio, and acid catalyst concentration. The reactions were analyzed by LC-TOF and revealed several correlations according to the mechanism shown (Scheme 2).

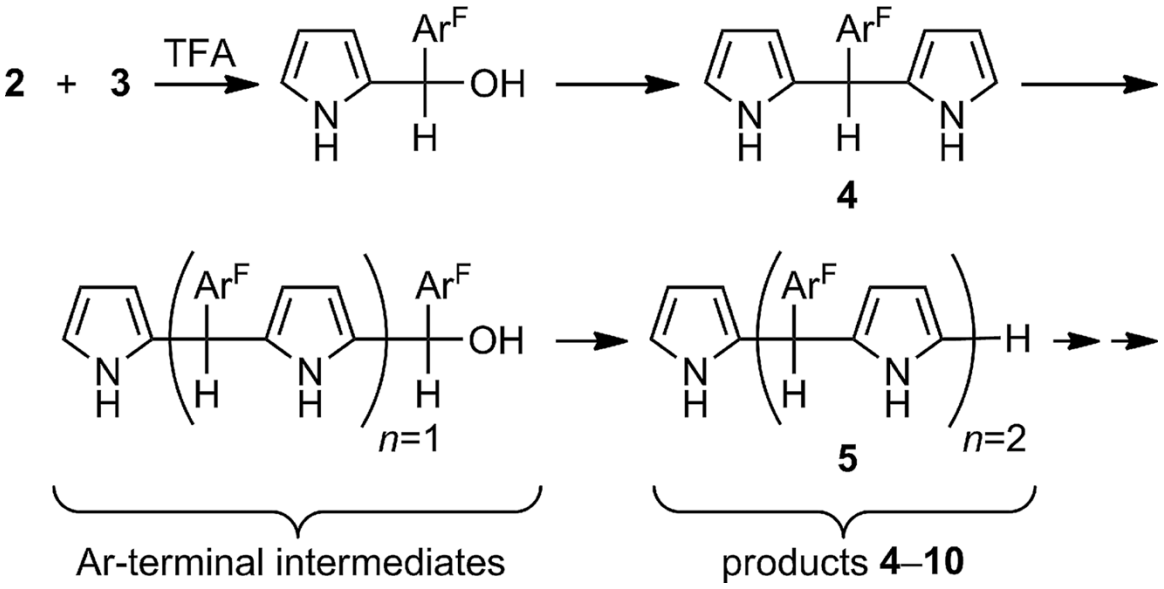


Scheme 2. Mechanism of condensation of **2** and **3**.

It became quickly apparent that a clean condensation could be optimized to achieve the predominant production of linear, fully alternating pyrrole-capped oligomers. We sought to optimize the conditions for the formation of oligomers **4**-**10**, expecting that compound **6** would prove to be a favorable precursor to **1** by oxidation (Scheme 3).

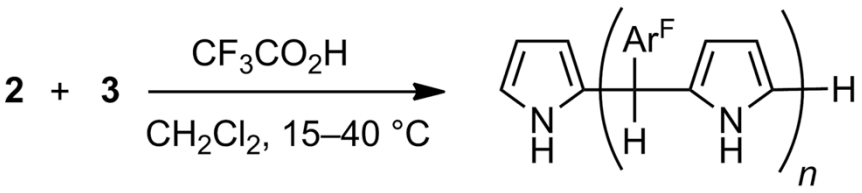


| # | *n* | Yield [%] |
|---|---|---|
| **4** | 1 | 20.0 |
| **5** | 2 | 18.4 |
| **6** | 3 | 22.4 |
| **7** | 4 | 15.9 |
| **8** | 5 | 8.2 |
| **9** | 6 | 4.3 |
| **10** | 7 | 1.7 |

Scheme 3. Selective preparation of oligomers **4**-**10**.

The best conditions for generating a predominance of the fully capped species included increased reaction concentration and increased number of pyrrole equivalents. However, under concentrated reagent conditions or as a neat mixture, the reaction is strongly exothermic and the exotherm is uncontrollable on a scale above 5 mmol. We therefore performed a series of automated screens to optimize the parameters of temperature, dilution, pyrrole equivalents, and trifluoroacetic acid (TFA) catalyst loading. Elevated reaction temperatures were found to lead to a flattening of the oligomer distribution favoring **7**-**10** and still larger oligomers while decreasing the contribution of **6** to the final product mixture. Dilution with dichloromethane was evaluated to moderate the reaction and control the exotherm. The initial observations from these dilution experiments revealed the presence of Ar-terminal intermediates in the product mixture (Scheme 2) and a prevalence of higher-massed products (10). The presence of Ar-terminal intermediates in the product mixture was especially undesirable, even in small amounts, due to their eventual conversion upon subsequence oxidation to the porphyrin that we found difficult to separate from **1**. Therefore, additional equivalents of pyrrole were screened to achieve the complete pyrrole-capping of oligomers and this had the added benefit of sharply curtailing the product distribution past

the desired product **6**. Under the optimized conditions for the scale-up procedure (20 g of **2**), the yield of compound **6** was maximized (Figure 1) with a favorable exponential decline of higher oligomers (11, 12). In order to unambiguously characterize the products of this reaction and to confirm the predominance of **6** in the product mixture, a smaller scale reaction mixture (1.5 g of **2**) was purified by preparative HPLC affording the individual yields shown in Scheme 3.

Full characterization of the individual products form this reaction required an appreciation of the stereoisomerism inherent to oligomeric species with sequential stereogenic centers (13). Although standard reversed phase HPLC analysis of products **4**-**10** gave no separation of the stereoisomers present, chiral supercritical fluid (SFC) experiments (Figure 2, left) readily separated individual isomeric species present in the products **4**-**7**. In addition, high-field $^1$H NMR spectra (Figure 2, right) revealed individual methane resonances for multiple stereoisomers in these fractions. Although **4** showed a single peak

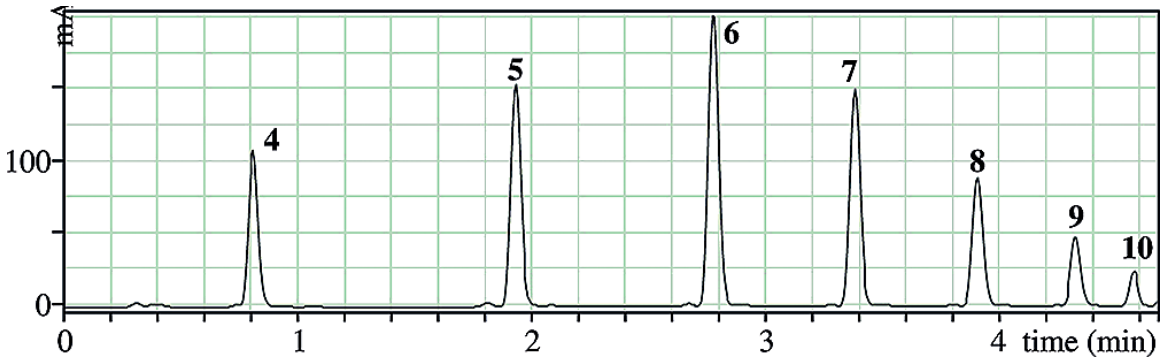


Figure 1. HPLC analysis (Agilent 2.1 x 50 mm Eclipse Plus C8, 60-100% ACN/$H_2O$, 254 nm) of the product mixture from teh reaction of 2.8 equiv. of **3** with aldehyde **2** in $CH_2Cl_2$ (2.0 *M*) with 1.9 mol-% TFA at 15-40 °C.

under each measurement, the product **5** gave a 1:1 ratio of *dl* and *meso* isomers in the $^1$H NMR spectrum and a 1:2:1 ratio in the chiral SFC analysis consistent with a statistical ratio of these isomers produced under the reaction conditions. In contrast, a non-statistical distribution of isomers was apparent from the analysis of **6** (0.27:0.32:0.29:0.12 ratio in SFC and 0.31:0.57:0.12 ratio by $^1$H NMR) (14). Finally, the spectra of **7** appeared to show the

expected six isomeric species in the $^1$H NMR spectrum while giving a complex series of peaks in the SFC analysis. Importantly, the isolation and unambiguous characterization of these linear fully alternating pyrrole-capped oligomers including **6,** demonstrates that for this perfluorophenyl series the entire acid-catalyzed sequence of reactions operates as a simple condensation without any pyrrole-pyrrole coupling events or cyclization to corrole precursors (15, 16).

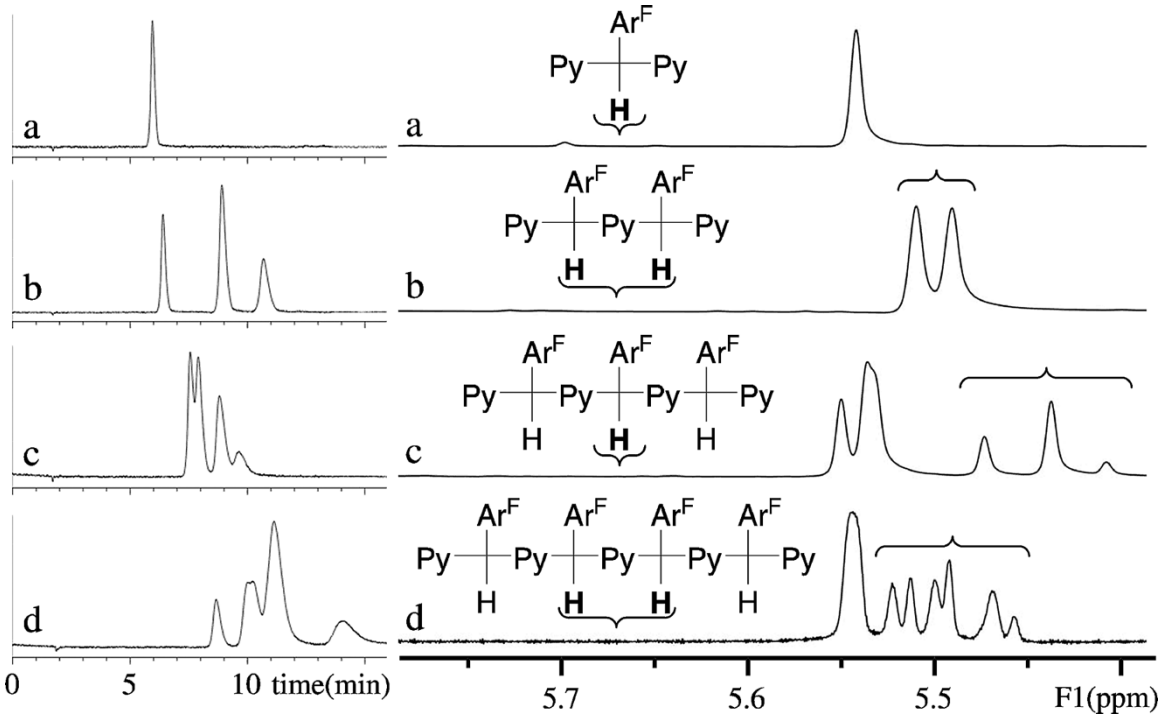


Figure 2. SFC chromatographic analysis (two Chiralcel® 4.6 X 260 mm AD-H columns, 7% 2-propanol in $CO_2$ at 40 °C, 3 mL/min) and $^1$H NMR (600 MHz, $C_6D_6$) analysis of the purified products **4**-**7** (spectra **a**-**d**).

The controlled DDQ (2,3-dihcloro-5,6-dicyano-1,4-benzoquinone) oxidation of the crude reaction mixture presents an additional challenge in the corrole-forming process. In preparative runs, the generation of electrophilic species from the crude mixture of **4**-**10** can lead to competing polymerization reactions, thus decreasing the isolate yield of **1**. We screened conditions for optimization using samples of pure **6** prepared above and then evaluated the factors necessary to achieve a high yield of **1** on the preparative scale from the mixture of **4**-**10**. Gratifyingly, the pure isomer **6** was effectively converted to corrole **1** in

84% isolated yield when treated with a THF solution of 3.3 equiv. of DDQ in dichloromethane at 15 ˚C. Corrole **1** was readily observed during the initial phase of the DDQ addition suggesting that the three $2e^-$ oxidations proceed as a cascade to the stable corrole rather than an accumulation of sequentially oxidized species. Based on this observation, it is reasonable to believe that the key intramolecular cyclization event occurs immediately after reaction with the first equivalent of DDQ followed by two facile oxidations to **1** as shown below (17).

When approaching the oxidation of the unpurified mixture of **4**-**10**, experimental conditions were evaluated in order to minimize the intermolecular electrophilic reactions that could compete with the cyclization shown in Scheme 4. The conditions described for the aforementioned oligomerization (Scheme 3) were chosen to minimize the contribution of oligomer **4** which generated an undesirable contribution of electrophilic species. In addition, removal of excess pyrrole in vacuo prior to the DDQ oxidation step dramatically reduced the formation of polymeric byproducts and simplified the chromatographic purification of **1**. Under the optimized scale-up procedure (beginning with 20 g of **2**, Scheme 2 and Scheme 4), the addition of a THF solution containing 1.0 equiv. of DDQ to the dichloromethane solution of **4**-**10** at 5 ˚C afforded **1** in 17.0% yield after chromatographic purification and recrystallization.

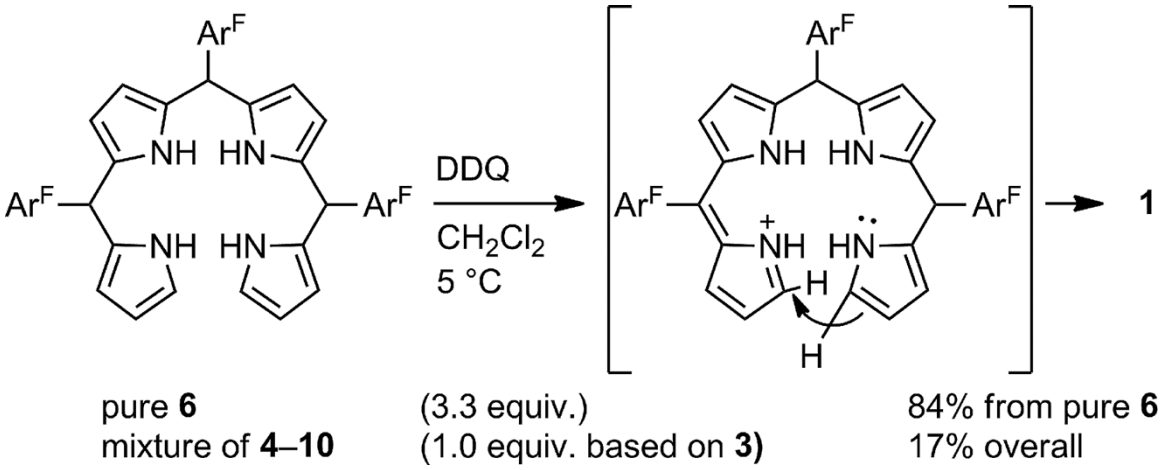


Scheme 4. DDQ oxidation of **6** leading to corrole **1**.

Although the crystal structure of **1** has been previously reported, we found that crystals of the formula **1**•(ace)$_2$ were obtained readily from acetone by slow evaporation.

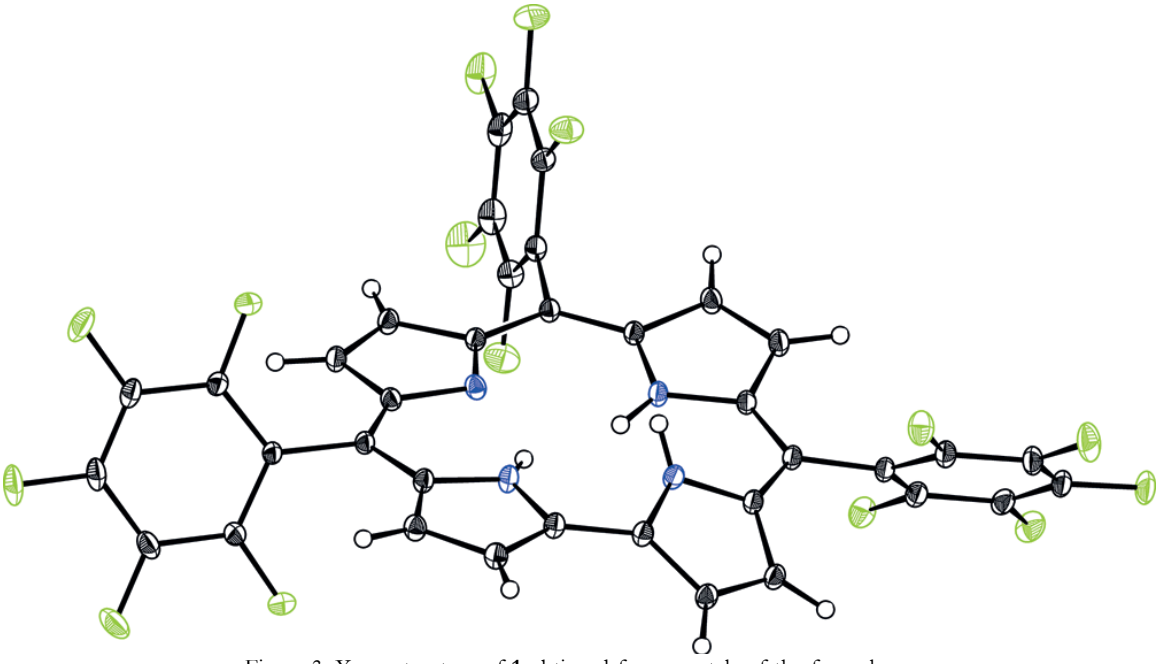

Figure 3. X-ray structure of **1** obtianed from crystals of the formula **1**•(ace)$_2$.

The X-ray structure shown in Figure 3 was freely refined to reveal the hydrogen atom coordinates within the corrole ring system (18).

## Conclusions

We have revisited the mechanism of corrole oligomerization and cyclization steps in an effort to achieve a scalable synthesis with an increased yield (19). Isolated precursor **6**, upon selective oxidation, afforded a favorable yield of 84% while a scalable synthesis directly from **2** and **3** without intermediate purification afforded 17.0% of the corrole **1** over two steps. This speaks to the intricacy of the oxidation of the bulk reaction mixture and the requirement for the optimization of both steps individually. We hope that these advances in mechanistic understanding will facilitate the further development of the corrole field due to more facile access to corrole ligands.

**Experimental Section**

A mixture of **2** (20 g, 0.102 mol), dihchloromethane (15 mL) and **3** (20 mL, 19.3 g 0.29 mol) in a 500 mL round-bottomed flask was placed in an ice-water bath. When the internal temperature reached 15 ˚C, 1.0 mL of a 5% *v/v* trifluoroacetic acid solution (0.075 g of TFA, 0.65 mmol) in dichloromethane was added with rapid stirring. After the initial exotherm subsided, an additional 2.0 mL of the 5% TFA solution was added. After 30 min, the mixture was filtered through anhydrous magnesium sulfate and concentrated at 0.5 Torr and 40 ˚C. The viscous liquid was redissolved in dichloromethane (50 mL) and concentrated again at 0.5 Torr and 40 ˚C. A solution of DDQ (22.7 g, 0.10 mol) in tetrahydrofuran (200 mL) was added to the resulting mixture of **4-10** (Figure 1) in dichloromethane (4000 mL) at 5 ˚C over 40 min. After stirring for 6h at room temperature, the mixture was evaporated to a volume of 400 mL, diluted with hexane (400 mL) and filtered. The crude product was purified by flash chromatography over silica (1320 g) with 25% dichloromethane/hexanes and recrystallized from dichloromethane/hexanes to afford 4.58 g of **1** (17.0% yield) in two crops.

**Acknowledgements**

The authors acknowledge the Doheny Eye Institute, Sanofi, the Gordon and Betty Moore Foundation, Caltech, and the National Institutes of Health (NIH) (grant number RR027690) for financial and infrastructural support. The authors are grateful to Professor Zeev Gross for ongoing support in these efforts and suggestions on the presentation of this work. The authors also wish to thank Dr. David VanderVelde for assistance in obtaining NMR spectra of compounds **4-10** and Prof. Brian Stoltz for helpful discussions.

---

[1] a) Z. Gross, N. Galili, I. Saltsman, *Angew. Chem. Int. Ed.* **1999**, *38*, 1427–1429; *Angew. Chem.* **1999**, *111*, 1530; b) Z. Gross, N. Galili, I. Saltsman, *Angew. Chem.* **1999**, *111*, 1530–1533.

[2] Z. Gross, N. Galili, L. Simkhovich, I. Saltsman, M. Botoshansky, D. Bläser, R. Boese, I. Goldberg, *Org. Lett.* **1999**, *1*, 599– 602.

[3] a) J. Y. Hwang, D. J. Lubow, D. Chu, J. Sims, F. Alonso-Valen- teen, H. B. Gray, Z. Gross, D. L. Farkas, L. K. Medina-Kauwe, *J. Controlled Release* **2012**, *163*, 368–373; b) H. Agadjanian, J. Ma, A. Rentsendorj, V. Valluripalli, J. Y. Hwang, A. Mah- ammed, D. L. Farkas, H. B. Gray, Z. Gross, L. K. Medina- Kauwe, *Proc. Natl. Acad. Sci. USA* **2009**, *106*, 6105–6110; c) J. Y. Hwang, D. J. Lubow, J. D. Sims, H. B. Gray, A. Mah- ammed, Z. Gross, L. K. Medina-Kauwe, D. L. Farkas, *J. Bi omed. Opt.* **2012**, *17*, 015003; d) C. M. Blumenfeld, B. F. Sadtler, G. E. Fernandez, L. Dara, C. Nguyen, F. Alonso-Valenteen, L. Medina-Kauwe, R. A. Moats, N. S. Lewis, R. H. Grubbs, H. B. Gray, K. Sorasaenee, *J. Inorg. Biochem.* **2014**, *140*, 39–44.

[4] a) L. Flamigni, D. T. Gryko, *Chem. Soc. Rev.* **2009**, *38*, 1635– 1646; b) H. Lei, A. Han, F. Li, M. Zhang, Y. Han, P. Du, W. Lai, R. Cao, *Phys. Chem. Chem. Phys.* **2014**, *16*, 1883–93.

[5] Q. Wang, Y. Zhang, L. Yu, H. Yang, M. H. Mahmood, H.-Y. Liu, *J. Porphyrins Phthalocyanines* **2014**, *18*, 316–325.

[6] C. M. Blumenfeld, R. H. Grubbs, R. A. Moats, H. B. Gray, K. Sorasaenee, *Inorg. Chem.* **2013**, *52*, 4774–4776.

[7] A. Johnson, I. Kay, *J. Chem. Soc.* **1965**, 1620–1629.

[8] R. Paolesse, S. Licoccia, M. Fanciullo, *Inorg. Chim. Acta* **1993**, *203*, 107–114.

[9] G. R. Geier III, J. S. Lindsey, *J. Chem. Soc. Perkin Trans. 2* **2001**, 677–686.

[10] The specific conditions for the condensation of equimolar amounts of **2** and **3** affording cyclic and Ar-terminal products have been previously reported, see: L. Simkhovich, I. Goldberg, Z. Gross, *Org. Lett.* **2003**, *5*, 1241–1244.

[11] Although reaction of **2** and **3** can be treated as a classical step- growth oligomerization to generate a weight distribution of oligomers **4–10** favoring compound **6**, the strong predominance of **6** obtained in this procedure arises from the attenuated reac- tivities of the sequential intermediates **4–10** and the lower rela- tive reactivity of pyrrole, see: P. J. Flory, *Principles of Polymer Chemistry*, Cornell University Press, New York, **1953**, ch. 8.

[12] On the 20 g scale presented in this work, the condensation reac- tion was evaluated under both air and nitrogen atmosphere and the product distribution shown in Figure 1was found to be identical under both conditions. Molar response factors mea- sured at 254 nm for the purified oligomers **4–10** are provided in the Supporting Information and increase with the number of chromophoric aryl residues present in each oligomer.

[13] E. L. Eliel, S. H. Wilen, *Stereochemistry of Organic Compounds*, Wiley, New York, **1994**.

[14] A random statistical distribution expected for **6** would consist of equal proportions of *d*, *l*, *meso*1 and *meso*2 isomers that would afford a 1:1:2 ratio of peaks in the 1H NMR spectrum.

[15] Our finding is in accordance with the report by Lee (ref.[16b]) and a report by Gryko (ref.[16c]) in which the isolation of analogous corrole precursors similar to **6** was reported.

[16] a) D. T. Gryko, K. Jadach, *J. Org. Chem.* **2001**, *66*, 4267–4275; b) J.-W. Ka, W.-S. Cho, C.-H. Lee, *Tetrahedron Lett.* **2000**, *41*, 8121–8125; c) B. Koszarna, D. T. Gryko, *J. Org. Chem.* **2006**, *71*, 3707–3717.

[17] The key cyclization of an electron-deficient intermediate during the DDQ oxidation of **6** could also involve a radical intermediate analogous to that shown in Scheme 4. The progress of the DDQ oxidation of **6** is shown in the Supporting Information and may exhibit features particular to this electron-deficient perfluoroaryl series.

[18] Of the two possible tautomeric representations of **1**, the structure presented in Figure 3 unambiguously reveals the position of the three central hydrogen atoms. As shown in

Scheme 1, two hydrogen atoms are found on the intact bipyrrole subunit and one hydrogen atom is shared within the top tautomeric portion of corrole **1**. See the Supporting Information for more details. CCDC-1052621 contains the supplementary crystallographic data for this paper. These data can be obtained free of charge from The Cambridge Crystallographic Data Centre via www.ccdc.cam.ac.uk/data_request/cif.

[19] In addition to the procedures presented in ref.[1,2], one can compare this work with previously reported procedures for the preparation of **1**, see: a) I. H. Wasbotten, T. Wondimagegn, A. Ghosh, *J. Am. Chem. Soc.* **2002**, *124*, 8104–8116; b) D. T. Gryko, B. Koszarna, *Org. Biomol. Chem.* **2003**, *1*, 350–357; c) D. K. Dogutan, S. A. Stoian, R. McGuire Jr., M. Schwalbe, T. S. Teets, D. G. Nocera, *J. Am. Chem. Soc.* **2011**, *133*, 131–140.

**Supplementary Experimental and Characterization**

**Representative Screening Results from the Optimization of Oligomerization and Oxidation Steps:** Screening experiments of pyrrole:aldehyde ratio, TFA catalyst concentration, solvent, and temperature were prepared using the Freeslate Core Module 2 on a scale of 1 mmol and the crude reaction mixtures were analyzed by LCMS at multiple timepoints. Using the measured relative molar response factors at 254 nM of 1.0, 2.2, 3.5, 5.1, 6.7, 8.4 for the purified compounds **4**-**9**, respectively, the UV integrations for each oligomer were converted to the per cent of theoretical yield of each oligomer. A representative optimization for pyrrole:aldehyde molar ratio is shown in Figure 1 below. Optimization experiments for the DDQ oxidation step were conducted in a similar fashion using 4,4'-di-*tert*-butylbiphenyl as an internal standard. In practice, the optimum number of equivalents of DDQ and the yield of **1** were dependent on the composition of **4**-**10** present in the oligomer sample subject to oxidation with the best results obtained when oligomer **4** was present in lesser amounts. A representative optimization for the molar ratio of DDQ:starting aldehyde on the mixture of **4**-**10** is shown in Figure 2 below.

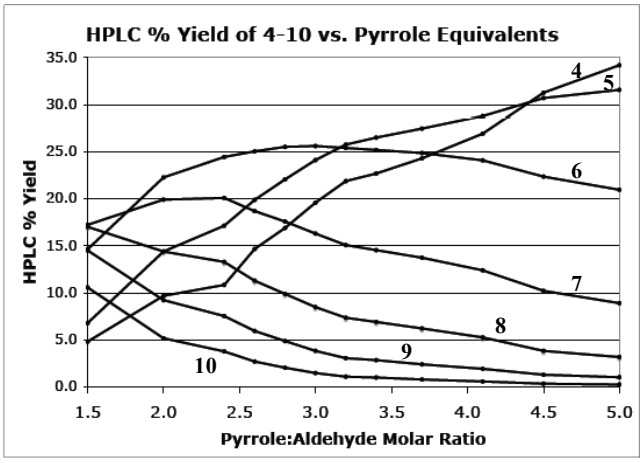


Supplementary Figure 2: HPLC % Yield of **4-10** vs. Pyrrole Equivalents.

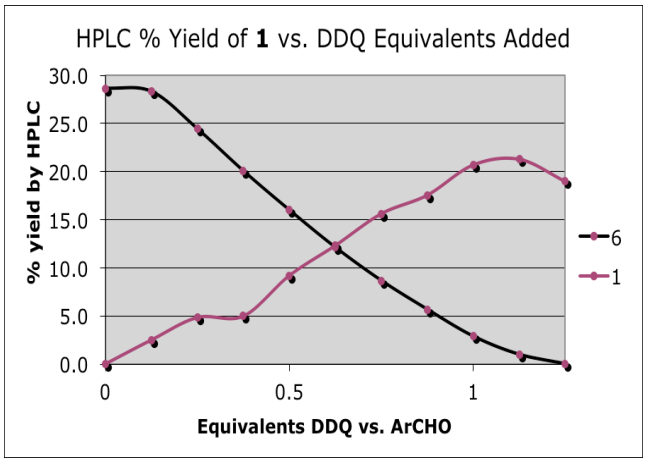


Supplementary Figure 1: HPLC % Yield of **1** vs. DDQ equivalents

**Procedure for the preparation and preparative HPLC separation of compounds 4-10:**

To a 20 mL scintillation vial with stirbar was added a solution of pentafluorobenzaldehyde (1.50 g, 7.65 mmol, 1.0 equiv.) in dichloromethane (2.25 mL) followed by pyrrole (2.25 mL, 2.18 g, 32.4 mmol, 4.2 equiv.). The mixture was cooled to 15 °C and a solution of 1:19 v/v trifluoroacetic acid in dichloromethane (75 µL, .05 mmol, 0.006 equiv.) was added. After stirring for 10 minutes at 15 – 20 °C, an additional 75 µL of the trifluoroacetic acid solution was added and the mixture was allowed to stir at room temperature for 20 minutes.

The reaction mixture was directly purified by reversed phase preparative HPLC (in 12 injections of 500 μL each) on a 30 x 250 mm XDB-C18 column (5 μM particle size) using an Agilent 1200 preparative HPLC with a flow rate of 50 mL/min (85-100% acetonitrile/water) and UV detection at 254 nM. The fractions containing compounds **4-10** were separately collected in ice-cooled receivers and rotary evaporated to dryness. Care was taken to minimize exposure to air and light during the handling and storage of **4-10**. After dissolving in ether, the products were transferred to individual vials and evaporated to afford the pure compounds **4-10** which were pumped under high vacuum for 4 hours.

2,2'-((perfluorophenyl)methylene)bis(1H-pyrrole)

$C_4H_4N$-$CH(C_6F_5)$-$C_4H_4N$ (**4)** was obtained as an off-white solid (478 mg, 20.0% yield). $^1$H NMR (600 MHz, $CD_2Cl_2$): δ 8.20 (br s, 2H), 6.73 (dt, 2H, $J$ = 1.5, 2.7 Hz), 6.14 (q, 2H, $J$ = 3.0 Hz), 6.01 (t, 2H, $J$ = 3.2 Hz), 5.91 (s, 1H). HR(ESI)-MS (M-H) (M = $C_{15}H_9F_5N_2$): Calcd 311.0602, obsd 311.0587.

2,5-bis((perfluorophenyl)(1H-pyrrol-2-yl)methyl)-1H-pyrrole

$C_4H_4N$-$[CH(C_6F_5)$-$C_4H_3N]$-$CH(C_6F_5)$-$C_4H_4N$ (**5)** was obtained as an orange viscous liquid (393 mg, 18.4% yield). $^1$H NMR (600 MHz, $CD_2Cl_2$): δ 8.20 (br s, 2H), 8.07 and 8.04 (pair of s, 1H, dl and meso), 6.72 (q, 2H, $J$ = 2.3 Hz), 6.11 (m, 2H), 5.96 (s, 2H), 5.92 (t, 2H, $J$ = 2.4 Hz), 5.84 (s, 2H). HR(ESI)-MS (M-H) (M = $C_{26}H_{13}F_{10}N_3$): Calcd 556.0866, obsd 556.0851.

5,5'-((perfluorophenyl)methylene)bis(2-((perfluorophenyl)(1H-pyrrol-2-yl)methyl)-1H-pyrrole)

$C_4H_4N$-$[CH(C_6F_5)$-$C_4H_3N]_2$-$CH(C_6F_5)$-$C_4H_4N$ (**6)** was obtained as a yellow powder (459 mg, 22.4% yield). $^1$H NMR (600 MHz, $CD_2Cl_2$): δ 8.20 (br s, 2H), 8.00 – 8.10 (m, 2H), 6.73 (m, 2H), 6.12 (m, 2H), 5.96 (m, 2H), 5.86-5.91 (m, 4H), 5.84 (s, 2H), 5.78 and 5.77 (pair of s, 1H). HR(ESI)-MS (M-H) (M = $C_{37}H_{17}F_{15}N_4$): Calcd 801.1130, obsd 801.1110.

2,5-bis((perfluorophenyl)(5-((perfluorophenyl)(1H-pyrrol-2-yl)methyl)-1H-pyrrol-2-yl)methyl)-1H- pyrrole

$C_4H_4N$-[$CH(C_6F_5)$-$C_4H_3N$]$_3$-$CH(C_6F_5)$-$C_4H_4N$ (**7)** was obtained as an orange viscous liquid (318 mg, 15.9% yield). $^1$H NMR (600 MHz, $CD_2Cl_2$): δ 8.20 (br s, 2H), 8.00 (m, 3H), 6.71 (m, 2H), 6.10 (m, 2H), 5.96 (m, 2H), 5.90 (m, 2H), 5.87 (m, 4H), 5.83 (s, 2H), 5.76 (pair of s, 2H). HR(ESI)-MS (M-H) (M = $C_{48}H_{21}F_{20}N_5$): Calcd 1046.1394, obsd 1046.1395.

5,5'-((perfluorophenyl)methylene)bis(2-((perfluorophenyl)(5-((perfluorophenyl)(1H-pyrrol-2- yl)methyl)-1H-pyrrol-2-yl)methyl)-1H-pyrrole)

$C_4H_4N$-[$CH(C_6F_5)$-$C_4H_3N$]$_4$-$CH(C_6F_5)$-$C_4H_4N$ (**8)** was obtained as an orange viscous liquid (162 mg, 8.2% yield). $^1$H NMR (600 MHz, $CD_2Cl_2$): δ 8.18 (br s, 2H), 8.03 (m, 4H), 6.71 (m, 2H), 6.10 (m, 2H), 5.95 (m, 2H), 5.89 (m, 2H), 5.87 (m, 6H), 5.83 (s, 2H), 5.76 (m, 3H). HR(ESI)-MS (M-H) (M = $C_{59}H_{25}F_{25}N_6$): Calcd 1291.1658, obsd 1291.1627.

2,5-bis((perfluorophenyl)(5-((perfluorophenyl)(5-((perfluorophenyl)(1H-pyrrol-2-yl)methyl)-1H-pyrrol- 2-yl)methyl)-1H-pyrrol-2-yl)methyl)-1H-pyrrole

$C_4H_4N$-[$CH(C_6F_5)$-$C_4H_3N$]$_5$-$CH(C_6F_5)$-$C_4H_4N$ (**9)** was obtained as a light brown viscous liquid (85 mg, 4.3% yield). $^1$H NMR (600 MHz, $CD_2Cl_2$): δ 8.18 (br s, 2H), 8.02 (m, 5H), 6.70 (m, 2H), 6.09 (m, 2H), 5.95 (m, 2H), 5.89 (m, 2H), 5.87 (m, 8H), 5.83 (s, 2H), 5.76 (br s, 4H). HR(ESI)-MS (M-H) (M = $C_{70}H_{29}F_{30}N_7$): Calcd 1536.1922, obsd 1536.1883.

5,5'-((perfluorophenyl)methylene)bis(2-((perfluorophenyl)(5-((perfluorophenyl)(5-((perfluorophenyl)(1H-pyrrol-2-yl)methyl)-1H-pyrrol-2-yl)methyl)-1H-pyrrol-2-yl)methyl)-1H-pyrrole

$C_4H_4N$-[$CH(C_6F_5)$-$C_4H_3N$]$_6$-$CH(C_6F_5)$-$C_4H_4N$ (**10)** was obtained as a light brown viscous liquid (32 mg, 1.8% yield). $^1$H NMR (600 MHz, $CD_2Cl_2$): δ 8.18 (br s, 2H), 8.02 (m,

6H), 6.70 (m, 2H), 6.09 (m, 2H), 5.94 (m, 2H), 5.90 (m, 2H), 5.87 (m, 10H), 5.82 (s, 2H), 5.75 (br s, 5H). HR(ESI)-MS (M-H) (M = $C_{81}H_{33}F_{35}N_8$): Calcd 1781.2186, obsd 1781.2135.

**Procedure for the DDQ oxidation of purified oligomer 6:**

In a 40 mL scintillation vial with stirbar, a solution of oligomer **6** (364 mg, 0.45 mmol) in 25 mL dichloromethane was treated by the dropwise addition over 10 minutes of a solution of 2,3-dichloro-5,6- dicyano-1,4-benzoquinone (341.5 mg, 1.50 mmol, 3.3 equiv.) in 1.5 mL tetrahydrofuran at 15 °C. The reaction was allowed to proceed with stirring at 15 °C for 20 minutes. After filtration of the cold reaction mixture through Celite®, the filtrated was concentrated to dryness. The residue was immediately taken up in 1:3 dichloromethane-hexane and purified by column chromatography on silica using 1:3 dichloromethane-hexanes as eluent. The corrole **1** was obtained as a dark purple powder (305 mg, 84% yield).

**Preparation of Tris(pentafluorophenyl)corrole (1):**

To an open 500 mL round-bottomed flask equipped with a stir bar was added pentafluorobenzaldehyde (20.0 g, 0.102 mole), dichloromethane (15 mL) followed by freshly distilled pyrrole (20 mL, 19.3 g,

0.29 mole, 2.8 equiv.). The mixture was placed in an ice-water mixture with stirring and when the internal temperature reached 15 °C, 1.0 mL of a 5% by volume trifluoroacetic acid solution (0.075 g of TFA, 0.65 mmol) in dichloromethane was added in one portion with rapid stirring. After 3 minutes, the solution temperature had risen to 40 °C while stirring in the ice-water bath was continued. (It was found that allowing the temperature to rise in this manner ensured that the reaction mixture remained homogeneous and this procedure produced the most favorable distribution of the oligomers **4-10**.) Once the temperature subsided to 30 °C, an additional 2.0 mL of trifluoroacetic acid solution (0.15 g of TFA, 1.3 mmol) was added and the reaction was removed from the bath and allowed to proceed at room temperature for 30 minutes. The reaction mixture was filtered through anhydrous magnesium sulfate and concentrated to a viscous liquid by rotary

evaporation using a vacuum pump at 0.5 torr and 50 °C. Complete removal of excess pyrrole was achieved by dissolving in 50 mL dichloromethane and rotary evaporation a second time. Analysis of the oligomeric mixture by LC-TOF confirmed the presence of oligomers **4-10** in relative contributions shown in Figure 1. Integration of the UV signal (254 nm) of the HPLC chromatogram revealed that the desired peak corresponding to oligomer **6** represented 25.7% of the total integration for the oligomers **4-10**. (Using the measured relative molar response factors at 254 nM of 1.0, 2.2, 3.5, 5.1, 6.7, 8.4 for the purified compounds **4-9**, respectively, we estimated that the mole fraction of the desired oligomer **6** in this mixture was approximately 26% in reasonable agreement with the isolated yield of **6** obtained in the preparative HPLC procedure above.) The mixture of oligomers **4-10** was subject to discoloration by air oxidation and was therefore used without delay.

The crude mixture of **4-10** was dissolved in dichloromethane (4000 mL), transferred to a 5L round bottomed flask with stirbar and cooled to 5 °C using an ice-water mixture. A solution of 2,3-dichloro- 5,6-dicyano-1,4-benzoquinone (22.7 g, 0.100 mole, 1.00 equiv. based on starting aldehyde) in tetrahydrofuran (200 mL) was added dropwise with stirring over 40 minutes while the reaction mixture was maintained at 5 °C. After completion of the addition (the complete consumption of **6** and the generation of **1** in the reaction mixture could be monitored by LCMS), the reaction mixture was stirred at room temperature for 6 hours. The resulting product mixture was then concentrated to a volume of 400 mL, diluted with 400 mL hexane and filtered to remove the hydroquinone byproduct. After rotary evaporation, the material was dissolved in dichloromethane (100 mL) with heating until dissolved and flash silica gel (120 g) was added followed by hexane (300 mL). The warm mixture was loaded without delay onto a column of 1200g flash (40-60 uM) silica gel prepared with 1:3 dichloromethane-hexanes. Upon elution of the column with 1:3 dichloromethane-hexane as eluant, the strongly colored corrole containing fraction was concentrated. [It was desirable to efficiently separate the less polar orange contaminant (described and characterized by Gross[3]) during this chromatography procedure in order to ensure the successful purification of **1** by recrystallization.] The

crude corrole **1** was dissolved in dichloromethane (120 mL) with heating and hexane was added (180 mL). The mixture was heated to evaporate about half of the dichloromethane from the mixture inducing the crystallization of a significant portion of the product. After cooling the mixture to 0 °C, the first crop of **1** was collected by filtration and washing with cold hexane (3.75 g, 13.9% yield). The filtrate was combined with mixed fractions from the first column chromatography and repurified by column chromatography to afford, after recrystallization, an additional crop of **1** (0.83 g, 3.1% yield). The combined yield of tris(pentafluorophenyl)corrole (**1**) was 4.58 g, (17.0% yield). $^{1}$H NMR (600 MHz, $CD_2Cl_2$): δ 9.17 (d, 2H, *J* = 3.5 Hz), 8.83 (d, 2H, *J* = 3.5 Hz), 8.61-8.66 (m, 4H). HR(ESI)-MS (M+H) (M = $C_{37}H_{11}F_{15}N_4$): Calcd 797.0817, obsd 797.0825.

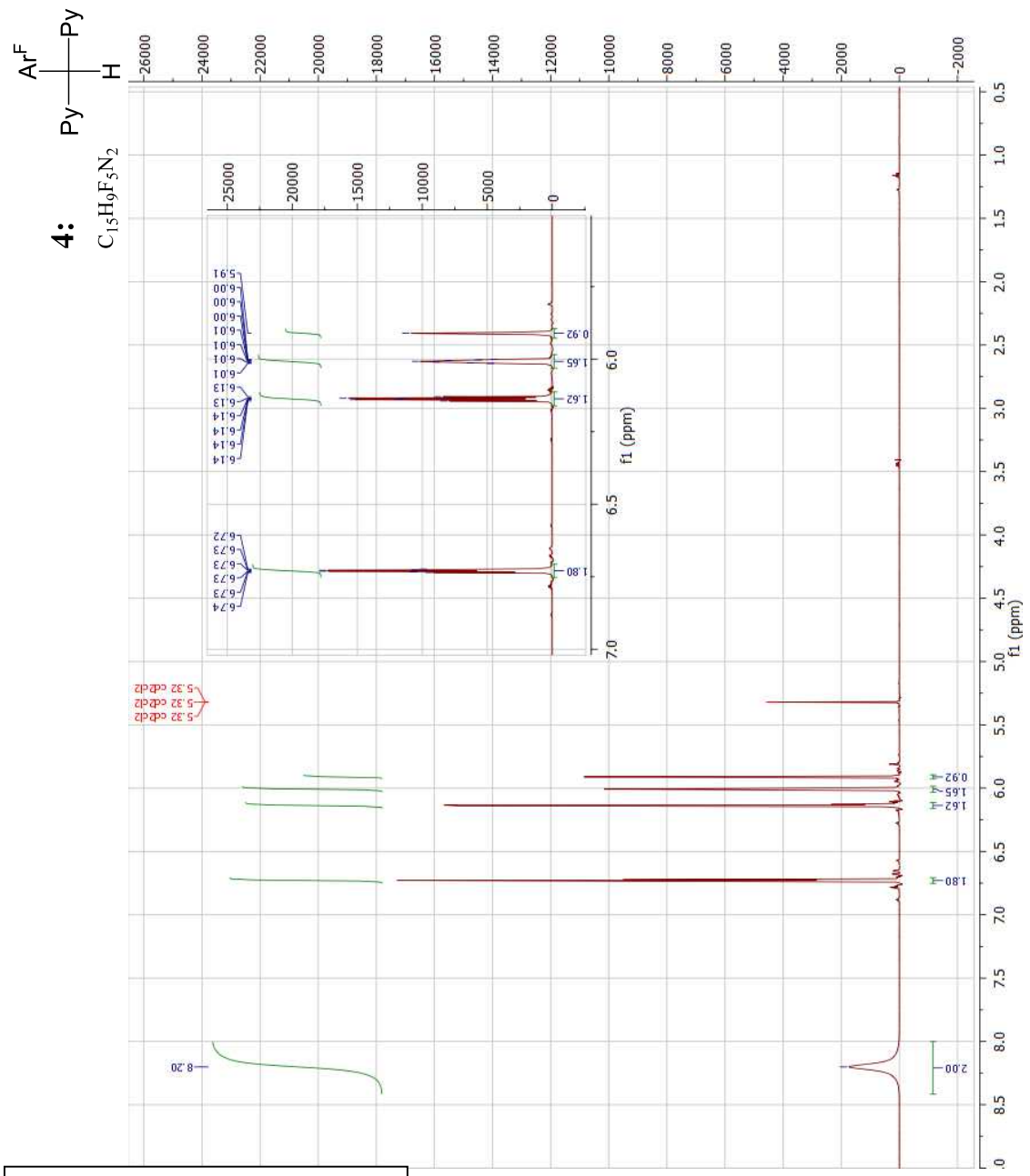


$^1$H NMR of **4** in $CD_2Cl_2$

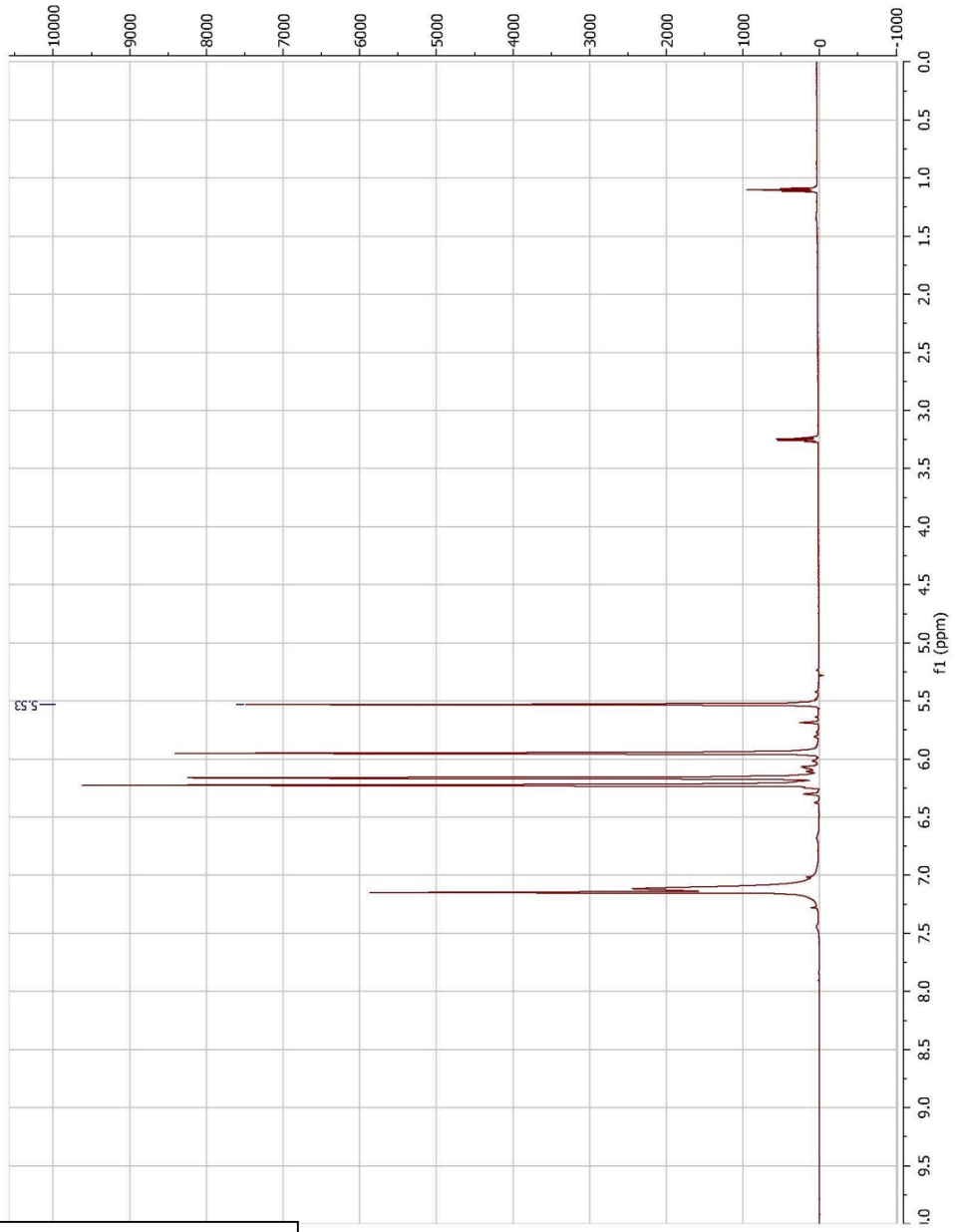


$^{1}$H NMR of **4** in $C_6D_6$

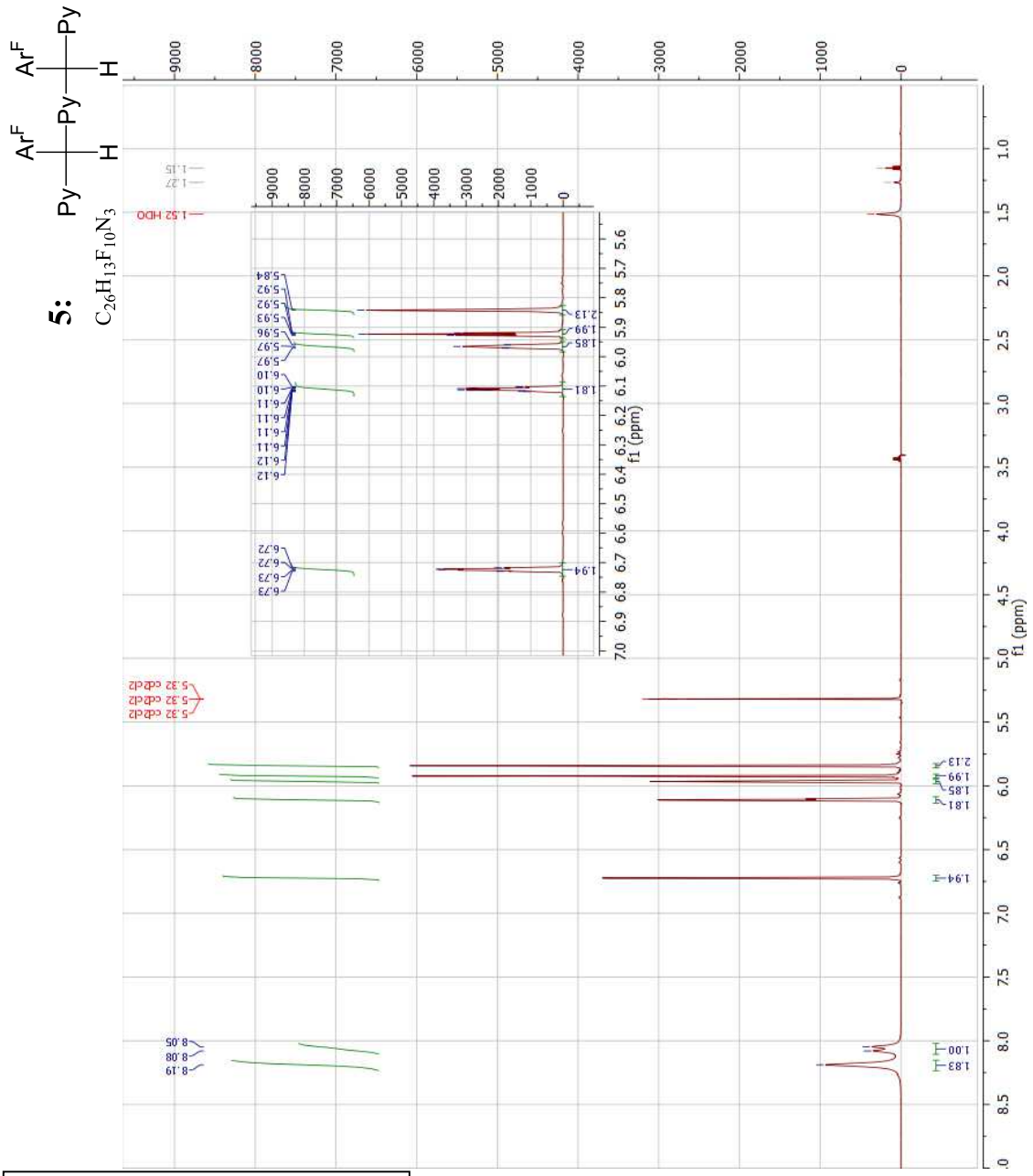


$^1$H NMR of **5** in $CD_2Cl_2$

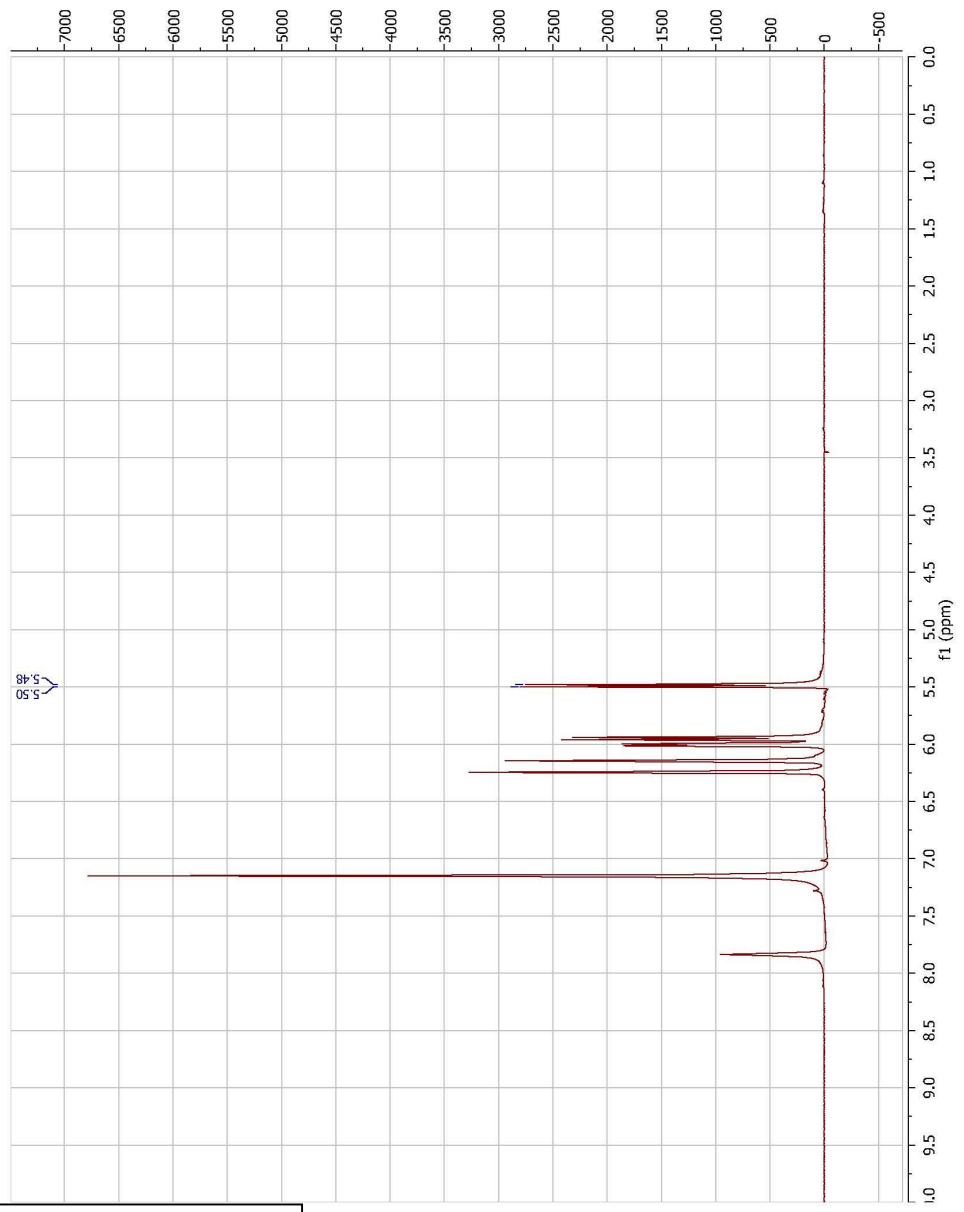


$^{1}$H NMR of **5** in $C_6D_6$

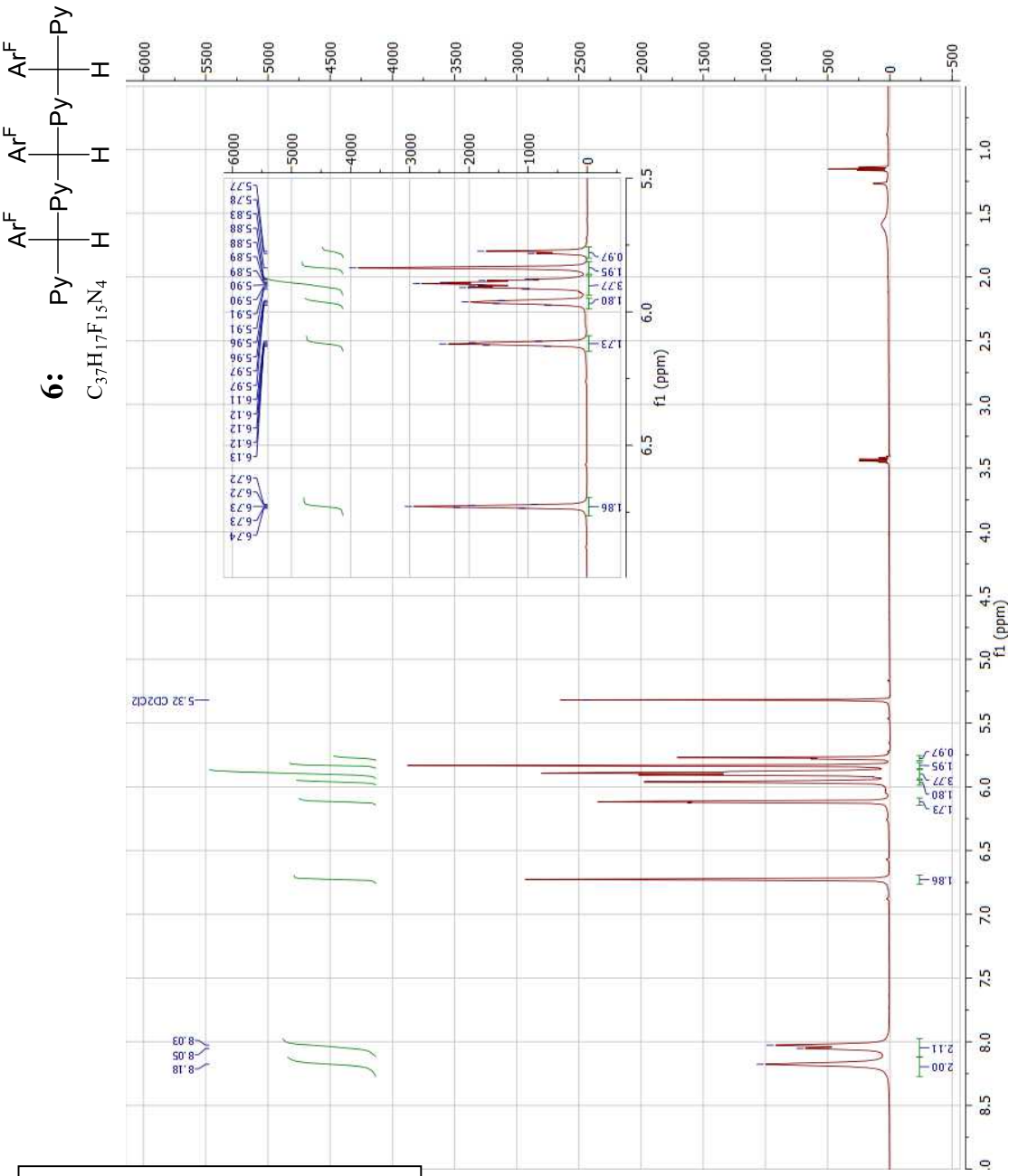


$^1$H NMR of **6** in $CD_2Cl_2$

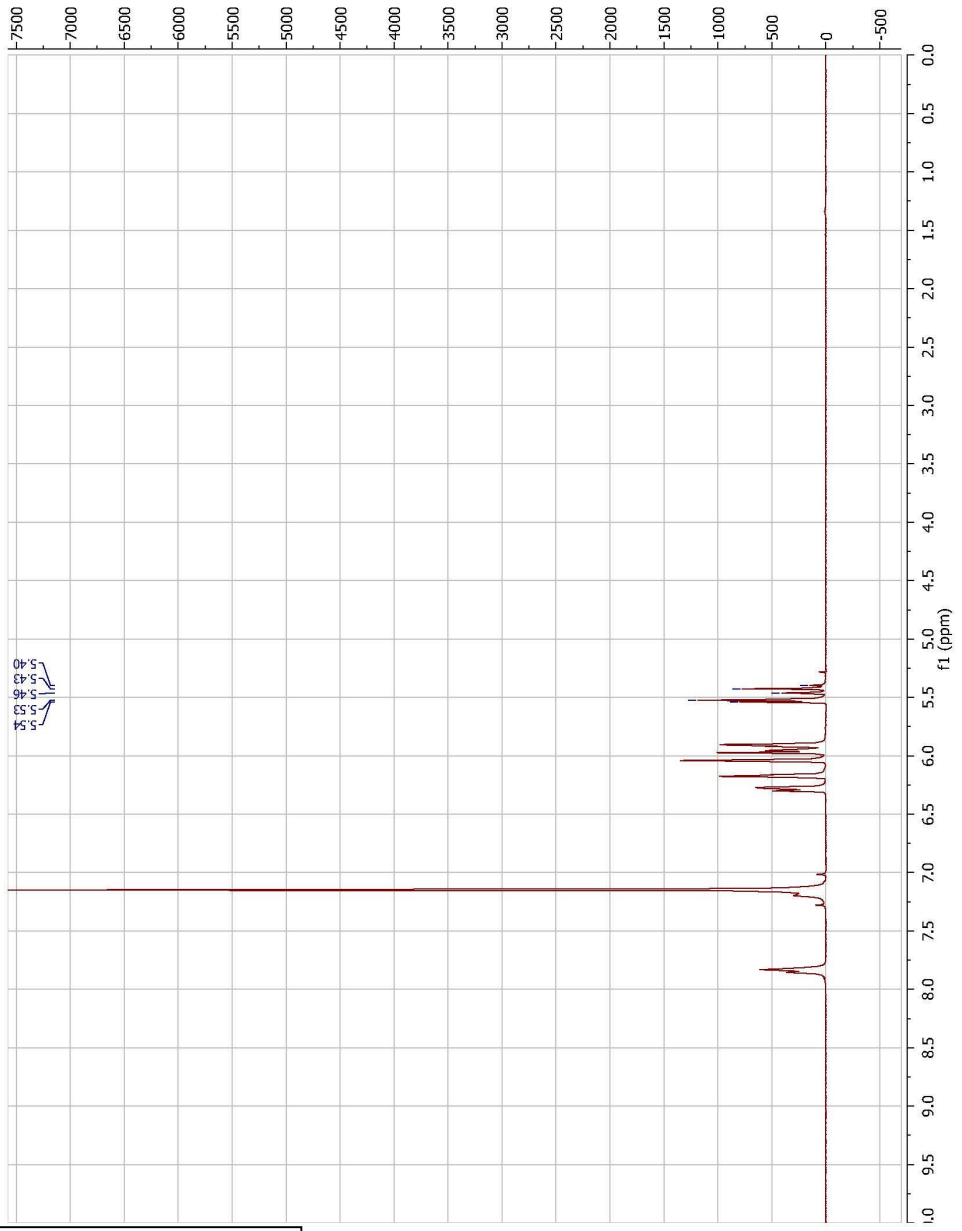


$^1$H NMR of **6** in $C_6D_6$

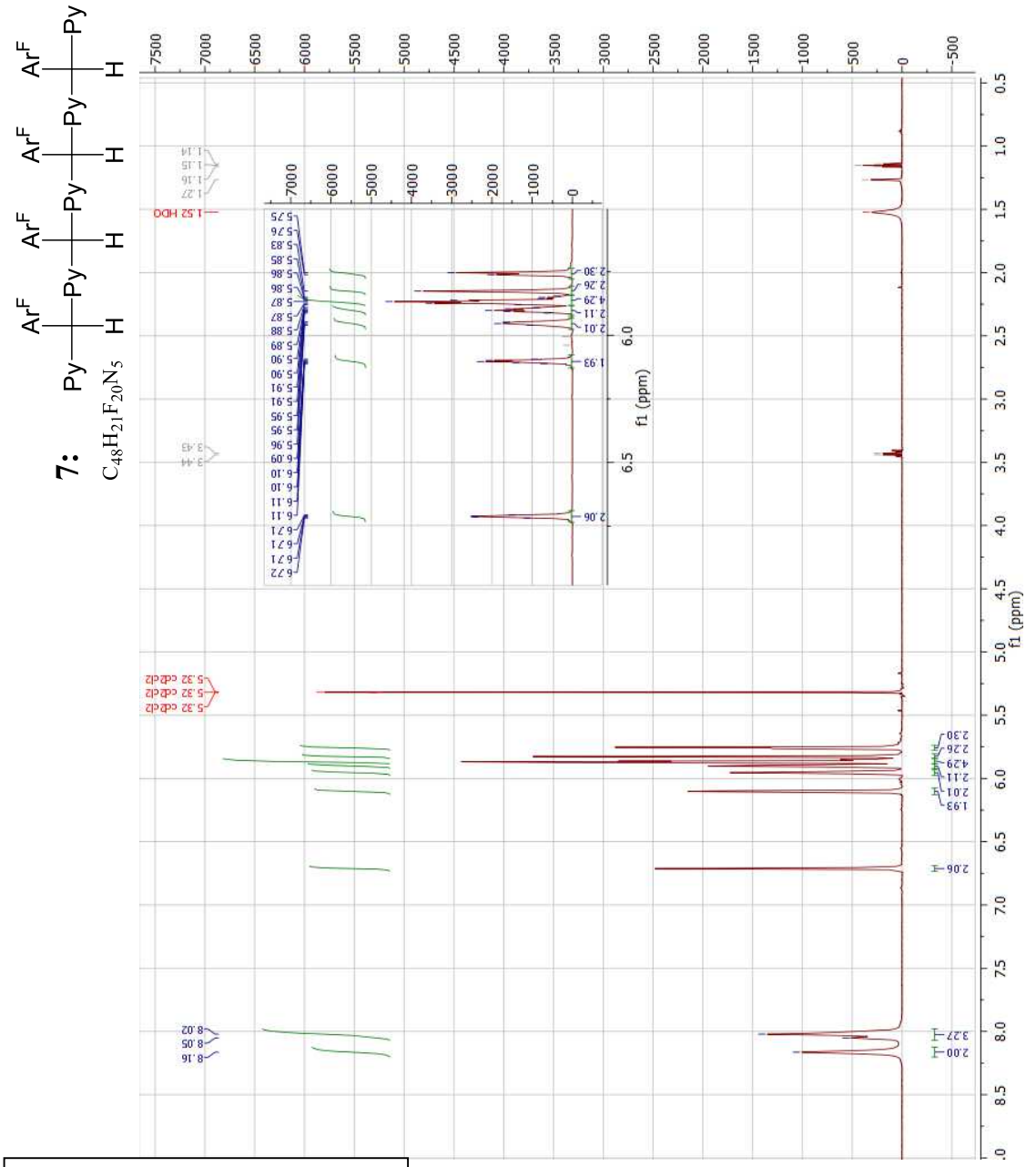


$^1$H NMR of **7** in $CD_2Cl_2$

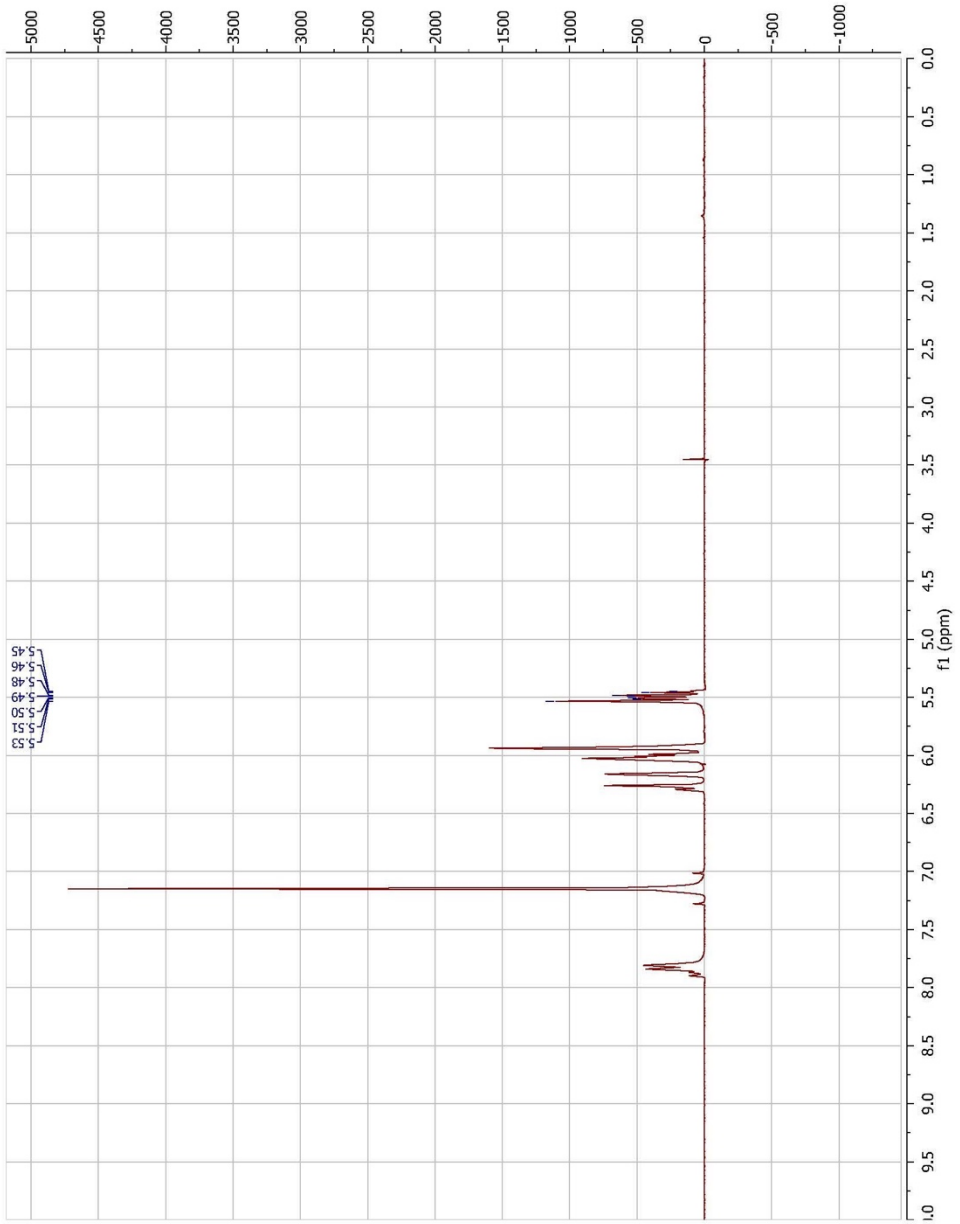


$^1$H NMR of **7** in $C_6D_6$

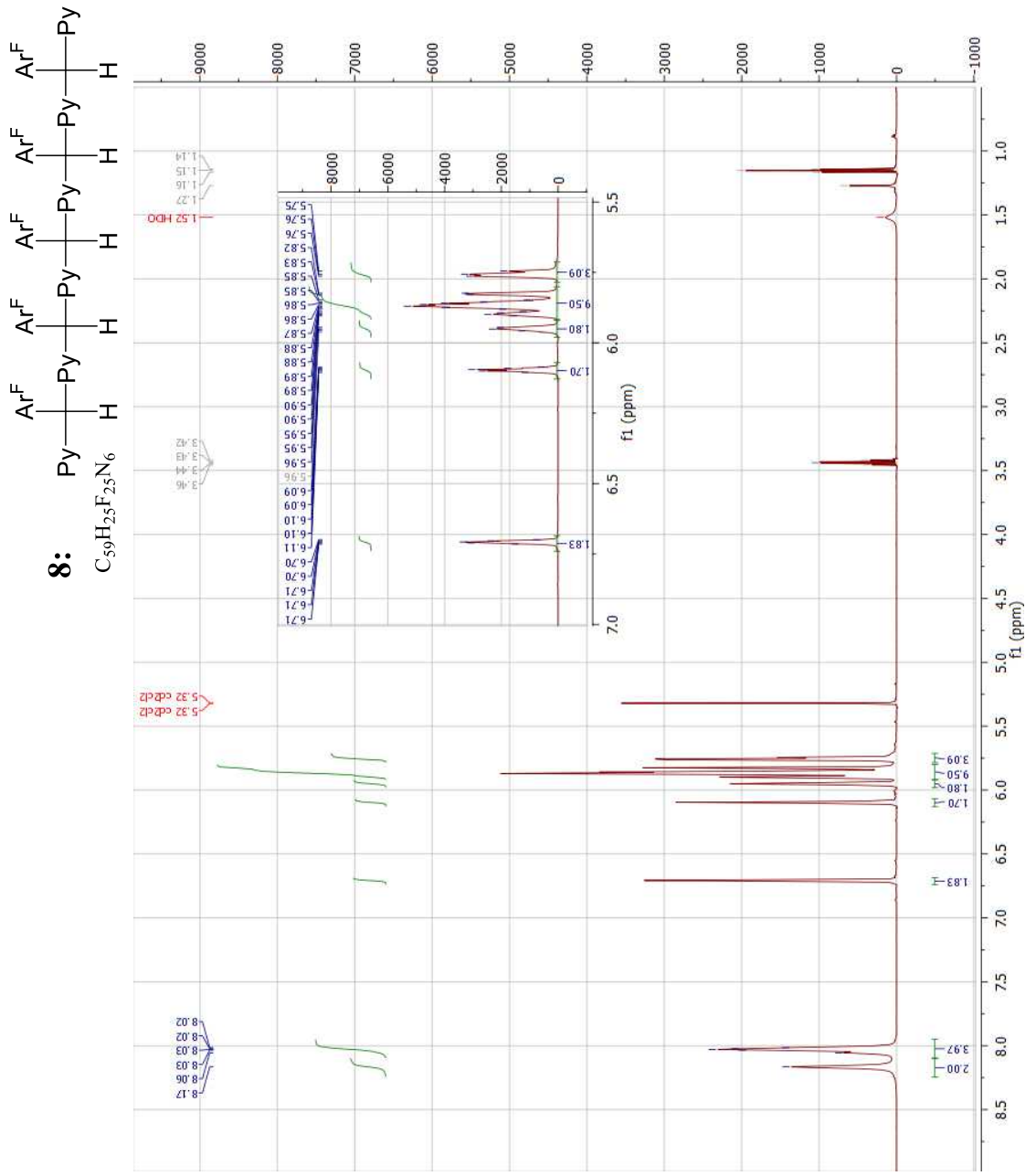


$^1$H NMR of **8** in $CD_2Cl_2$

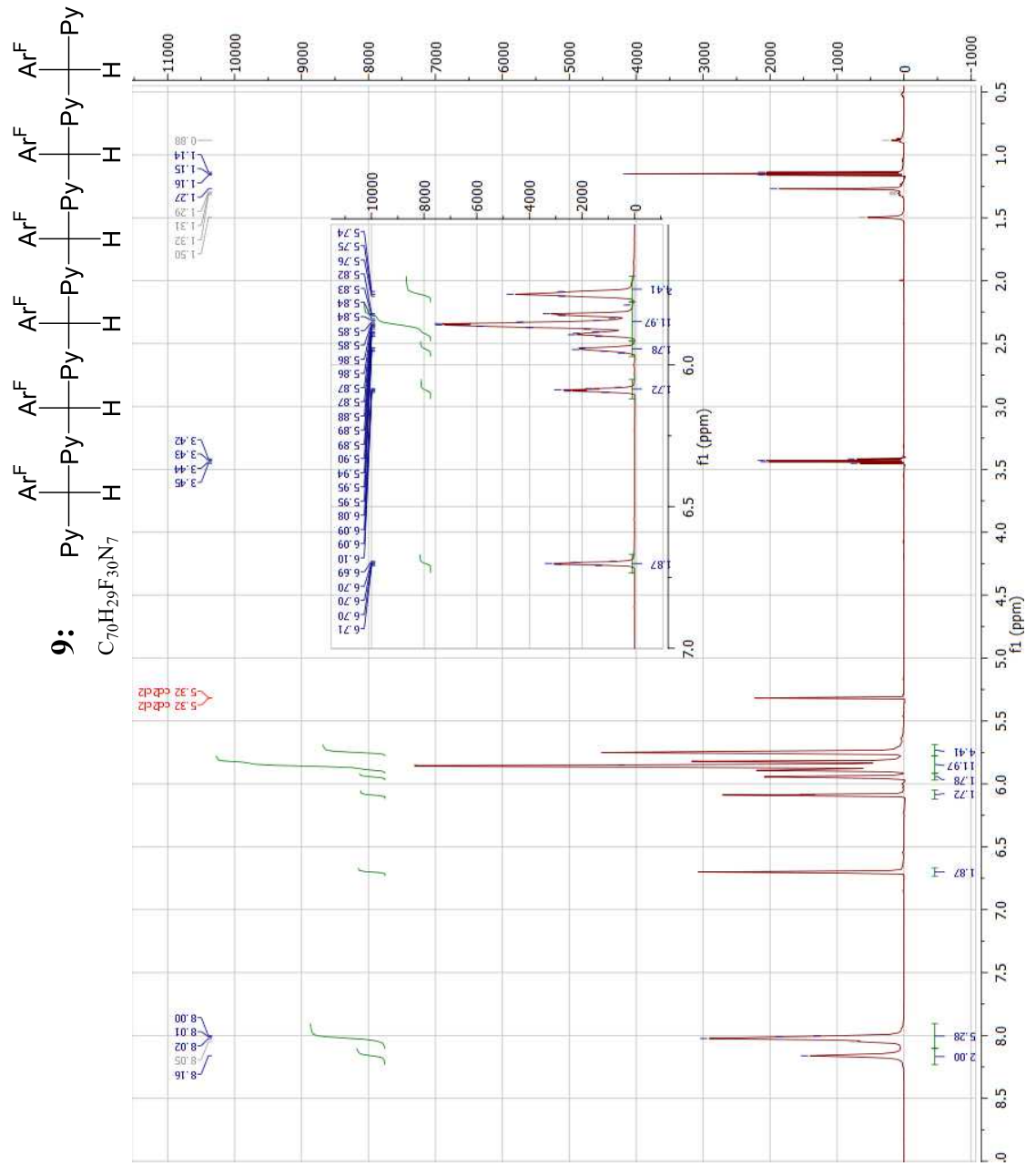


$^1$H NMR of **9** in $CD_2Cl_2$

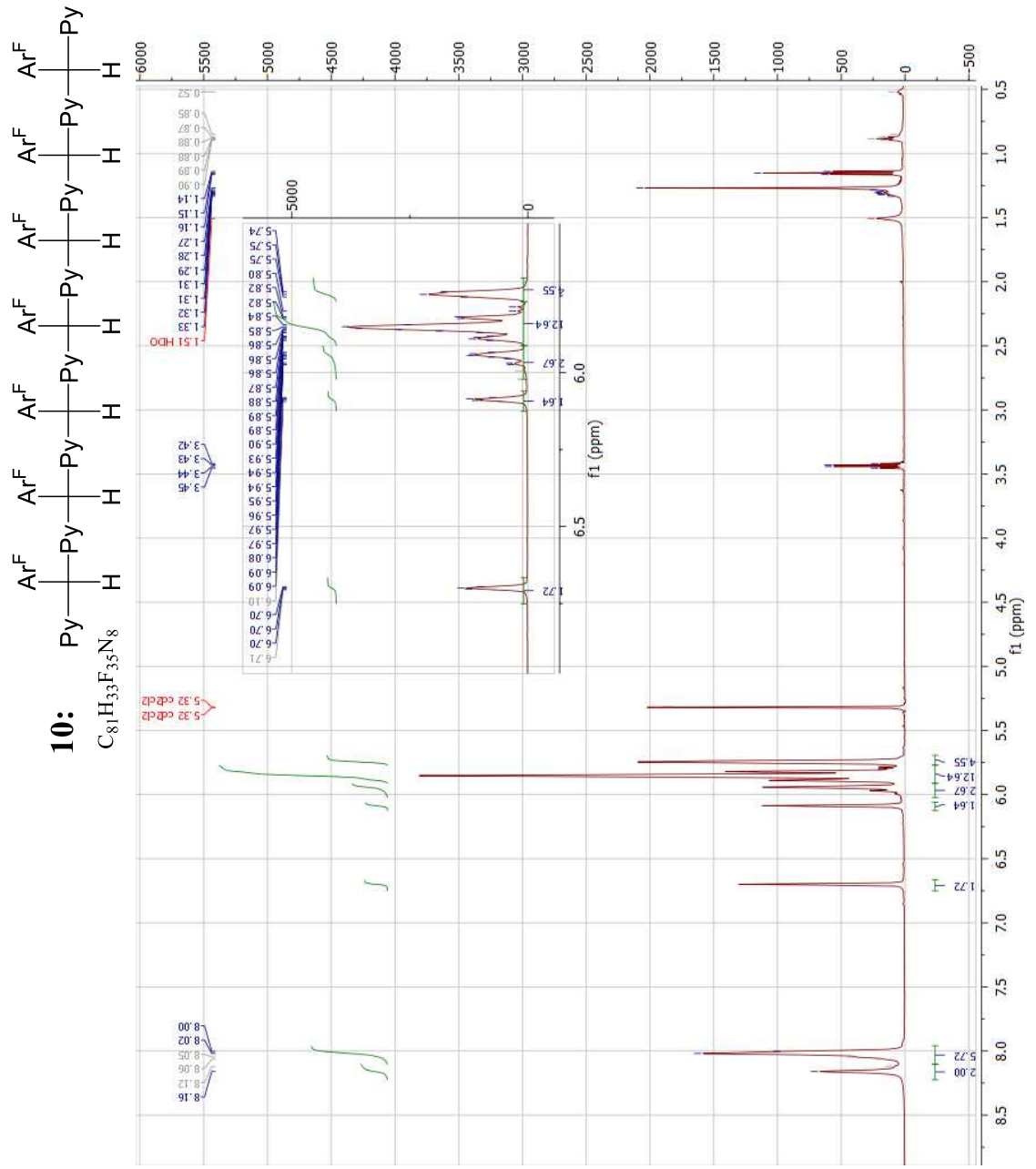


$^1$H NMR of **10** in $CD_2Cl_2$

**X-Ray Structure Determination**

Diffraction data ($\omega$-and $\phi$-scans) were collected on a Bruker AXS KAPPA APEX II diffractometer using an APEX II CCD detector with Triumph graphite monochromated Mo $K_\alpha$ fine-focus sealed tube radiation ($\lambda$ = 0.71073 Å) equipped with an Oxford 700 Cryostream low-temperature cooler set to 100 K. The structure was solved by direct methods using SHELXT[i] and refined against $F^2$ on all data by full-matrix least squares with SHELXL[1] using OLEX2[2].

Compound A14375 crystallizes in the monoclinic space group $P2_1/c$ (#14) as large (several mm in length) purplish-red crystals with a metallic luster. The asymmetric unit consists of one corrole and two acetone solvent molecules. Except for the minor orientation of one disordered perfluorophenyl group, all non-hydrogen atoms were refined anisotropically. The central pentafluorophenyl group is disordered 92:08 by an ~4° tilt parallel to the plane of the phenyl ring. The minor component was refined isotropically and restrained to have the same geometry as the major component. One of the two acetones is disordered 80:20 over two positions. There may be some small disorder in the other as well. All hydrogen atoms on the corrole were located in difference maps and freely refined. The methyl groups on the solvent acetone molecules were refined as rotating groups with $U_{iso}$ values 1.5 times the $U_{eq}$ of the bonded atom. There is a hydrogen bond from a pyrrole nitrogen to one acetone oxygen. The out of pyrrole plane distances for the hydrogens H1, H2, and H4 are 0.37, 0.09, and 0.10Å respectively. The angles between the pyrrole planes (N1-N2, N2-N3, N3-N4, N4-N1 respectively) are 157.0, 167.2, 6.6, and 25.5°. The overall conformation of the corrole is similar to that in a structure of an *m*-xylene solvate reported by Gross[3] in which the hydrogen parameters were not refined.

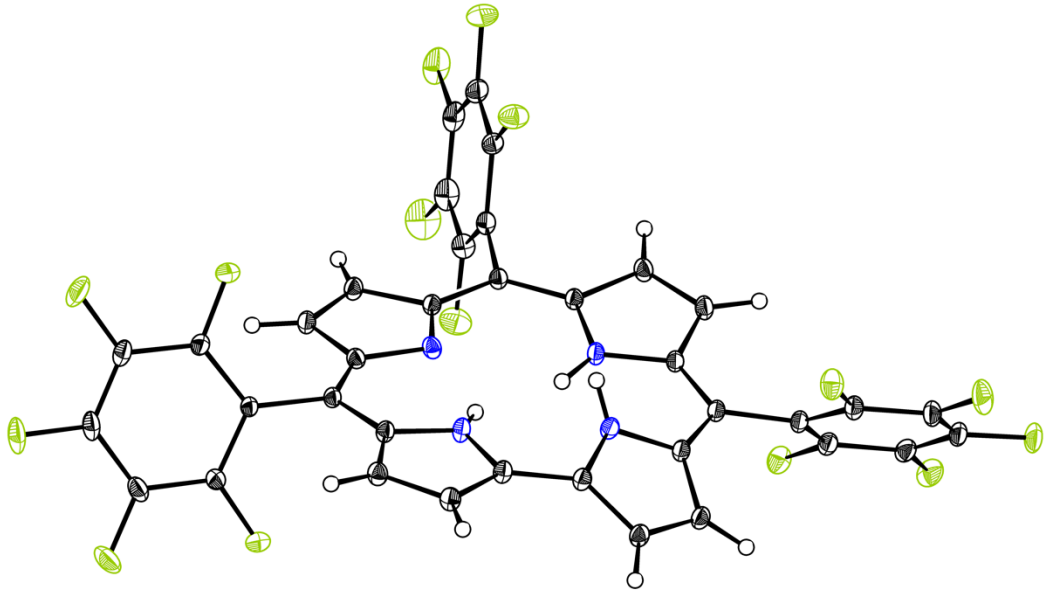

**References:**

(1) Sheldrick, G. M. (2008). *Acta Cryst.* **A64**, 112-122.

(2) Dolomanov, O.V.; Bourhis, L.J.; Gildea, R.J.; Howard, J.A.K.; Puschmann, H. (2009). *J. Appl. Cryst.* **42**, 339-341.

(3) Gross, Z.; Galili, N.; Simkhovich, L.; Saltsman, I.;Botoshansky, M.; Blaser, D.; Boese, R.; Goldberg, I. (1999). *Org. Lett.* **1**, 599-602.

*Chapter 2*

# DECORATING METAL OXIDE SURFACES WITH FLUORESCENT CHLOROSULFONATED CORROLES

The work presented in this chapter was the first corrole work I published. When I first arrived at Caltech, I sought to scale the synthesis of a carboxylated corrole for tumor diagnostic purposes. Naturally, this project went horribly and the reproduction of literature seemed impossible. Luckily, I was introduced to Karn Sorasaenee, a wonderful researcher at Children's Hospital Los Angeles, and former Gray group postdoctoral fellow. He suggested that instead we investigate nanoparticle imaging systems based on corrole chemistry.

We were inspired by some work in Jeremy Weaver's (a former Gray group member) thesis, in which he utilized sulfonic acid functionalized corroles for dye sensitized solar cells. These materials were efficient, however, the dye molecules tended to leach from the surface into the electrolyte solution. To access covalently coupled materials we carried out a dreaded chlorosulfonation reaction but left the chlorosulfonyl group intact. The notion behind coupling the dyes to the surface was inspired by the use of chlorosulfonation in organic chemistry. The sulfonyl chloride synthetic handle reacts readily with nucleophiles including hydroxyl groups. We went on to react the hydroxyl-bearing surface of titanium dioxide with the chlorosulfonyl group on the corrole ring, to produce a stable, covalent bond in the form of a sulfonic ester.

Having achieved success with the freebase molecule, we investigated two routes to metallated species. We concluded that it was necessary to carefully install metals following chlorosulfonation. The metallated complexes tended to decompose under chlorosulfonation conditions. This was somewhat expected as the chlorosulfonation required the use of neat chlorosulfonic acid.

In preparing these materials we imaged them using confocal fluorescence microscopy. The aluminum corrole nanoconjugate was by far the brightest material. This helped us elect the

imaging candidate described in the following chapter. This work really began my interest in surface functionalization…it's been a good run so far!

# DECORATING METAL OXIDE SURFACES WITH FLUORESCENT CHLOROSULFONATED CORROLES



**Abstract:**

We have prepared 2,17-bis(chlorosulfonyl)-5,10,15-tris(pentafluorophenyl)corrole (**1**), 2,17-bis(chlorosulfonyl)-5,10,15-tris(pentafluorophenyl)-corrolatoaluminum(III) (**1-Al**), and 2,17-bis(chlorosulfonyl)-5,10,15-tris(pentafluorophenyl)-corrolatogallium(III) (**1-Ga**). The metal complexes **1-Al** and **1-Ga** were isolated and characterized by electronic absorption and NMR spectroscopies, as well as by mass spectrometry. Relative emission quantum yields for **1**, **1-Al**, and **1-Ga**, determined in toluene, are 0.094, 0.127, and 0.099, respectively. Reactions between **1**, **1-Al**, and **1-Ga** and $TiO_2$ nanoparticles (NPs) result in corrole—$TiO_2$ NP conjugates. The functionalized NP surfaces were investigated by solid-state Fourier transform infrared and X-ray photoelectron spectroscopies and by confocal fluorescence imaging. The fluorescence images for **1-Al**—$TiO_2$ and **1-Ga**—$TiO_2$ suggest a promising application of these NP conjugates as contrast agents for noninvasive optical imaging.

In recent years, molecular imaging has attracted much attention in the medical field for both the diagnosis of and intervention against disease.[1] Although a myriad of imaging modalities have enormously contributed to biomedical research,[2] probe development is still a very high priority.[3] Historically, small-molecule and biomolecule contrast agents have been prepared and studied in the context of their corresponding imaging modalities.[4] More recently, nanomaterial probes, such as quantum dots and iron oxide nanoparticles (NPs), have been developed and employed in molecular imaging.[5] Studies of and interests in these nanomaterials as contrast agents also suggest the possibility of extensive probe development in biomedical imaging. In this study, we focus on the use of versatile fluorescent small

molecules, namely, corroles, as potential contrast agents in optical imaging. Corroles are facilely modified using multiple approaches including both aromatic and asymmetric substitution at the *meso*-aryl position as well as modification at the β-pyrrolic positions, making these tetrapyrrolic macrocycles strong candidates for readily tunable imaging systems.[6]

Recently, there has been much effort in developing these macrocycles as optical dyes because of their unique fluorescence properties.[7] Previous imaging studies employing corroles have only been pursued with noncovalent assemblies between the macrocycle and proteins.[8] For the first time, we report the use of corroles as synthons for optical imaging agents with applications involving covalently bound NPs. The preparation of the parent free-base macrocycle 2,17-bis(chlorosulfonyl)-5,10,15-tris(pentafluorophenyl)corrole (**1**) has been reported;[9] however, before our work, the metalated species had not been prepared. Here we report the preparation and characterization of **1**, 2,17-bis(chlorosulfonyl)-5,10,15-tris(pentafluorophenyl)-corrolatoaluminum(III) (**1-Al**), and 2,17-bis(chlorosulfonyl)-5,10,15-tris(pentafluorophenyl)corrolatogallium(III) (**1-Ga**). In addition, spectroscopic and photophysical studies, which serve as a fundamental platform for further development of these bis-chlorosulfonated corroles as building blocks for optical contrast agents, will be addressed. We will also discuss surface modification reactions by which **1**, **1-Al**, and **1-Ga** can be covalently coupled to $TiO_2$ NP surfaces as well as surface characterization of the $TiO_2$—corrole nanoconjugates.

Corrole **1** has been prepared according to the literature.[9] Metal-insertion reactions of **1** with $AlMe_3$ in a toluene/pyridine mixture at 0 ˚C and $GaCl_3$ in pyridine at reflux afford the products **1-Al** (26% yield) and **1-Ga** (39% yield), respectively (Scheme 1). Both **1-Al** and **1-Ga** were isolated by solvent extraction and obtained as green solids after evaporation to dryness. The metalated products were further purified by acetone/methylene chloride assisted filtration followed by the removal of solvents in vacuo.

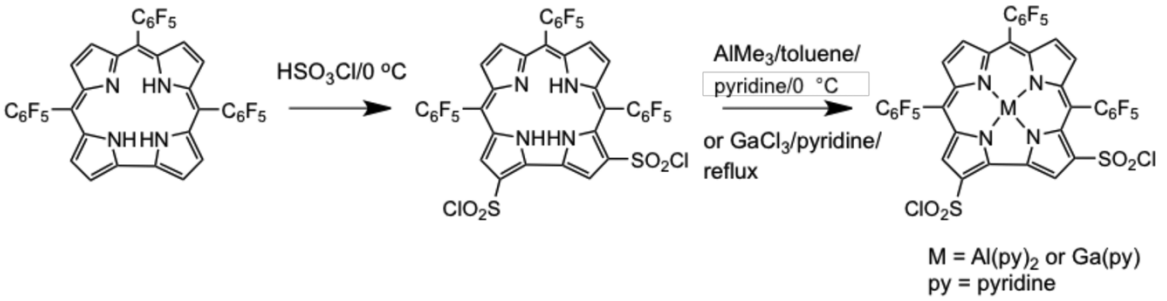


Scheme 5. Preparation of Metalated **1**

Electronic absorption spectra for **1**, **1-Al**, and **1-Ga** obtained in degassed toluene solutions reveal the signature Soret and Q bands for these tetrapyrrolic macrocycles (Figure 1). The electronic absorption data for the chlorosulfonated corroles are also given in Table 1. Compared to the parent compound **1**, each of the metalated chlorosulfonated corroles **1-Al** and **1-Ga** exhibits a sharper Soret band with a vibronic shoulder to the left (characteristic of the metalated species) that is blue-shifted at 424 and 426 nm, respectively, as shown in Figure 1. The Q bands for both **1-Al** and **1-Ga** are also narrower and are observed at 592 and 588 nm, respectively. This could be further explained by the presence of a single absorbing species for the metalated corroles, while the nonmetalated corrole could exhibit two tautomeric forms.[10g,h]

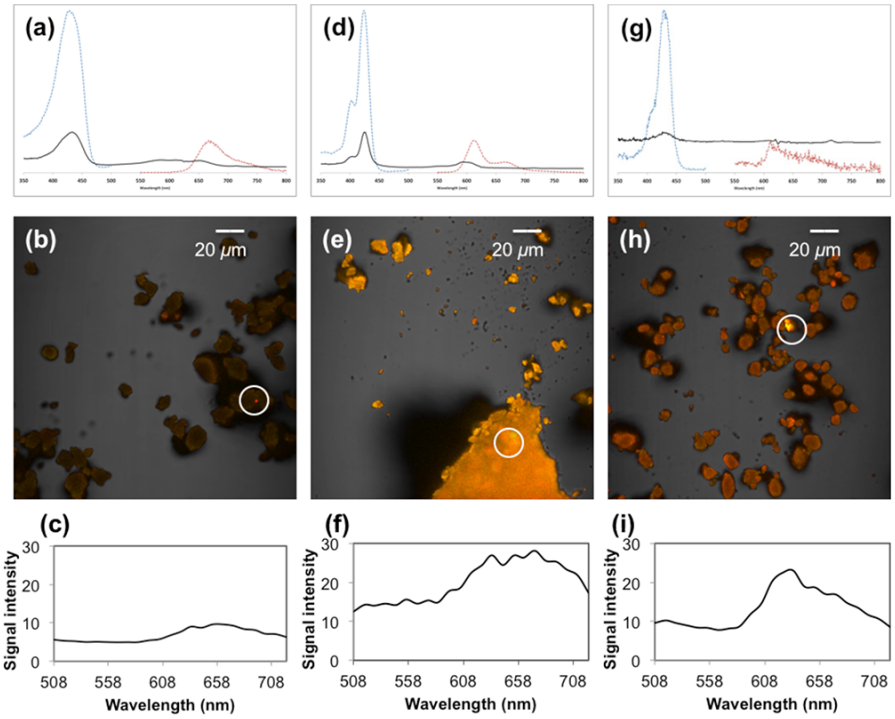


Figure 4. First row: Absorption (black), excitation (blue), and emission (red) spectra for 1 (a), 1-Al (d), and 1-Ga (g). Second row: Superimposed confocal fluorescence pseudocolor and bright-field images for 1−TiO2 (b), 1-Al−TiO2 (e), and 1-Ga−TiO2 (h). Third row: Fluorescence profiles of 1−TiO2 (c), 1-Al−TiO2 (f), and 1-Ga−TiO2 (i) aggregates with $\lambda_{ex}$ = 405 nm. The white circles represent the selected areas from which the corresponding spectral profiles were derived.

| | electronic absorption[a] | fluorescence[a] | | |
|---|---|---|---|---|
| corrole | $\lambda_{max}$[b] (nm) | $\lambda_{ex}$ (nm) | $\lambda_{em}$ (nm) | $\phi_{em}$[c] |
| 1 | 430 (S), 580 (Q) | 426 | 670 | 0.094 |
| 1-Al | 424 (S), 592 (Q) | 420 | 611 | 0.127 |
| 1-Ga | 426 (S), 588 (Q) | 427 | 609 | 0.099 |

[a]The measurements were performed in degassed toluene. [b]The maximum absorption wavelengths are reported for both Soret (S) and Q bands. [c]The relative emission quantum yields were determined using tetraphenylporphyrin as the standard.

Table 1. Electronic Spectroscopic Data for Chlorosulfonated Corroles **1**, **1-Al**, and **1-Ga in Toluene Solutions**

Similar to the other pentafluorophenyl corroles, **1**, **1-Al**, and **1-Ga** exhibit bright fluorescence, particularly **1-Al**, with a large Stokes shift.[10] Excitation into the Soret or Q bands results in an emission spectral profile similar to that with $\lambda_{em}$ observed around 600—

670 nm (Figure 1) accompanied by a vibronic band to the red of the major emission peak for the three corroles. The excitation and emission wavelengths observed are set out in Table 1. We note that chlorosulfonated metallocorroles **1-Al** and **1-Ga** follow the expected trend for fluorescence in which $\lambda_{em}$ (611 nm) for the slightly more electropositive **1-Al** is more red-shifted compared to $\lambda_{em}$ (609 nm) for **1-Ga** because of a destabilized highest occupied molecular orbital.[11] The quantum yield measurements, relative to tetraphenylporphyrin,[12] with $\lambda_{ex}$ = 355 nm for **1**, **1-Al**, and **1-Ga** reveal $\phi_{em}$ = 0.094, 0.127, and 0.099, respectively. As expected, the aluminum chlorosulfonated corrole exhibits the highest relative quantum yield, consistent with the previously reported relative quantum yield for the nonsulfonated aluminum(III) corrole.[10b,c] The $\phi_{em}$ trend for all three chlorosulfonated corroles is comparable to that reported elsewhere for nonsulfonated comounds.[10a-c]

On the basis of modification of the chlorosulfonyl group with alcohols producing sulfonic esters (13), we report the covalent modification of a chlorosulfonyl group with a new hydroxyl platform, namely, $TiO_2$ NPs with hydroxylated surfaces, as an example of the versatility of chlorosulfonated corroles and their potential uses in optical imaging applications. Corrole coupling to $TiO_2$ NPs was performed following enhanced hydroxylation of the surface using $H_2O_2$. The NPs bearing the hydroxylated surfaces were mixed with pyridine solutions of corrole and heated to reflux. After repeated washing with copious amounts of $CH_2Cl_2$, acetone, and water and drying under high vacuum, green powders were obtained. The electronic absorption spectra of the colloidal suspensions of **1**—$TiO_2$, **1-Al**—$TiO_2$, and **1-Ga**—$TiO_2$ nanoconjugates in phosphate-buffered saline (pH 7.4) reveal maximum absorptions centered around 425 and 600 nm for the Soret and Q bands, respectively (Table 2). These peak maxima are in agreement with the spectroscopic properties of the corresponding cororle (Table 1). We also note that the Soret band splitting for **1**—$TiO_2$ is similar to the splitting observed for its amphiphilic molecular counterpart 2,17-disulfonato-5,10,15-tris-(pentafluorophenyl) corrole in an aqueous solution at physiological pH, supporting the presence of the sulfonate linkage on the corrole anchored to $TiO_2$ surfaces. The splitting pattern, however, is not observed for the metalloconjugates

**1-Al**—$TiO_2$ and **1-Ga**—$TiO_2$, due to the presence of metal bound to deprotonated nitrogen atoms.[10b-d,h]

| | electronic absorption | $SO_2$ vibrational frequency ($cm^{-1}$) | | |
|---|---|---|---|---|
| conjugate | $\lambda_{max}$ (nm) | sym | asym | F(1s) binding energy (eV) |
| **1**–$TiO_2$ | 415, 430 (S), 591, 621 (Q) | 1153 | 1410 | 691 |
| **1-Al**–$TiO_2$ | 427 (S), 576, 610 (Q) | 1244 | 1431 | 690 |
| **1-Ga**–$TiO_2$ | 423 (S), 589, 610 (Q) | 1160 | 1450 | 688 |

Table 2. Electronic Absorption, Vibrational, and X-ray Photoelectron Spectroscopic Data for Corrole–$TiO_2$ Nanoconjugates **1**–$TiO_2$, **1-Al**–$TiO_2$, and **1-Ga**–$TiO_2$

Characterization of the fine green powder of **1**—$TiO_2$, **1-Al**—$TiO_2$, and **1-Ga**—$TiO_2$ with Fourier transform infrared spectroscopy reveals vibrational absorption bands around 1150—1250 $cm^{-1}$ assigned to the symmetric stretching of $SO_2$ groups as well as those around 1400—1450 $cm^{-1}$ assigned to asymmetric starching of $SO_2$ groups of covalent sulfonates.[14] The presence of these vibrational signatures suggests that the corroles are covalently attached to the surface of $TiO_2$ through a sulfonate linkage. The vibrational frequencies for these $TiO_2$—corrole nanoconjugates are listed in Table 2. X-ray photoelectron spectroscopy was performed to study the elemental presence of the surface of the NP conjugates (Table 2). High-resolution scans for the spectra of the conjugates revealed F(1s) binding energy peaks between and 691 eV,[15] suggesting the presence of corresponding (pentafluorophenyl)corroles attached to the $TiO_2$ surface.

Confocal fluorescence microscopy images of aggregates of the nanoconjugates **1**—$TiO_2$, **1-Al**—$TiO_2$, and **1-Ga**—$TiO_2$ in the solid state (Figure 1) were taken with the samples illuminated at $\lambda_{ex}$ = 405 nm and $\lambda_{em}$ recorded from 508 to 722 nm. The images for **1-Al**—$TiO_2$ and **1-Ga**—$TiO_2$ (Figure 1e,h) exhibit fluorescence areas on the NPs compared to the relatively darker image for **1**—$TiO_2$. The fluorescence signals observed with various intensities across the $TiO_2$ samples for **1-Al**—$TiO_2$ and **1-Ga**—$TiO_2$ also suggest that the

$TiO_2$ surfaces are not evenly functionalized because of material aggregation. More detailed studies of the quenching of the fluorescence of **1**—$TiO_2$ are underway in our laboratories. Upon closer inspection, however, of selected fluorescence areas (white circles) on all three images, spectral profiles representing the nanoconjugates **1**—$TiO_2$, **1-Al**—$TiO_2$, and **1-Ga**—$TiO_2$ were obtained (Figure 1c,f,i). We note that these spectral profiles and fluorescence signal intensities are in agreement with the fluorescence spectra (Figures 1a,d,g) obtained from the molecular corroles **1**, **1-Al**, and **1-Ga**.

In summary, we have prepared $TiO_2$ nanoconjugates whose surfaces were covalently modified with fluorescent chlorosulfonated corroles through sulfonic ester formation. The nanoconjugate **1-Al**—$TiO_2$ exhibits the most intense fluorescence based on the spectral plot obtained from confocal fluorescence microscopy images. This finding is in line with the fluorescence behavior (high relative $\phi_{em}$) of **1-Al**. Further biological and imaging experiments involving these fluorescent nanoconjugates as potential contrast agents for optical imaging are underway in our laboratories.

**Acknowledgements**

We thank the CHLA Radiology Endowment Fund, Sanofi, and Doheny Eye Institute for financial support. We thank Esteban Fernandez, George Rossman, Bruce Brunscwig, Zeev Gross, and Michael Lichterman for their help and discussion on this work. We thank Mona Shahgholi (CCE Division Multiuser Mass Spectrometry Lab at Caltech) for her help with electrospray ionization mass spectrometry experiments.

**References**

(1) (a) Tempany, C. M.; McNeil, B. J. *JAMA* **2001**, *285*, 562. (b) Herschman, H. R. *Science* **2003**, *302*, 605. (c) Weissleder, R.; Pittet, M. J. *Nature* **2008**, *452*, 580. (d) Mura, S.; Couvreur, P. *Adv. Drug Delivery Rev.* **2012**, *64*, 1394.

(2) (a) Ntziachristos, V.; Ripoll, J.; Wang, L. V; Weissleder, R. *Nat. Biotechnol.* **2005**, *23*, 313. (b) Borsook, D.; Becerra, L.; Hargreaves, R. *Nat. Rev. Drug Discovery* **2006**, *5*, 411.

(3) Willmann, J. K.; Van Bruggen, N.; Dinkelborg, L. M.; Gambhir, S. S. *Nat. Rev. Drug Discovery* **2008**, *7*, 591.

(4) Winter, P. M.; Caruthers, S. D.; Kassner, A.; Harris, T. D.; Chinen, L. K.; Allen, J. S.; Lacy, E. K.; Zhang, H.; Robertson, J. D.; Wickline, S. A.; Lanza, G. M. *Cancer Res.* **2003**, 5838.

(5) (a) Endres, P. J.; Paunesku, T.; Vogt, S.; Meade, T. J.; Woloschak, G. E. *J. Am. Chem. Soc.* **2007**, *129*, 15760. (b) Xie, J. *Inorg. Chem.* **2008**, *47*, 5564. (c) Zhang, W.; Zhou, X.; Zhong, X. *Inorg. Chem.* **2012**, *51*, 3579. (d) Rodriguez-Liviano, S.; Becerro, A. I.; Alcantara, D.; Grazu, V.; De la Fuente, J. M.; Ocaña, M. *Inorg. Chem.* **2013**, *52*, 647.

(6) (a) Gross, Z.; Galili, N.; Saltsman, I. *Angew. Chem., Int. Ed.* **1999**, *38*, 1427. (b) Sankar, J.; Anand, V. G.; Venkatraman, S.; Rath, H.; Chandrashekar, T. K. *Org. Lett.* **2002**, *4*, 4233. (c) Ngo, T. H.; Puntoriero, F.; Nastasi, F.; Robeyns, K.; Van Meervelt, L.; Campagna, S.; Dehaen, W.; Maes, W. *Chem. Eur. J.* **2010**, *16*, 5691.

(7) (a) Mahammed, A.; Gray, H. B.; Weaver, J. J.; Sorasaenee, K.; Gross, Z. *Bioconjugate Chem.* **2004**, *15*, 738. (b) Li, C.-Y.; Zhang, X.-B.; Han, Z.-X.; Akermark, B.; Sun, L.; Shen, G.-L.; Yu, R.-Q. *Analyst* **2006**, *131*, 388.

(8) (a) Agadjanian, H.; Weaver, J. J.; Mahammed, A.; Rentsendorj, A.; Bass, S.; Kim, J.; Dmochowski, I. J.; Margalit, R.; Gray, H. B.; Gross, Z.; Medina-Kauwe, L. K. *Pharm. Res.* **2006**, *23*, 367. (b) Agadjanian, H.; Ma, J.; Rentsendorj, A.; Valluripalli, V.; Hwang, J. Y.; Mahammed, A.; Farkas, D. L.; Gray, H. B.; Gross, Z.; Medina-Kauwe, L. K. *Proc. Natl. Acad. Sci. U.S.A.* **2009**, *106*, 6105.

(9) (a) Mahammed, A.; Goldberg, I.; Gross, Z. *Org. Lett.* **2001**, *3*, 3443. (b) Saltsman, I.; Mahammed, A.; Goldberg, I.; Tkachecko, E.; Botoshansky, M.; Gross, Z. *J. Am. Chem. Soc.* **2002**, *124*, 7411.

(10) (a) Bendix, J.; Dmochowski, I. J.; Gray, H. B.; Mahammed, A.; Simkhovich, L.; Gross, Z. *Angew. Chem., Int. Ed.* **2000**, *112*, 4214. (b) Mahammed, A.; Gross, Z. *J. Inorg. Biochem.* **2002**, *88*, 305. (c) Weaver, J. J.; Sorasaenee, K.; Sheikh, M.; Goldschmidt, R.; Tkachenko, E.; Gross, Z.; Gray, H. B. *J. Porphyrins Phthalocyanines* **2004**, *08*, 76. (d) Sorasaenee, K.; Taqavi, P.; Henling, L. M.; Gray, H. B.; Tkachenko, E.; Mahammed, A.; Gross, Z. *J. Porphyrins Phthalocyanines* **2007**, *11*, 189. (e) Kowalska, D.; Liu, X.; Tripathy, U.; Mahammed, A.; Gross, Z.; Hirayama, S.; Steer, R. P. *Inorg. Chem.* **2009**, *48*, 2670. (f) Yang, Y.; Jones, D.; Von Haimberger, T.; Linke, M.; Wagnert, L.; Berg, A.; Levanon, H.; Zacarias, A.; Mahammed, A.; Gross, Z.; Heyne, K. *J. Phys. Chem. A* **2012**, *116*, 1023. (g) Ivanova, Y. B.; Savva, V. A.; Mamardashvili, N. Z.; Starukhin, A. S.; Ngo, T. H.; Dehaen, W.; Maes, W.; Kruk, M. M. *J. Phys. Chem. A* **2012**, *116*, 10683. (h) Kruk, M.; Ngo, T. H.; Savva, V.; Starukhin, A.; Dehaen, W.; Maes, W. *J. Phys. Chem. A* **2012**, *116*, 10704. (i) Kruk, M.; Ngo, T. H.; Verstappen, P.; Starukhin, A.; Hofkens, J.; Dehaen, W.; Maes, W. *J. Phys. Chem. A* **2012**, *116*, 10695.

(11) (a) Hush, N.; Dyke, J. *Dalton Trans.* **1974**, 395. (b) Ghosh, A.; Wondimagegn, T.; Parusel, A. B. J. *J. Am. Chem. Soc.* **2000**, *122*, 5100.

(12) Seybold, P. G.; Gouterman, M. *J. Mol. Spectrosc.* **1969**, *31*, 1.

(13) Reynolds, D.; Kenyon, W. *J. Am. Chem. Soc.* **1950**, *72*, 1584.

(14) Socrates, G. *Infrared and Raman Characteristic Group Frequencies: Table and Charts*; John Wiley & Sons: Chichester, U.K., 2001; p 218.

(15) Barron, A. R., Ed. *Physical Methods in Chemistry and Nano Science*; Connexions: Houston, TX, 2012; p 365.

**Supplementary Experimental**

**Materials.** 2 M $AlMe_3$ in toluene (Aldrich), $GaCl_3$ (Aldrich), $HSO_3Cl$ (Aldrich), 21 nm nanopowder $TiO_2$ (Aldrich), 30% $H_2O_2$ (EMD) were obtained commercially and used as received. The starting material *5*,*10*,*15*-tris(pentafluorophenyl) corrole ($H_3$tpfc) was prepared based on the literature method.[1] The solvents pyridine and toluene were dried over a column. Acetone and dichloromethane used were both of reagent and spectroscopic grades depending on the applications.

**Chemical Preparation.** All preparations were carried out under Ar(g) atmosphere unless otherwise noted.

1. **Corrole Preparation.** Preparation of 2,17-bischlorosulfonato-5,10,15-tris(pentafluorophenyl) corrole ($H_3$tpfc$(SO_2Cl)_2$; **1**) was performed according to the literature procedure.[2] The metallocorroles described in this study were prepared in the following manner.

**1.1. Preparation of 1-Al.** To the 20-mL toluene solution of 0.32 g of **1** (0.32 mmol) in a round bottom flask was added 0.8 mL of 2 M $AlMe_3$ (1.6 mmol) in toluene solution at an ice- bath temperature. The solution was stirred for 10 min followed by the addition of 1 mL anhydrous pyridine. The solution was allowed to stir for another 10 min over ice. The reaction was quenched by an addition of ice chips. The dark green solution was then extracted with $CH_2Cl_2$ and washed with water. The solvent was removed *in vacuo* and the dry deep green solid was redissolved in $CH_2Cl_2$ followed by filtration. The filtrate was brought to dryness to afford the dark green solid (0.098 g, 26% yield). ESI-MS ($CH_2Cl_2$): *m*/*z*: 1014.87 $[M-H]^-$ (Calculated for $C_{37}H_6N_4F_{15}Cl_2S_2O_4Al$: 1015.88); $^1$H-NMR (400 MHz, acetone-$d_6$, ppm): $\delta$ = 9.76 (*s*, 1 H), 9.25 (*s*, 1 H), 8.97 (*d*, 1 H), 8.85 (*d*, 1 H), 8.70 (*d*, 1 H), 8.58 (*d*, 1 H); $^{19}$F-NMR (376 MHz, acetone-$d_6$, ppm): -138.7 (*d*, 4 F), -140.0 (*d*, 2 F), -156.9 (*t*, 1 F), -157.5 (*t*, 1 F), -158.1 (*t*, 1 F), -164.9 (*m*, 2 F), -165.3 (*m*, 2 F), -167.0 (*m*, 2 F); UV-Vis (toluene:pyridine, 95:5): $\lambda_{max}$ ($\varepsilon$ $M^{-1}$ $cm^{-1}$) = 436 (4.08

$\times 10^4$), 625 ($7.66 \times 10^3$) nm.

**1.2. Preparation of 1-Ga.** To a heavy-walled Schlenk flask were added 0.20 g of **1** (0.20 mmol) and 0.57 g $GaCl_3$ (3.3 mmol) under Ar(g). The flask was chilled in $N_2$(l) and evacuated. 15 mL Degassed anhydrous pyridine (15mL) was added to the flask *via* vacuum transfer. The flask was subsequently sealed and allowed to warm to room temperature. The reaction vessel was heated to 120 °C for 1 h. The pyridine solution was diluted with $CH_2Cl_2$ and washed with water three times. The solution was then filtered through glass wool and partially concentrated for recrystallization with hexanes overnight. The product was then filtered, dried, and washed with a combination of acetone, $CH_2Cl_2$, and toluene. This filtrate collected was brought to dryness *in vacuo* to afford a dark green solid (0.092 g, 38% yield). ESI-MS ($CH_2Cl_2$:pyridine): *m*/*z*: 1056.81 $[M-H]^-$ (Calculated for $C_{37}H_8N_4F_{15}Cl_2S_2O_4Ga$: 1057.82); $^1$H-NMR (500 MHz, $CD_2Cl_2$, ppm): $\delta$ = 9.99 (*s*), 8.82 (*m*), 8.73 (*m*), 8.57 (*m*); $^{19}$F-NMR (376 MHz, acetone-$d_6$, ppm): -138.7 (*d*), -140.0 (*d*), -156.9 (*t*), -157.5 (*t*), -158.1 (*t*), -164.9 (*m*), -165.3 (*m*), -167.0 (*m*); UV-Vis (toluene:pyridine, 95:5): $\lambda_{max}$ ($\varepsilon$ $M^{-1}$ $cm^{-1}$) = 429 ($1.65 \times 10^4$), 611 ($5.61 \times 10^3$) nm.

2. **$TiO_2$ Surface activation.** To the solid $TiO_2$ nanoparticle (10 g) in a 2.0-L round bottom flask was added 1.2 L 30% $H_2O_2$ solution. The milky colloidal suspension was stirred under reflux for 5 h. Upon cooling, the off-white solid was isolated from the $H_2O_2$ solution by ultra- centrifugation at 4 ºC and washed with copious amount of water. The activated $TiO_2$ nano- particle ($TiO_2$–OH) collected was dried *in vacuo* for 12 h and stored dry in a vial prior to use.

3. **Surface Conjugation.** The following general procedure was employed for the conjugation of the corroles **1**, **1-Al**, and **1-Ga** to the activated $TiO_2$ nanoparticle surface: To the mixed solids containing the activated $TiO_2$ and corrole in a 25-mL round bottom flask was charged with anhydrous pyridine. The suspension turned green

immediately and was stirred under reflux before the reaction was stopped. The resulting green solid was isolated from the green solution by centrifugation and washed multiple times with dichloromethane, acetone, and deionized water until the centrifuge supernatant became colorless. The solid remained green, was dried *in vacuo*, and was stored until further use. The detailed preparation procedure for each corrole nanoconjugate is given as follows:

**3.1. Preparation of 1-$TiO_2$.** To a 25 mL round bottom flask were added 0.32 g $TiO_2$ OH and 0.028 g of **1** (28.1 $\mu$mol), which was subsequently cycled with argon and vacuum. After establishment of the inert atmosphere, 8 mL anhydrous pyridine was added to the flask and the reaction was set to reflux for 2 h. The resulting green solid was collected in a manner following the general centrifugation and washing procedures outlined above.

**3.2. Preparation of 1-Al-$TiO_2$.** To a 40 mL vial was added 1.18 g $TiO_2$–OH, which was subsequently cycled with argon and vacuum. To this flask, was added 5 mL anhydrous pyridine, followed by sonication to ensure even dispersion. In a second flask, was added 0.03 g of **1-Al** (25.5 $\mu$mol) and 7 mL anhydrous pyridine under Ar(g). This solution was stirred and then added to the $TiO_2$–OH precursor *via* syringe. The reaction was sealed and allowed to reflux for 2 h after which, the resulting green solid was collected in a manner following the general centrifugation and washing procedures outlined above.

**3.3. Preparation of 1-Ga-$TiO_2$.** To a 40 mL vial was added 0.84 g $TiO_2$–OH and 0.04 g of **1- Ga** (32.8 $\mu$mol), which was subsequently cycled with argon and vacuum. After establishment of the inert atmosphere, 8 mL anhydrous pyridine was added to the flask and the reaction was set to reflux for 2 h. The resulting green solid was collected in a manner following the general centrifugation and washing procedures outlined above.

**Supplementary References**

1. Gross, Z.; Galili, N.; Saltsman, I. *Angew. Chem. Intl. Ed.* **1999**, *38*, 1427.

2. (a) Mahammed, A.; Goldberg, I.; Gross, Z. *Org. Lett.* **2001**, *3*, 3443. (b) Saltsman, I.; Mahammed, A.; Goldberg, I.; Tkachecko, E.; Botoshansky, M.; Gross, Z. *J. Am. Chem. Soc.* **2002**, *124*, 7411.

*Chapter 3*

# CELLULAR UPTAKE AND CYTOTOXICITY OF A NEAR-IR FLUORESCENT CORROLE-$TiO_2$ NANCONJUGATE

As described in the previous chapter, we prepared and studied three corrole-nanoconjugates—the freebase, gallium, and aluminum systems. Based on initial confocal fluorescence microscopy of the conjugates and fluorescence quantum yield measurements of the unbound molecules, we identified the aluminum corrole naonconjugate as the brightest material, and therefore, the best possible candidate for optical imaging. Our hypothesis, was that all things equal, the brightest system would be the best candidate as improved brightness would allow for better visualization during deep tissue imaging.

The work described in this chapter required a lot of hands because of the extensive nature of the surface chemistry, microscopy, and biology involved. Nonetheless, initial tests were promising. An immortalized cell culture line, namely U87 glioblastoma, when treated appeared to uptake the nanoconjugate. Based on these promising results we tested for toxicity. We were pleasantly surprised that the conjugates exhibited very low levels of toxicity and that cells would proliferate even in the presence of fairly large quantities of the material. The following pages describe our results, which we published in 2014.

# CELLULAR UPTAKE AND CYTOTOXICITY OF A NEAR-IR FLUORESCENT CORROLE-$TiO_2$ NANCONJUGATE

Reproduced with permission from: Carl M. Blumenfeld, Bryce F. Sadtler, G. Esteban Fernandez, Lily Dara, Cathie Nguyen, Felix Alonso-Valenteen, Lali Medina-Kauwe, Rex A. Moats, Nathan S. Lewis, Robert H. Grubbs, Harry B. Gray, and Karn Sorasaenee. Journal of Inorganic Biochemistry, **2014,** 39-44. 

**Abstract:**

We are investigating the biological and biomedical imaging roles and impacts of fluorescent metallocorrole—$TiO_2$ nanoconjugates as potential-near infrared optical contrast agents *in vitro* in cancer and normal cell lines. The $TiO_2$ nanoconjugate labeled with the small molecule 2,17-bis(chlorosulfonyl)-5,10,15-tris(pentafluorophenyl)corrolato aluminum (III) (**1-Al**—$TiO_2$) was prepared. The nanoparticle **1-Al**—$TiO_2$ was characterized by transmission electron microscopy (TEM) and integrating-sphere electronic absorption spectroscopy. TEM images of three different samples of $TiO_2$ nanoparticles (bare, $H_2O_2$ etched, and **1-Al** functionalized) showed similarity in shapes and sizes with an average diameter of 29 nm for **1-Al**—$TiO_2$. Loading of **1-Al** on the $TiO_2$ surfaces was determined to be *ca.* 20-40 mg **1-Al**/g $TiO_2$. Confocal fluorescence microscopy (CFM) studies of luciferase-transfected primary human glioblastoma U87-Luc cells treated with the nanoconjugate **1-Al**—$TiO_2$ as the contrast agent in various concentrations were performed. The CFM images revealed that **1-Al**—$TiO_2$ was found inside the cancer cells even at low doses (0.02—2 μg/mL) and localized in the cytosol. Bioluminescence studies of the U87-Luc cells exposed to various amounts of **1-Al**—$TiO_2$ showed minimal cytotoxic effects even at higher doses (2—2000 μg/mL) after 24 h. A similar observation was made using primary mouse hepatocytes (PMH) treated with **1-Al**—$TiO_2$ at low doses (0.0003—3 μg/mL). Longer incubation times (after 48 and 72 h for U87-Luc) and higher doses (> 20 μg/mL **1-Al**—$TiO_2$ for U87-Luc and > 3 μg/mL **1-Al**—$TiO_2$ for PMH) showed decreased cell viability.

## 1. Introduction

Small molecules, biomolecules, and biocompatible materials for molecular imaging have played an important role in recent advances in biomedical and drug development research [1-3]. Application of contrast agents is required by many imaging modalities and allows for better understanding of biochemical pathways, physiological processes, and disease pathologies [4-8]. Many small molecules and biomolecules that function as molecular imaging contrast agents have been utilized in both preclinical and clinical settings [9]. Recent efforts have focused on nanomaterials, a start contrast to traditional small molecules and oligomers [10, 11]. Aside from the sizes of these materials, including volumes and surface areas, which essentially provide a canvas for numerous small molecule labeling, they exhibit properties not generally found in either bulk materials or discreet molecules [12-14]. Examples of widely used and studied nanomaterials for biomedical imaging include quantum dots for optical imaging and superparamagnetic iron oxides for magnetic resonance imaging [10, 11].

In our work, we have employed semiconductor nanoparticulate titanium(IV) oxide ($TiO_2$) covalently decorated with fluorescent corroles as a new class of optical imaging contrast agents for the study of cellular uptake and cytotoxic effects in cancer and normal cells. $TiO_2$, found in several different crystalline structures, such as rutile, anatase, and brookite, has been used in a number of contexts, including photocatalysis, dye-sensitized solar cells, and photochromic devices [15-19]. $TiO_2$ nanoparticles exhibit a wealth of intrinsic properties dependent upon several factors, including surface area, crystalline phase, and single crystallinity. We have exploited the facile nature with which the surface can be decorated with corroles, which were selected as optical dyes. Many studies have shown that 5,10,15-trispentafluorophenyl corrole and its derivatives exhibit bright and robust fluorescence signals in the near-IR region ($\lambda_{em} \geq 600$ nm) and are therefore considered suitable candidates for optical imaging [20-23]. In addition, the chemical versatility of corroles, allowing for various metalation [24-26] and substitution [27, 28] reactions, as well as their biological stability [29-31] makes them attractive contrast agents.

Previously we reported the syntheses, spectroscopic characterizations, and spectral confocal fluorescence imaging results for a family of corrole-$TiO_2$ nanoconjugates, namely **1**—$TiO_2$, **1-Al**—$TiO_2$, and **1-Ga**—$TiO_2$ [32]. The $TiO_2$ nanoparticle surfaces were covalently labeled with chlorosulfonated corroles through a sulfonic ester linkage (Scheme 1).

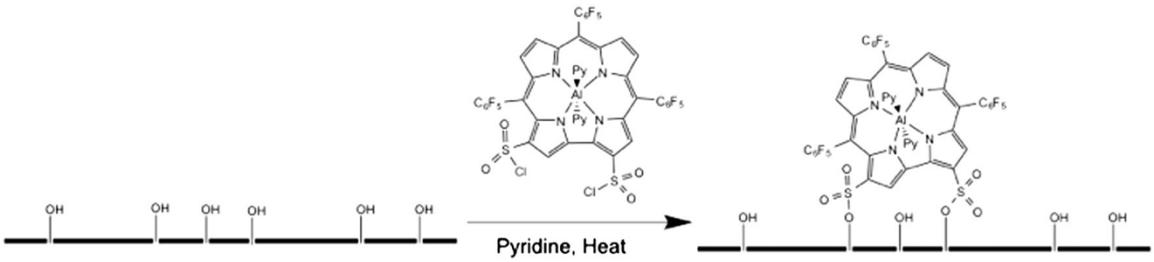


Scheme 6. $TiO_2$ surface labeling with **1-Al** forming sulfonic ester linkages between the corrole and the surface.

Because **1-Al**—$TiO_2$ exhibits the brightest fluorescence, consistent with the emission properties of related molecular Al corroles [26, 32, 33], we chose this nanoconjugate as a model to study cellular uptake and cytotoxic effects.

## 2. Experimental

### *2.1 Reagents and materials*

Preparation of the Al(III)tpfc($SO_2Cl$)$_2$ (**1-Al**) and the nanoconjugate **1-Al**—$TiO_2$ was reported previously [32]. D-Luciferin potassium salt (Promega), Hoechst 34580 (Invitrogen™), Hoechst 33258 (Invitrogen™), Sytox Green (Invitrogen™), and FM® 1-43FX (Invitrogen™) were used as received according to the provider's instruction.

### *2.2 Physical Methods*

Characterization of **1-Al** was performed by $^1$H NMR, $^{19}$F NMR, electronic absorption, and fluorescence spectroscopies, and was reported previously [32]. Surface characterization of **1-Al**—$TiO_2$ is outlined as follows.

*2.2.1. Transmission electron microscopy*

The morphologies of the $TiO_2$ nanoparticles before and after surface functionalization were imaged using an FEI Tecnai F30ST transmission electron microscope (TEM) operated at an acceleration voltage of 300 kV. Images were recorded using a Gatan CCD camera. For TEM analysis, a small quantity of $TiO_2$ particles was dispersed in isopropyl alcohol (IPA) by sonication. The dispersions were drop-cast onto C-flat™ holey carbon films on a 200 mesh Cu TEM grid (Electron Microscopy Sciences).

*2.2.2. Absorption spectroscopy*

Calculation of the corrole **1-Al**'s loading on the surface of $TiO_2$ was based on the absorbance values obtained from the integrating sphere electronic absorption measurements described as follows.

Thin film transflectance measurements were used to determine **1-Al** loading on the $TiO_2$ nanoparticles. Both $H_2O_2$-etched and **1-Al**-functionalized nanoparticles were dispersed in a polydimethylsiloxane (PDMS) polymer matrix. PDMS was chosen as it provides a transparent matrix for measuring the optical properties of porous solids [34]. The weights of the $TiO_2$ nanoparticles, the PDMS base (Sylgard® 184 silicone elastomer base from Dow Corning), and the curing agent (Sylgard® 184 silicone elastomer curing agent from Dow Corning) are provided in Table A.1. The nanoparticles were first dispersed in a minimal amount of IPA by sonication. The dispersion of $TiO_2$ nanoparticles in IPA was then mixed with the PDMS base and curing agent using a vortex mixer. The mixtures were cast into films onto quartz substrates and allowed to cure in air for 12 h followed by curing in a drying oven at 60° for 2 h.

Transflectance spectra of the $H_2O_2$-etched and **1-Al**-functionalized $TiO_2$ nanoparticle films were measured using a Cary 5000 UV–vis-NIR spectrometer from Agilent Technologies equipped with an integrating sphere (External DRA 1800), a PMT detector, a quartz-iodine lamp for the visible region (350–800 nm), and a deuterium lamp for the ultravi-

olet region (300–350 nm). Because the $TiO_2$ nanoparticles diffusely scattered the incident illumination, the PDMS films were placed in the center of the integrating sphere to collect both the transmitted, T, and the reflected, R, (including the spectrally reflected and diffusely scattered) light with the PMT detector. The transflectance measurements allowed for the absorbance, A, of the films to be determined by $A = -\log(T + R)$. The concentration, C, of **1-Al** within the PDMS films was then calculated using the Beer–Lambert law, $A = \varepsilon Cl$, where $\varepsilon$ is the extinction coefficient of the dye and l is the film thickness (determined by profilometry, see below) [35–37]. The absorbance values at 426 and 595 nm (corresponding to the Soret and Q bands of the dye, respectively) for the PDMS film containing the **1-Al**-functionalized $TiO_2$ nanoparticles, the estimated extinction coefficients of **1-Al** at these wavelengths, and the film thicknesses are provided in Table A.2. The absorbance values for the PDMS film containing the non-functionalized, $H_2O_2$-etched $TiO_2$ nanoparticles at these wavelengths are also provided, which were subtracted from the absorbance values of the **1-Al**-functionalized $TiO_2$ nanoparticles. The **1-Al**-loading was determined to be 24 mg of **1-Al** per gram of $TiO_2$ based on the absorbance value of the Soret band and 38 mg of dye per gram of $TiO_2$ based on the absorbance value of the Q band.

Thickness profiles of the PDMS films were measured using a Bruker DektakXT stylus surface profilometer. The diameter of the diamond- tipped stylus was 2 μm and a weight of 1 mg was applied to the film. The stylus was scanned at a rate of 250 μm/s. The thickness profiles were used to measure the average path length through the PDMS films during the transflectance measurements.

*2.2.3. Hydrodynamic size and surface charge measurements*

The mean particle size was determined by dynamic light scattering (DLS, Malvern ZEN 3600 Zetasizer Nano) measurements. Samples of **1-Al**–$TiO_2$ suspended in PBS pH 7.2 were pipetted into a low volume quartz cuvette with appropriate concentrations. At least nine measurements were performed for each sample. Each measurement comprised 20 runs with an average of 34,000 particle counts per second. The data represent the particle size distribution parameter, which reports the most frequent particle size in the sample accounting

for the intensity fluctuations of larger particles. The particle intensity was computed using Zetasizer Software version 7.01 applying the Stokes–Einstein equation to correlate the change in the scattering intensity and particle movements. Plots showing the average size of the nanoparticle aggregates are shown in Fig. A.1. The surface charge of **1-Al**–$TiO_2$ in PBS pH 7.2 was examined through ζ potential measurements (Malvern ZEN 3600 Zetasizer Nano). The average ζ potential was calculated from 20 measurements with 10–100 runs for each depending on the variation of the particles.

*2.3. Cell culture and cell viability assay*

Pathogen-free U87-LUC cell line (TSRI Small Animal Imaging and Research Laboratory) [38] was grown in a 75-mL flask in Dulbecco's Minimal Essential Medium (DMEM) in 5% $CO_2$ at 37 °C. The cell culture medium was supplemented with 10% fetal bovine serum (FBS) and 1% antibiotic primocin. The cell culture medium was replenished every 2 days and the cells were passaged once they reached 80% confluence. Primary mouse hepatocytes (PMH) were isolated and cultured as previously described [39].

For U87-Luc cell culture experiments, cells plated in an 8-chamber slide (Nunc™ Lab-Tek™, Thermo Scientific) were treated with **1-Al**–$TiO_2$ suspended in PBS over a range of 0.002 μg/mL to 2000 μg/mL. A primary stock solution (6.3 mg **1-Al**–$TiO_2$ in 1 mL PBS) was prepared. The primary stock solution was further diluted to prepare secondary and tertiary stock solutions. Various amounts of stock solutions were added to the 8-chamber glass slide plated with cells to give the aforementioned range of concentrations. The final volume of each chamber was 300 μL. After treatment, the treated cells and controls were incubated in the dark in 5% $CO_2$ at 37 °C for a period of 24, 48, and 72 h. The cells were imaged using a cooled IVIS® animal imaging system (Xenogen, Alameda, CA USA) linked to a PC running with Living Image™ software (Xenogen) along with IGOR (Wavemetrics, Seattle, WA, USA) under Microsoft® Windows® 2000. This system yielded high signal-to-noise images of luciferase signals emerging from the cells. Before imaging, 20 μL of 5 mg/mL luciferin in normal saline were added to each well. An integration time of 1 min with binning of 5 min was used for luminescent image acquisition. The signal intensity was

quantified as the flux of all detected photon counts within each well using the Living Image™ software package. All experiments were performed in triplicate.

For PMH cell culture experiments, the cells were plated in a 6-chamber slide (Falcon®, Primaria™). After 3 h, media was exchanged (DMEM-F12) and the cells were treated with **1-Al**–$TiO_2$ suspended in PBS over a range of 0.0003 to 300 μg/mL. A primary stock solution (6.3 mg **1-Al**–$TiO_2$ in 1 mL PBS) was prepared. The primary stock solution was further diluted to prepare secondary and tertiary stock solutions. Various amounts of stock solutions were added to the 6-chamber glass slide plated with cells to give the aforementioned range of concentrations. The final volume of each chamber was 2000 μL. After 24 or 48 h of treatment, cells were double stained with Hoechst 33258 (8 mg/mL) and Sytox Green (1 mM). Quantitation of total and necrotic cells (Sytox Green positive) was performed by counting cells in at least five different fields using ImageJ, as previously described [39]. All experiments were done in triplicate.

*2.4. In vitro confocal fluorescence microscopy*

The U87-Luc cells were seeded at 20,000 cells per well on an 8-chamber slide (Nunc™ Lab-Tek™, Thermo Scientific) and allowed to grow overnight. Cells were washed with PBS and were incubated in serum free media mixed 1:1 with **1-Al**–$TiO_2$ for 24, 48, and 72 h at 37 °C over a concentration range similar to that of the U87-Luc cell viability assay (0.002 μg/mL to 2000 μg/mL). Cells were then washed 3 × with PBS and stained with Hoechst 33258 and FM® 1-43FX stains. The stained cells were kept chilled on ice without fixation until just prior to imaging. Z-stacked images were acquired with an LSM 710 confocal system mounted on an AxioObserver Z.1 inverted microscope equipped with a 40 ×/1.2 C-APOCHROMAT water-immersion lens (Carl Zeiss Microimaging, Thornwood, NY). Two visible laser lines of 405 and 488 nm were used for fluorescence excitation. The Z-stacks were acquired with 0.5 μm slice intervals. The software ZEN 2010 was used for hardware control. To reduce blurring and noise in the raw images, they were processed with the 3D blind deconvolution algorithm of AutoQuant AutoDeblur software (Media Cybernetics, Silver Spring, MD) using the default settings for the laser scanning confocal

modality. ZEN and Fiji ImageJ software [40] were employed to further process the deconvolved images.

## 3. Results and discussions

### *3.1. Physical characterization of **1-Al**—$TiO_2$: TEM, DLS, and surface characterization*

TEM images of $TiO_2$ (Fig. 1) were taken before and after $H_2O_2$-etching and surface functionalization. The images established that the average particle size post-corrole functionalization is 29 nm with a standard deviation of 7 nm. These results were obtained through averaging over 44 particles. Absorption measurements of the particles embedded in a transparent polymer matrix, facilitated with the use of an integrating sphere to distinguish between absorption and diffuse scattering by the nanoparticles, indicated nearly identical absorption features in the molecular and conjugated species. These experiments afforded an approximate loading of 1-Al on the surfaces of *ca.* 20–40 mg/g $TiO_2$ (Fig. 2).

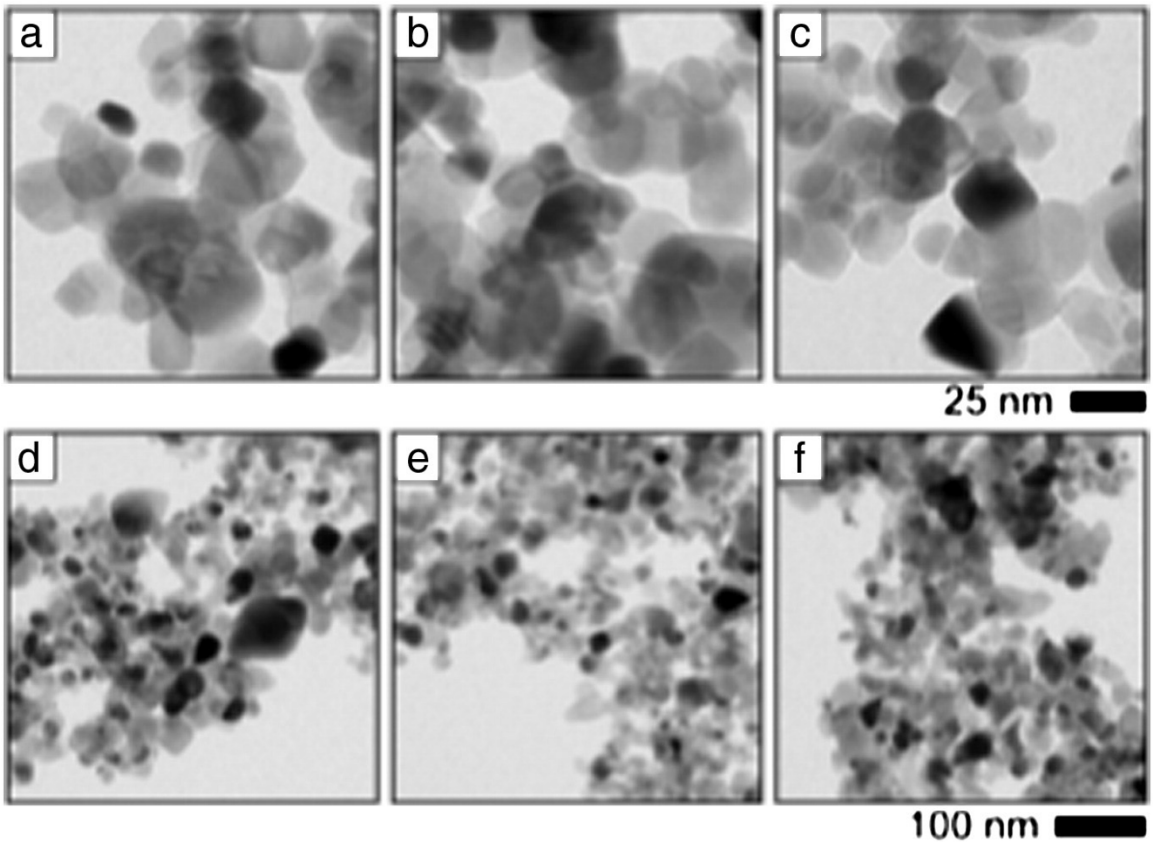


Figure 5. TEM images of $TiO_2$ nanoparticles before and after dye-functionalization. Images of the initial $TiO_2$ nanoparticles (a and d). Images of the nanoparticles after $H_2O_2$-etching (b and e). Images of the nanoparticles after **1-Al** functionalization (c and f). The top scale bar refers to images a, b, and c and the bottom scale bar refers to images d, e, and f.

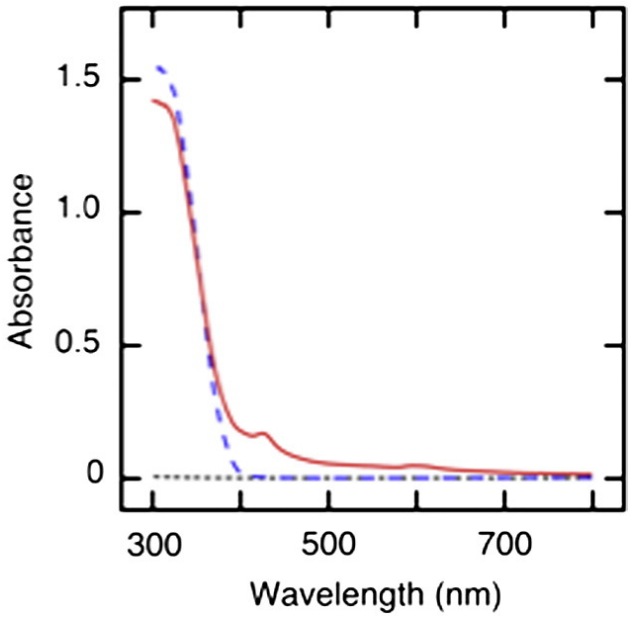


Figure 6. Absorbance spectra of $H_2O_2$-etched $TiO_2$ nanoparticles embedded in a PDMS polymer matrix before (blue, dashed line) and after **1-Al** functionalization (red, solid line), as well as the absorption spectrum of PDMS on quartz (black, dotted line). The absorption spectra were measured in transflectance mode where both transmitted and reflected light were collected employing an integrating sphere.

The hydrodynamic nature of **1-Al**–$TiO_2$ in PBS measured by the DLS method revealed great heterogeneity in size of the aggregates. While the average size of **1-Al**–$TiO_2$ in PBS was measured to be 200 nm in diameter, smaller and larger aggregates were observed. In addition, zeta (ζ) potential measurements of **1-Al**–$TiO_2$ in PBS exhibited moderate stability and revealed a negatively charged surface with a ζ potential of − 27.4 (±1.25) mV at the concentration of 50 μg/mL.

*3.2. Confocal fluorescence microscopy and uptake of **1-Al**—$TiO_2$ by U87-Luc cells*

Treatment of the luciferase-transfected glioblastoma cell U87-Luc with a wide range of **1-Al**–$TiO_2$ concentrations revealed internalization of these nanoconjugates over a period of 24, 48, and 72 h as shown by CFM (Fig. 3). We also show the Z-stacked three-dimensional CFM images (Fig. 4) of U87-Luc cells treated with 0.02 μg/mL of **1-Al**–$TiO_2$ for 48 and 72 h from three different perspectives.

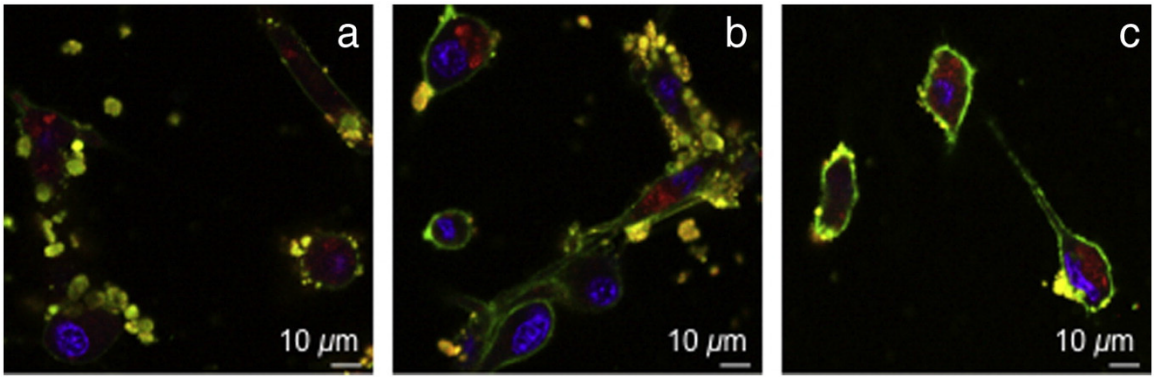


Figure 7. CFM images of U87-Luc cells incubated with 0.02 μg/mL **1-Al**—$TiO_2$ (red) for 24 h (a), 48 h (b), and 72 h (c) and stained with dyes to mark the membrane (green) and nucleus (blue).

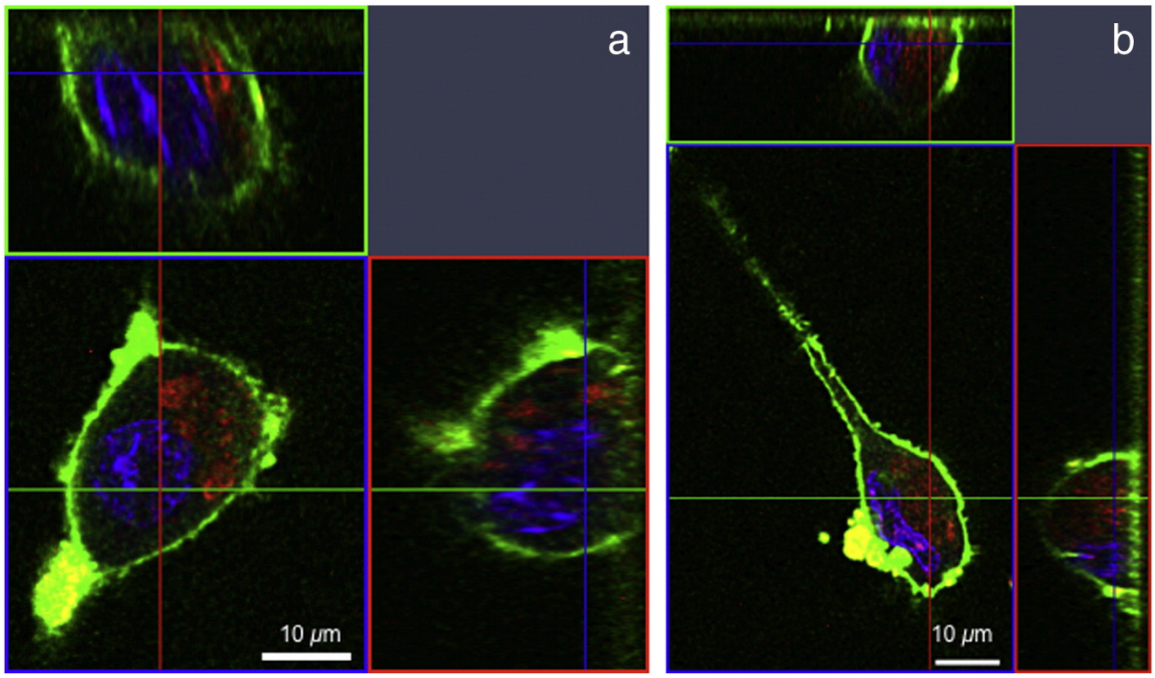


Figure 8. Z-Stacked CFM images of individual U87-Luc cells taken at 0.5 um z-slice intervals from top to bottom after (a) 48 h and (b) 72 h of treatment with 0.02 μg/ml **1-Al**—$TiO_2$.

The CFM images were taken after the cells were stained with nuclear and cell membrane dyes, and washed with media solution several times to remove unbound dyes and **1-Al**–$TiO_2$ nanoconjugates. The nucleus labeled with a Hoechst stain is colored blue ($\lambda_{ex}$ = 405; $\lambda_{em}$ = 460 nm), the membrane labeled with the dye FM® 1-43FX is colored green ($\lambda_{ex}$ = 488; $\lambda_{em}$ = 580 nm), and the nanoconjugate 1-Al–TiO2 is colored red ($\lambda_{ex}$ = 405; $\lambda_{em}$ = 634 nm).

While mechanisms of **1-Al**–$TiO_2$ uptake and localization into cells will be studied further, we propose that the **1-Al**–$TiO_2$ nanoconstruct is internalized through endocytosis, consistent with previous work [41–46]. We note that, based on confocal fluorescence imaging, the nanomaterial **1-Al**–modified $TiO_2$ appears to be suspended in the cytosol. This finding is consistent with the distribution pattern of $TiO_2$ nanoconjugates in HeLa cells in a previous study of 1D $TiO_2$ nanorods and nanoparticles labeled with fluorescein thiocyanate [43]. However, modified $TiO_2$ labeled with alizarin red S has been shown to have perinuclear localization in HeLa cells, in contrast to our observations with **1-Al**–$TiO_2$ [41,42]. Recent studies involving uptake of other modified $TiO_2$ nanoparticles in various cell lines, such as mouse fibroblasts and osteoblasts, suggested cellular internalization and distribution of $TiO_2$ nanoparticles at the endosome/lysosome and in the cytoplasm, in accord with our findings [44,45]. We note that internalization of **1-Al**–$TiO_2$ into glioblastoma cells can be observed at very low concentrations (0.02–2 μg/mL).

*3.3. Cytotoxicity in U87-Luc cells*

It is well documented that $TiO_2$ nanoparticles exhibit various degrees of cytotoxic activity upon photoactivation by UV–vis light due to formation of reactive oxygen species [43,44,46]. A study of water-soluble single-crystalline $TiO_2$ nanoparticles in melanoma A-375 cells revealed that in the absence of UV light the $TiO_2$ nanoparticles were essentially non-toxic and thus biocompatible [46]. However, upon irradiating these cells with UV light less than 20% of the melanoma cells survived at a $TiO_2$ concentration of 400 μg/mL. Therefore, in an attempt to understand the cytotoxic effects of the **1-Al**–$TiO_2$ conjugate independently of its phototoxic properties, we treated the glioblastoma cell U87-Luc in the

absence of UV–vis irradiation with the same range of **1-Al**–$TiO_2$ concentrations as in the cell internalization studies (0.002– 2000 μg/mL). The cells were incubated over a period of 24, 48, and 72 h prior to bioluminescence cell viability assays [38,47]. Based on the bioluminescence signal of the firefly luciferin from living U87-Luc cells, which is related to the level of cellular ATP, the cytotoxic assay showed that the nanoconjugate **1-Al**–$TiO_2$ had essentially no cytotoxic effect on the glioblastoma cells after 24 h of treatment (Fig. 5) and, therefore, could be considered biocompatible. The cytotoxic effect became more apparent as the cells were exposed to the corrole–$TiO_2$ nanoparticles for extended periods of time at higher concentrations (> 200 μg/mL). For example, only *ca.* 65% and *ca.* 30% of the bioluminescence signal from the live cells was observed after 48 h and 72 h treatments at 2000 μg/mL, respectively. Our viability study of the U87-Luc cells treated with **1-Al**–$TiO_2$ was also consistent with a study performed on mouse fibroblast cells, using the MTT assay, showing that the cytotoxic effects of $TiO_2$ at various concentrations (3–600 μg/mL) were negligible after 24 h of treatment, whereas the 48 h treatment of these cells with the nanoparticle showed a decrease in cell viability at higher concentrations [44]. Another study

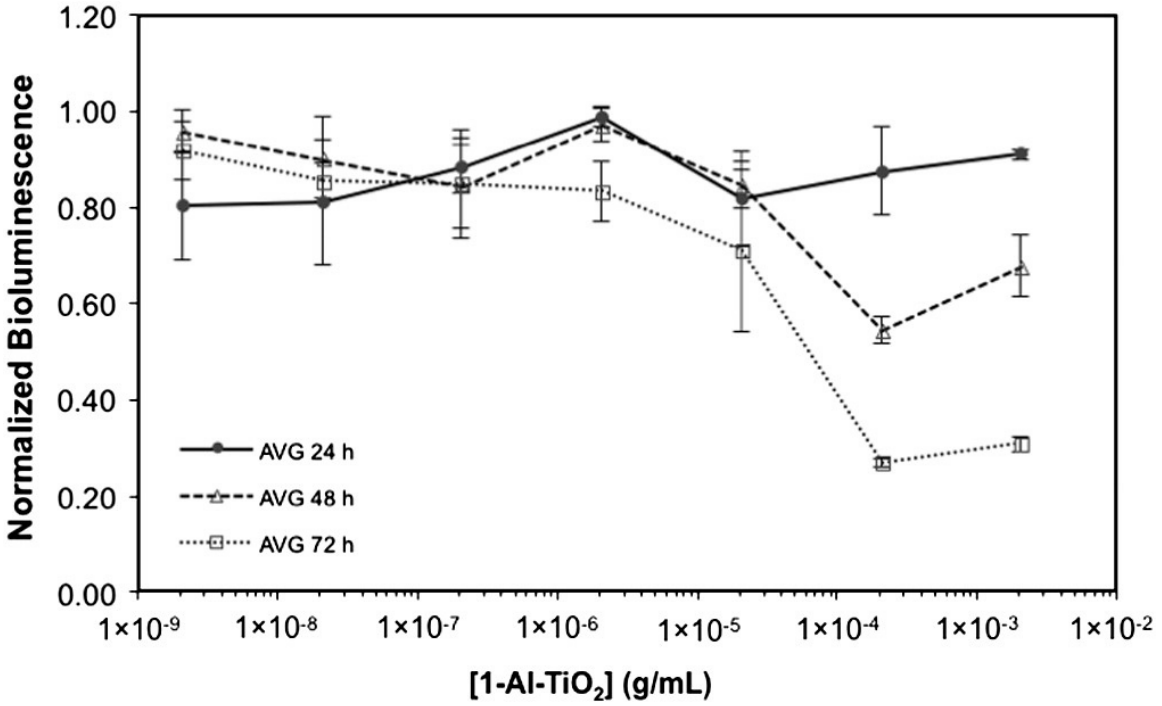


Figure 9. Cell viability plot of U87-Luc cells treated by **1-Al**–$TiO_2$ at various concentrations (0.002–2000 μg/mL) using a bioluminescence assay.

on the cytotoxicity effect of unmodified 1D and 3D $TiO_2$ nanostructures on HeLa cells also showed that these nanoparticles were relatively nontoxic at concentrations up to 125 μg/mL in the absence of light [43].

*3.4 Cytotoxicity in primary mouse hepatocytes*

Additionally, to determine the cytotoxic effect of the nanoconjugate **1-Al**–$TiO_2$ on non-cancerous cells, we treated primary mouse hepatocytes (PMH) with **1-Al**–$TiO_2$ at various concentrations (0.0003–300 μg/mL) for 24 and 48 h (Fig. 6) in the absence of UV–vis irradiation. Similar to the results observed for cancerous U87-Luc cells, **1-Al**–$TiO_2$ was essentially nontoxic in non-cancerous PMH at up to 3 μg/mL after both 24 and 48 h of treatment. Only at higher concentrations did the proportion of the live PMH drop below 80%. We note that the PMH behaved similarly after 24 h and 48 h treatments with various doses of **1-Al**–$TiO_2$, suggesting that low **1-Al**–$TiO_2$ concentrations had minimal cytotoxic effects on the viability of these non-cancerous cells. The PMH were more susceptible to the cytotoxic effects of **1-Al**–$TiO_2$ than the U87-Luc cells; it is reasonable that non-cancerous cells, especially primary cells, would be less tolerant towards exogenous non-native agents [48,49]. Nonetheless, the intense fluorescence exhibited by **1-Al** [26,33] would allow for the potential use of the nanoconjugate **1-Al**–$TiO_2$ as an optical imaging agent observable by confocal fluorescence microscopy even at low concentrations (0.02–2 μg/mL) below the cytotoxic thresholds for both cancerous and non-cancerous cells.

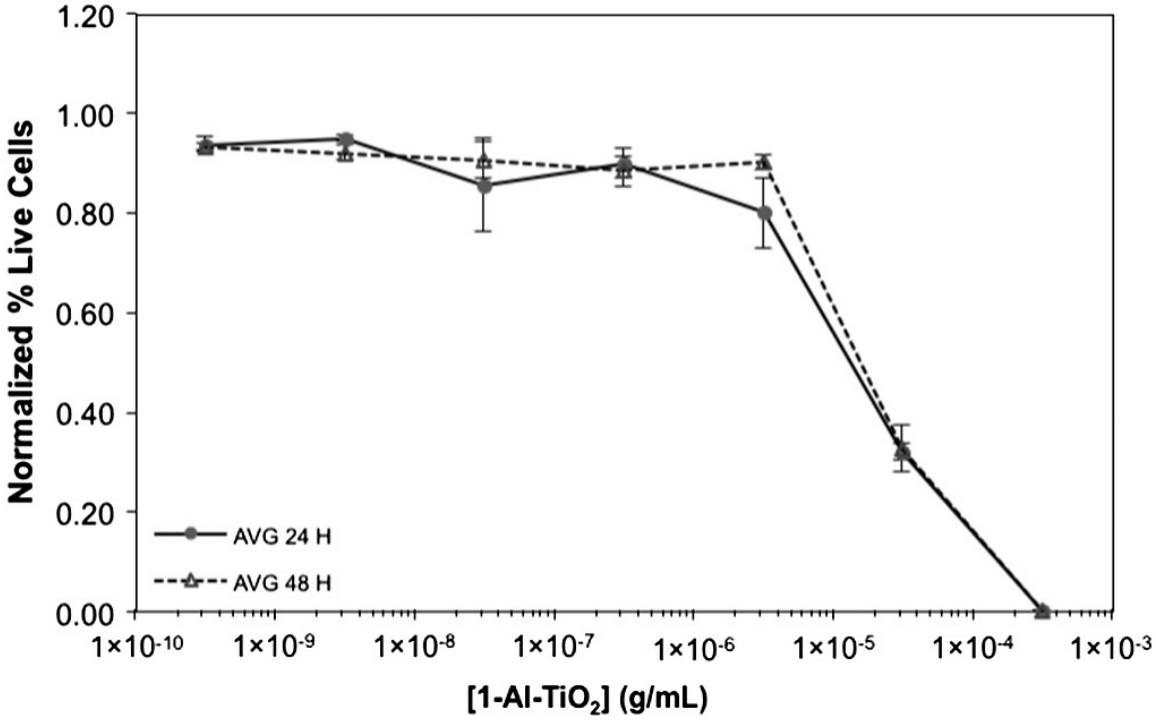


Figure 10. Cell viability plot of PMH treated with **1-Al**–$TiO_2$ at various concentrations (0.0003– 300 μg/mL) using a Syntox Green live-dead assay.

## 4. Conclusions

In summary, we report detailed characterization of **1-Al**–$TiO_2$, a nanoconjugate that potentially could be used as a metal oxide nanoprobe for optical imaging, owing to intense fluorescence as well as its biocompatibility. The biological studies suggest that **1-Al**–$TiO_2$ is essentially nontoxic at concentrations up to 3 and 2000 μg/mL for normal mouse liver cells and glioblastoma U87-Luc cells, respectively, within the first 24 h of treatment. The PMH viability, however, dropped at higher concentrations (> 3 μg/mL) after 24 h and 48 h treatments and the U87-Luc cell viability also declined at higher concentrations (> 20 μg/mL) after 48 h and 72 h treatments. We also would like to note, for example, that comparable to our PMH cytotoxic assay over the concentration range for **1-Al**–$TiO_2$ of 0.0003–300 μg/mL, superparamagnetic iron oxide nanoparticle used in MRI was studied for their cytotoxicity in

fetal stem cell lines over a low concentration range (5–35 μg/mL) [50]. Another example includes PDMAEMA-modified ZnO QDs functioning as contrast agents in monkey kidney cells over a concentration range of 50–800 μg/mL [51]. More importantly, our CFM studies demonstrated that the nanoconjugate **1-Al**–$TiO_2$ was internalized in U87-Luc cells even at a relatively low concentration (0.02 μg/mL). Although further detailed localization and internalization mechanism studies should be performed, our current work has revealed that there is random suspension of **1-Al**–$TiO_2$ in the cytosol even after 72 h treatment. Notably, the observation of near-IR fluorescence of **1-Al**–$TiO_2$ over a non-toxic concentration range (0.002–2000 μg/mL) in U87-Luc after 24 h treatment suggests that corrole–$TiO_2$ nanoconjugates could be very promising candidates for use as biological imaging agents.

**Acknowledgement**

We thank the CHLA Radiology Endowment Fund (K.S.), Sanofi (H.B.G.), Doheny Eye Institute (R.H.G.), and Beckman Institute Postdoctoral Fellowship (B.F.S.) for the support. We also thank Anahit Hovsepyan, Seda Mkhitaryan, Vazgen Khankaldyyan, and Gevorg Karapetyan for the help with the bioluminescence assays. Absorption measurements and profilometry were performed at the Molecular Materials Research Center, Beckman Institute, Caltech. We thank Carol M. Garland for the assistance in TEM imaging. B.F.S. and N.S.L. acknowledge the support from the "Light–Material Interactions in Energy Conversion" Energy Frontier Research Center funded by the US Department of Energy, Office of Science, Office of Basic Energy Sciences (DE-SC0001293).

**References**

[1] J.K. Willmann, N. van Bruggen, L.M. Dinkelborg, S.S. Gambhir, Nat. Rev. Drug Discov. 7 (2008) 591–607.

[2] B.A. Smith, B.D. Smith, Bioconjug. Chem. 23 (2012) 1989–2006.

[3] E.K.-H. Chow, D. Ho, Sci. Transl. Med. 5 (2013) 1–12.

[4] S. Keren, C. Zavaleta, Z. Cheng, A. de la Zerda, O. Gheysens, S.S. Gambhir, Proc. Natl.Acad. Sci. U. S. A. 105 (2008) 5844–5849.

[5] N.K. Devaraj, R. Weissleder, S.A. Hilderbrand, Bioconjug. Chem. 19 (2008) 2297–2299.

[6] S. Mather, Bioconjug. Chem. 20 (2009) 631–643.

[7] S.S. Kelkar, T.M. Reineke, Bioconjug. Chem. 22 (2011) 1879–1903.

[8] K. Wilson, K. Homan, S. Emelianov, Nat. Commun. 3 (2012) 1–10.

[9] P.M. Winter, S.D. Caruthers, A. Kassner, T.D. Harris, L.K. Chinen, J.S. Allen, E.K. Lacy, H. Zhang, J.D. Robertson, S.A. Wickline, G.M. Lanza, Cancer Res. 63 (2003) 5838–5843.

[10] P.J. Endres, T. Paunesku, S. Vogt, T.J. Meade, G.E. Woloschak, J. Am. Chem. Soc. 129 (2007) 15760–15761.

[11] J. Xie, Inorg. Chem. 47 (2008) 5564–5566.

[12] M.-C. Daniel, D. Astruc, Chem. Rev. 104 (2004) 293–346.

[13] J.P. Wilcoxon, B.L. Abrams, Chem. Soc. Rev. 35 (2006) 1162–1194.

[14] S.K. Murthy, Int. J. Nanomedicine 2 (2007) 129–141.

[15] D.V. Bavykin, J.M. Friedrich, F.C. Walsh, Adv. Mater. 18 (2006) 2807–2824.

[16] S.P. Albu, A. Ghicov, J.M. Macak, R. Hahn, P. Schmuki, Nano Lett. 7 (2007) 1286–1289.

[17] D.P. Macwan, P.N. Dave, S. Chaturvedi, J. Mater. Sci. 46 (2011) 3669–3686.

[18] B. O'Regan, M. Gratzel, Nature 353 (1991) 737–740.

[19] A. Fujishima, K. Honda, Nature 238 (1972) 37–38.

[20] Z. Gross, N. Galili, I. Saltsman, Angew. Chem. Int. Ed. 38 (1999) 1427–1429.

[21] J. Sankar, V.G. Anand, S. Venkatraman, H. Rath, T.K. Chandrashekar, Org. Lett. 4 (2002) 4233–4235.

[22] C.-L. Tsai, J.-C. Chen, W.-J. Wang, J. Med. Biol. Eng. 21 (2001) 7–13.

[23] Y. Huang, J. Tang, B.G. Swanson, A.G. Cavinato, M. Lin, B.A. Rasco, Carbohydr. Polym. 53 (2003) 281–288.

[24] J. Bendix, I.J. Dmochowski, H.B. Gray, A. Mahammed, L. Simkhovich, Z. Gross, Angew. Chem. Int. Ed. 39 (2000) 4048–4051.

[25] J.J. Weaver, K. Sorasaenee, M. Sheikh, R. Goldschmidt, E. Tkachenko, Z. Gross, H.B. Gray, J. Porphyrins, J. Porphyrins Phthalocyanines 08 (2004) 76–81.

[26] K. Sorasaenee, P. Taqavi, L.M. Henling, H.B. Gray, E. Tkachenko, A. Mahammed, Z. Gross, J. Porphyrins, J. Porphyrins Phthalocyanines 11 (2007) 189–197.

[27] A. Mahammed, I. Goldberg, Z. Gross, Org. Lett. 3 (2001) 3443–3446.

[28] I. Saltsman, A. Mahammed, I. Goldberg, E. Tkachenko, M. Botoshansky, Z. Gross, J. Am. Chem. Soc. 124 (2002) 7411–7420.

[29] A. Mahammed, H.B. Gray, J.J. Weaver, K. Sorasaenee, Z. Gross, Bioconjug. Chem. 15 (2004) 738–746.

[30] H. Agadjanian, J.J. Weaver, A. Mahammed, A. Rentsendorj, S. Bass, J. Kim, I.J. Dmochowski, R. Margalit, H.B. Gray, Z. Gross, L.K. Medina-Kauwe, Pharm. Res. 23 (2006) 367–377.

[31] H. Agadjanian, J. Ma, A. Rentsendorj, V. Valluripalli, J.Y. Hwang, A. Mahammed, D.L. Farkas, H.B. Gray, Z. Gross, L.K. Medina-Kauwe, Proc. Natl. Acad. Sci. U. S. A. 106 (2009) 6105–6110.

[32] C.M. Blumenfeld, R.H. Grubbs, R.A. Moats, H.B. Gray, K. Sorasaenee, Inorg. Chem. 52 (2013) 4774–4776.

[33] A. Mahammed, Z. Gross, J. Inorg. Biochem. 88 (2002) 305–309.

[34] M.D. Kelzenberg, S.W. Boettcher, J. A. Petykiewicz, D.B. Turner-Evans, M.C. Putnam, E.L. Warren, J.M. Spurgeon, R.M. Briggs, N.S. Lewis, H.A. Atwater, Nat. Mater. 9 (2010) 239–244.

[35] L. Ceriotti, K. Weible, N.F. De Rooij, E. Verpoorte, Microelectron. Eng. 67–68 (2003) 865–871.

[36] N. Shahzad, D. Pugliese, A. Lamberti, A. Sacco, A. Virga, R. Gazia, S. Bianco, M.I. Shahzad, E. Tresso, C.F. Pirri, J. Phys. Conf. Ser. 439 (2013) 1–12.

[37] D. Ryu, K.J. Loh, R. Ireland, M. Karimzada, F. Yaghmaie, A.M. Gusman, Smart Struct. Syst. 8 (2011) 471–486.

[38] J.S. Burgos, M. Rosol, R.A. Moats, V. Khankaldyyan, D.B. Kohn, M.D. Nelson Jr., W.E. Laug, Biotechniques 34 (2003) 1184–1188.

[39] G. Feng, N. Kaplowitz, J. Clin. Invest. 105 (2000) 329–339.

[40] J. Schindelin, I. Arganda-Carreras, E. Frise, V. Kaynig, M. Longair, T. Pietzsch, S. Preibisch, C. Rueden, S. Saalfeld, B. Schmid, J.-Y. Tinevez, D.J. White, V. Hartenstein, K. Eliceiri, P. Tomancak, A. Cardona, Nat. Methods 9 (2012) 676–682.

[41] K.T. Thurn, H. Arora, T. Paunesku, A. Wu, E.M.B. Brown, C. Doty, J. Kremer, G. Woloschak, Nanomedicine 7 (2011) 123–130.

[42] J. Blatnik, L. Luebke, S. Simonet, M. Nelson, R. Price, R. Leek, L. Zeng, A. Wu, E.M.B. Brown, Microsc. Microanal. 18 (2012) 134–142.

[43] J. Chen, H. Zhou, A.C. Santulli, S.S. Wong, Chem. Res. Toxicol. 23 (2010) 871–879.

[44] C.-Y. Jin, B.-S. Zhu, X.-F. Wang, Q.-H. Lu, Chem. Res. Toxicol. 21 (2008) 1871–1877.

[45] K. Cai, Y. Hou, Y. Hu, L. Zhao, Z. Luo, Y. Shi, M. Lai, W. Yang, P. Liu, Small 7 (2011) 3026–3031.

[46] J. Seo, H. Chung, M. Kim, J. Lee, I. Choi, J. Cheon, Small 3 (2007) 850–853. [47] S.J. Gould, S. Subramani, Anal. Biochem. 175 (1988) 5–13.

[48] A.P. Li, Primary Hepatocyte Cultures as an In Vitro Experimental Model for the Evaluation of Pharmacokinetic Drug–Drug Interactions, Adv. Pharmacol., 1997, pp. 103–130.

[49] J.G. Hengstler, D. Utesch, P. Steinberg, M. Ringel, N. Swales, K. Biefang, K.L. Platt, B. Diener, T. Böttger, T. Fischer, F. Oesch, Drug Metab. Rev. 32 (2000) 81–118.

[50] P. Zhang, W. Liu, Biomaterials 31 (2010) 3087–3094.

[51] V. Diana, P. Bossolasco, D. Moscatelli, V. Silani, L. Cova, PLoS ONE 8 (2013) e78435.

## Supplementary Materials

**Table A.1** Masses of $TiO_2$ nanoparticles, IPA, the PDMS base, and curing agent used to cast PDMS films, weight % $TiO_2$ in the films, film weight, and mass of $TiO_2$ per volume of PDMS.

| Sample | Mass $TiO_2$ (mg) | Mass IPA (g) | Mass PDMS base (g) | Mass PDMS curing agent (g) | Total weight (g) | Est. dry weight (g)[a] | Weight % $TiO_2$ | Film weight (g) | Mass $TiO_2$ /volume PDMS (g/L)[b] |
|---|---|---|---|---|---|---|---|---|---|
| Etched $TiO_2$ | 3.25 | 0.3234 | 0.9425 | 0.1154 | 1.3846 | 1.0676 | 0.30 | 0.2901 | 3.2 |
| **1-Al**-$TiO_2$ | 3.35 | 0.3683 | 0.9266 | 0.1220 | 1.4203 | 1.0593 | 0.32 | 0.2914 | 3.3 |

[a] *Separate measurements showed that 98% of the IPA evaporated during curing of the PDMS film.*
[b] *A value of 0.965 g/cm$^3$ was used for the density of PDMS.*

**Table A.2** Absorption values at 426 and 595 nm and thicknesses for PDMS films containing **1-Al**-functionalized and $H_2O_2$-etched $TiO_2$ nanoparticles, and estimated **1-Al** loading of the $TiO_2$ particles based on absorption measurements.

| Wavelength (nm) | 1-Al-functionalized $TiO_2$ absorbance | Film thickness (cm) | Est. dye extinction coefficient ($M^{-1}cm^{-1}$)[a] | Etched $TiO_2$ absorbance | Film thickness (cm) | 1-Al concentration (M) | 1-Al loading (mg of dye/g of $TiO_2$) |
|---|---|---|---|---|---|---|---|
| 426 | 0.170 | 0.054 | $4.08\times10^4$ | 0.005 | 0.054 | $7.5\times10^{-5}$ | 23 |
| 595 | 0.048 | 0.054 | $7.66\times10^3$ | 0.002 | 0.054 | $1.2\times10^{-4}$ | 36 |

[a] *Extinction coefficients measured in toluene:pyridine (95:5) mixture where the Soret band has an absorption maximum at 436 nm and the Q band has an absorption maximum at 625 nm.*

*Chapter 4*

# DRUG CAPTURE MATERIALS BASED ON GENOMIC DNA-FUNCTIONALIZED MAGNETIC NANOPARTICLES

The final chapter of my thesis is taken from a manuscript that we (my collaborators and I) intend to submit for review and publication around the time of my defense. This project originated from a conversation with a few MDs during a Caltech-UCSF consortium meeting. Mariam Aboian and Caroline Jordan presented work from the Hetts group in the Department of Interventional Radiology at UCSF. These doctors discussed an idea that seemed outlandish in principle but completely useful in practice. They wanted to make chemotherapy regimens less toxic. The Hetts group insisted that by removing chemotherapeutic drugs from the bloodstream after the site of activity, systemic toxicity could be reduced—that meant patients would not be nearly as sick from therapy, improving adherence and prognosis.

The Hetts group shared that they were using DNA as a filtration medium for removing DNA targeting drugs including doxorubicin. The problem they experienced was with device construction. With my background in surface functionalization, I suggested we investigate the use of synthetic DNA on the surface of nanoparticles to help structure devices that could be coated. Little did I know that synthetic DNA could truly be as expensive as I found it to be. More than that, synthetic DNA took months to get our hands on, at least at the scale we needed to make nanoparticle functionalized materials.

Nonetheless, a synthetic approach worked for drug capture, but marginally, and cost dictated that the technology would not be scalable. Bob and I met to discuss results, at which point we thought about using commercially available genomic DNA. It was cheap and abundant but nearly impossible to do chemistry with. After enough brainstorming, we concluded that the only types of chemistry we could do on DNA were crosslinking and alkylating, in line with modern chemotherapeutics. So that was what I did. I prepared what I thought to be an analogue to cisplatin on the surface of iron-oxide using silane linkages bearing diamines.

When reacted with DNA derived from herring, the platinum complex reacted affording a DNA coated nanoparticle. Additional thought went into other methods and we concluded that multi-arm nitrogen mustards would be even more reactive than the platinum species…and they were cheaper!

Michael Schulz, a truly wonderful postdoc, joined in on the project not long after. He helped devise many of the studies we used to evaluate the efficacy of our materials. The project started to pick up traction and after a few months we saw efficacy for drug capture even in whole porcine blood. Nonetheless, the following chapter details the synthesis and evaluation of drug capture materials based on the genomic DNA covalent functionalization of metal-oxide surfaces.

# DRUG CAPTURE MATERIALS BASED ON GENOMIC DNA-FUNCTIONALIZED MAGNETIC NANOPARTICLES

**Authors:** Carl M. Blumenfeld†, Michael D. Schulz†, Mariam S Aboian, Mark W. Wilson, Terilyn Moore, Steven W. Hetts, Robert H. Grubbs*

**One Sentence Summary:** Iron-oxide nanoparticles were functionalized with genomic DNA and used to sequester doxorubicin and other chemotherapy agents from biological solutions both *in vivo* and *in vitro*.

**Abstract:** Chemotherapy agents are notorious for producing severe side-effects. One approach to mitigating this off-target damage is to deliver the chemotherapy directly to a tumor via transarterial infusion, or similar procedures, and then sequestering any chemotherapeutic that enters systemic circulation. Materials capable of such drug capture have yet to be fully realized. We report the first covalent attachment of genomic DNA to surfaces (iron-oxide nanoparticles). With these magnetic materials, we captured three common chemotherapy agents—doxorubicin, cisplatin, and epirubicin—from biological solutions. We achieved >80% capture of doxorubicin from human serum in 1 minute, with 98% capture in 10 minutes, all at physiologically relevant concentrations. Finally, the *in vivo* efficacy of these materials was demonstrated in a porcine model, which showed an 82% reduction in doxorubicin concentration over the length of a particle-coated device. The efficacy of these materials indicates that drug capture is a viable strategy for mitigating chemotherapy-associated side-effects.

The systemic toxicity of chemotherapy is a widely recognized problem in oncology. Off-target damage often persists indefinitely, adversely affects patient survival, and restricts dose and treatment options.[1,2] Direct administration of chemotherapy agents to the tumor via transarterial chemoembolization, or similar procedures, followed by sequestration of any chemotherapeutic that enters systemic circulation would mitigate this damage if materials capable of such drug capture were fully realized.[3,4]

Hepatocellular carcinoma (HCC) is the third leading cause of cancer-related deaths worldwide.[5] Liver transplantation is the most definitive approach for treatment; however, less than 30% of HCC patients are eligible.[6] Direct delivery of drug to a tumor via intraarterial chemotherapy (IAC) and its variant, transarterial chemoembolization (TACE), is often used as a bridge to transplantation, shrinking HCC or at least controlling its growth through recurrent treatments until curative transplant is possible. In cases where surgery is untenable, chemotherapy is often the only recourse. Targeted therapy, however, does not completely eliminate side-effects.

Three of the most common drugs used to treat HCC are doxorubicin (DOX), epirubicin (EPI), and cisplatin (**Fig. 1c**), all of which act on DNA.[7] DOX and EPI function by intercalating between DNA base pairs, while cisplatin is a DNA crosslinker that functions by binding to guanine.[8,9] A major problem for these anticancer compounds is toxicity in non-targeted tissues. DOX and EPI toxicity can result in cardiomyopathy and congestive heart failure.[8–10] Similarly, cisplatin elicits side-effects including extensive nephrotoxicity and neurotoxicity.[11,12] To reduce the likelihood of cardiac toxicity, cumulative dosage of DOX is generally limited by clinicians to 400-450 mg/m$^2$, though lower cumulative dosages (300 mg/m$^2$) are known to increase the risk of congestive heart failure.[13,14] Still, a single standard dose of DOX (50-75mg) can result in severe side-effects, yet higher dosages of DOX are known to be associated with greater tumor suppression. Consequently, a balance must be struck in order to maximize drug dose, leading to better tumor suppression, while simultaneously avoiding catastrophic off-target toxicity. Although limiting a patient's lifetime cumulative dose is the most effective way to avoid cardiotoxicity, this approach necessarily limits anti-cancer efficacy.[15]

The unwanted systemic toxicity of chemotherapy agents has inspired a number of more targeted approaches. One such approach is TACE, during which liver blood flow is occluded in conjunction with administration of high dose chemotherapy directly to the tumor.[3,16] Both during TACE and after liver blood flow is restored, however, up to 50% of residual chemotherapeutics enter systemic circulation and cause off-target toxicity.[17]

Efforts have been made toward reducing non-targeted toxicity during TACE. In 2014 Patel and coworkers proposed chemotherapy filtration devices ("ChemoFilters") that employed sulfonated ion-exchange resins with affinity for DOX. Such a device could be deployed via catheter in the hepatic vein, "downstream" from the site of chemotherapy administration, where it can intercept any residual chemotherapy agents before they reach the heart and enter systemic circulation. They demonstrated a 52% reduction in DOX concentration from porcine serum over 10 minutes, and showed that such a device could be successfully deployed during a simulated TACE procedure.[3] In 2016, the "ChemoFilter" approach inspired the development of more elaborate block copolymer membranes for DOX capture, which achieved up to 90% removal of DOX in 31 minutes from phosphate buffered saline (PBS).[4]

Inspired by the ChemoFilter concept, we designed and synthesized DNA-functionalized materials based on magnetite ($Fe_3O_4$) nanoparticles, capable of rapidly capturing chemotherapy agents. Central to our approach is the direct covalent attachment of genomic DNA. Functionalizing surfaces with DNA has historically involved tagging either the backbone or bases of synthetic DNA with an appropriate moiety, or attaching the DNA via a reactive end-group. These approaches are highly useful and enable complete control of the DNA sequence used resulting in the development of numerous interesting materials;[18–25] however, they are limited by the relatively high cost of synthetic DNA. The synthesis of large amounts of such materials would be prohibitively expensive for most applications.

Functionalization with genomic DNA is an alternative approach that may be appropriate for certain applications; however, this approach is relatively unexplored. Pierre and coworkers recently synthesized magnetic nanoparticles with surface-bound intercalating groups, and showed that such materials can bind to genomic DNA.[26] To our knowledge, however, no one has reported the covalent attachment of genomic DNA to a surface. Here, we report two methods of attaching genomic DNA to nanoparticles, both on multi-gram scale (**Fig. 1a**). We show that the resulting materials are capable of removing DNA-targeting

chemotherapy agents from solution both rapidly and in the presence of potential biological intereferents (e.g., serum proteins and other blood components).

DNA-alkylating agents are a common motif in chemotherapy. By forming covalent crosslinks between DNA strands, these drugs prevent the DNA from being accurately duplicated, ultimately leading to apoptosis. To attach genomic DNA to magnetic nanoparticles, we used an approach analogous to DNA-alkylating/crosslinking drugs (**Fig. 1a**). The first approach was inspired by cisplatin. To synthesize IONP-Pt-DNA samples, the hydroxylated surface of magnetite was silylated with N-(2-aminoethyl)-3-aminopropyltrimethoxysilane exposing a chelating diamine functionality. This sample was treated with an excess of potassium tetrachloroplatinate to create an analogue of cisplatin by which DNA could be anchored to the surface. Cisplatin's cytotoxicity is thought to stem from its coordination with nucleophilic N7-sites of purine bases, resulting in crosslinks.[27] We hoped to accomplish DNA crosslinking to the surface through this mechanism. The sample was then exposed to DNA to produce IONP-Pt-DNA.

The second approach was modeled on nitrogen mustard chemotherapy agents. IONP-HN3-DNA samples were prepared first by functionalizing magnetite with 4-aminobutyltriethoxysilane to install free amines on the surface. This particle was then treated with excess tris(2-chloroethyl)amine hydrochloride (HN3•HCl) to create a scaffold for DNA functionalization. HN3•HCl, the hydrochloride salt of the nitrogen mustard HN3, undergoes aziridinium formation when deprotonated, and is attacked readily by the nucleophilic moieties of DNA.[28] The functionalized particle was exposed to DNA resulting in IONP-HN3-DNA. Both materials were characterized by scanning electron microscopy, electron dispersive scattering, elemental analysis, and infrared spectroscopy (see Supplementary Information).

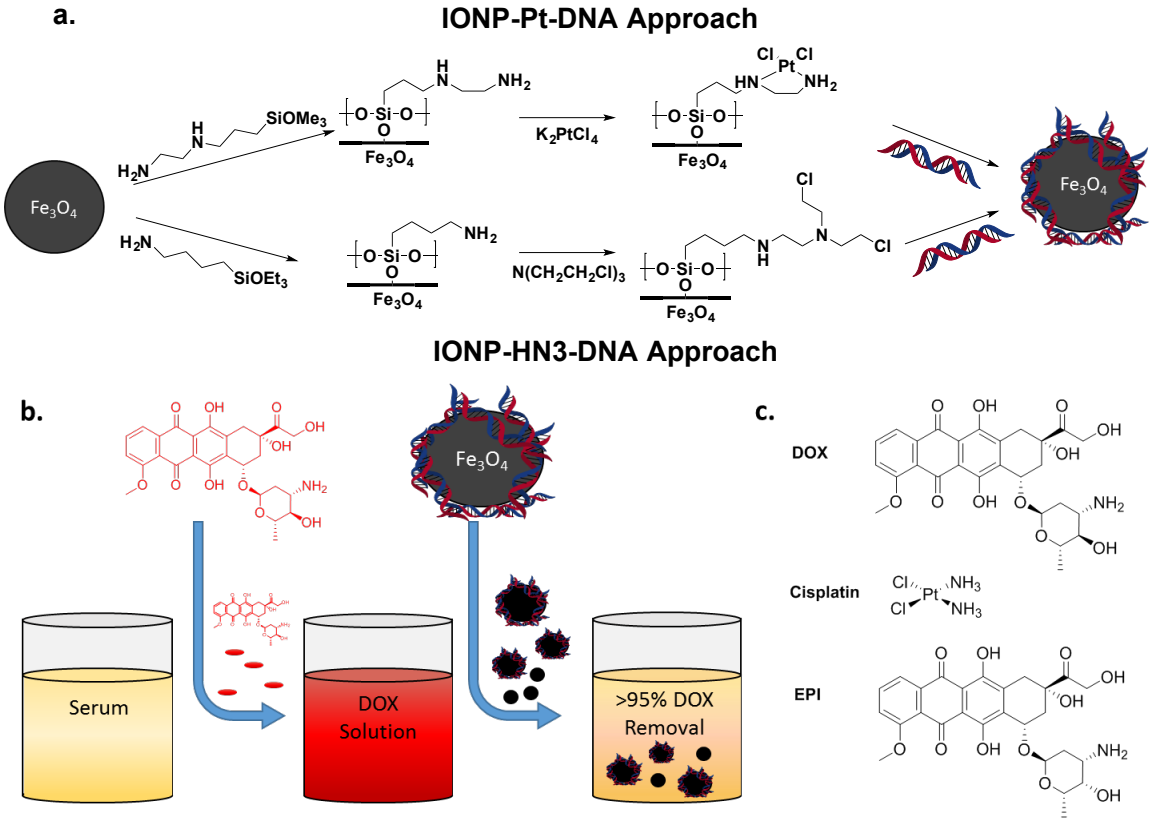


Figure 11: a. Two synthetic approaches for covalently mounting genomic DNA onto iron-oxide nanoparticle (IONP) surfaces. b. Drug capture concept. c. Three common chemotherapy agents used in this study.

In order to evaluate the efficacy of our materials at scavenging chemotherapy agents from solution we studied DOX-binding in human serum at 37 °C to approximate the biological environment in which these materials would have to operate. We found that IONP-HN3-DNA was able to capture 93% of DOX, on average, from a 0.05 mg/mL solution in 25 minutes, while IONP-Pt-DNA averaged 79% (**Fig. 2a**). In both cases, the kinetics were extremely rapid, with about 50% of DOX capture occurring within one minute in the case of IONP-Pt-DNA and over 65% DOX capture occurring within one minute for IONP-HN3-DNA. Based on these results, we carried out all further tests with IONP-HN3-DNA.

Interestingly, both materials were highly effective, despite the known binding of DOX with serum albumin. It is known that DNA intercalation is the kinetically more favorable process,[29,30] and we believe that this kinetic advantage enabled our material to capture DOX from serum solution, despite the thermodynamics being in favor of serum binding overall. We posit that over longer timescales, serum binding would be the dominant process; however, since TACE is a relatively short procedure (<1 h), we believe that kinetic factors will dominate in the performance of any material or device.

Drug capture was also evaluated in porcine whole blood, by measuring DOX plasma concentration over time. We observed some DOX removal due to binding to the non-plasma blood components, which we cannot deconvolute from capture by our materials. Nevertheless, there is rapid reduction of DOX concentration in the blood plasma within 1 minute after exposure to our material, reaching a 92% reduction in DOX plasma concentration over 10 minutes, in stark contrast to the control experiment (**Fig. 2b**). This experiment conclusively demonstrates that our materials are capable of capturing DOX from whole blood.

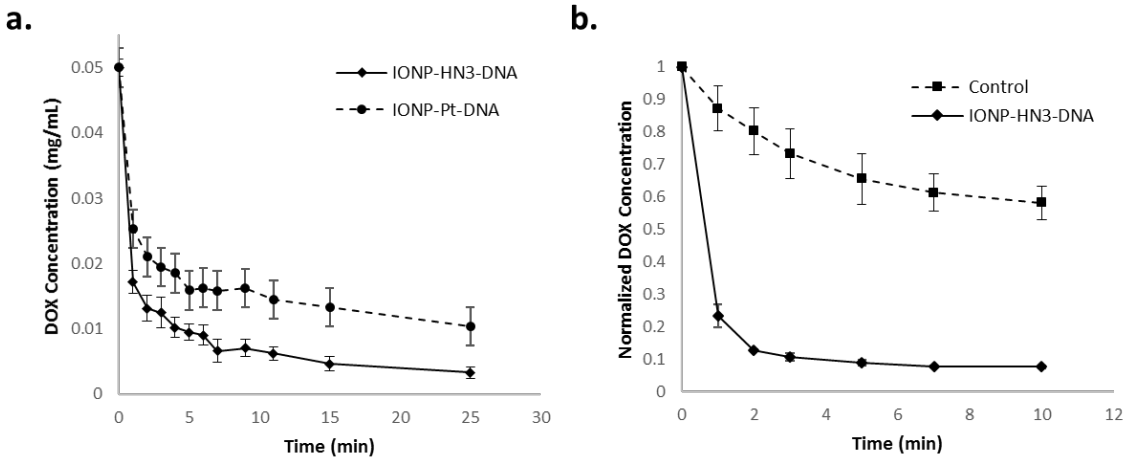


Figure 12: Decrease in DOX concentration in human serum, determined by fluorescence, as a result of DOX capture by IONP-HN3-DNA and IONP-Pt-DNA; 100±5 mg particle in 20 mL (0.05 mg/mL), 1 mg total DOX, 37 °C; error bars = 1 standard deviation (n=3). b. Decrease in DOX plasma concentration as a result of DOX capture by IONP-HN3-DNA from porcine whole blood; 100±5 mg IONP-HN3-DNA in 20 mL (0.05 mg/mL), 1 mg total DOX, 37 °C; error bars = 1 standard deviation (n=3).

To better understand the DOX-capture capacity of IONP-HN3-DNA, we performed a series of experiments in which nanoparticle loading was systematically varied (**Fig. 3a**, further data in the Supplementary Information). These experiments revealed a roughly linear trend in DOX-capture as a function of the amount of particle added, up to a plateau around 100 mg material added per mg DOX, resulting in ~90% DOX capture in 10 minutes. Further DOX capture appears less favorable after this point. We believe this plateau is the result of competition with serum binding, which makes that portion of DOX unavailable for capture by our particles, as well as the typical kinetic effects of diminishing concentration. The absorption of DOX onto the particles was further verified by performing confocal fluorescence microscopy (**Fig. 3b** and **Fig. 3c**). This technique allowed visualization of the fluorescence of DOX bound to the surface of the particles.

Our approach is general for all DNA-targeting chemotherapy agents. To demonstrate this fact, we performed further experiments on two additional common DNA-targeting chemotherapeutics: cisplatin and EPI. We performed an initial cisplatin-binding experiment in PBS solution with IONP-HN3-DNA and monitored the decrease of cisplatin concentration by inductively coupled plasma-mass spectrometry. Approximately 20% of the cisplatin was captured from solution over 30 minutes, with little improvement over longer time periods (see Supplementary Information). We confirmed the presence of captured cisplatin on the surface of the particles by x-ray photoelectron spectroscopy.

Along with DOX and cisplatin, EPI is among the most commonly used chemotherapeutic agents for treating HCC. We evaluated the efficacy of our materials for capturing EPI using a set of experiments analogous to those we used with DOX (see Supplementary Information). Our particles were highly effective at sequestering EPI from serum, with 68% captured after 25 minutes. The sequestered amount would lead to a reduction in unwanted side-effects if achieved *in vivo*.

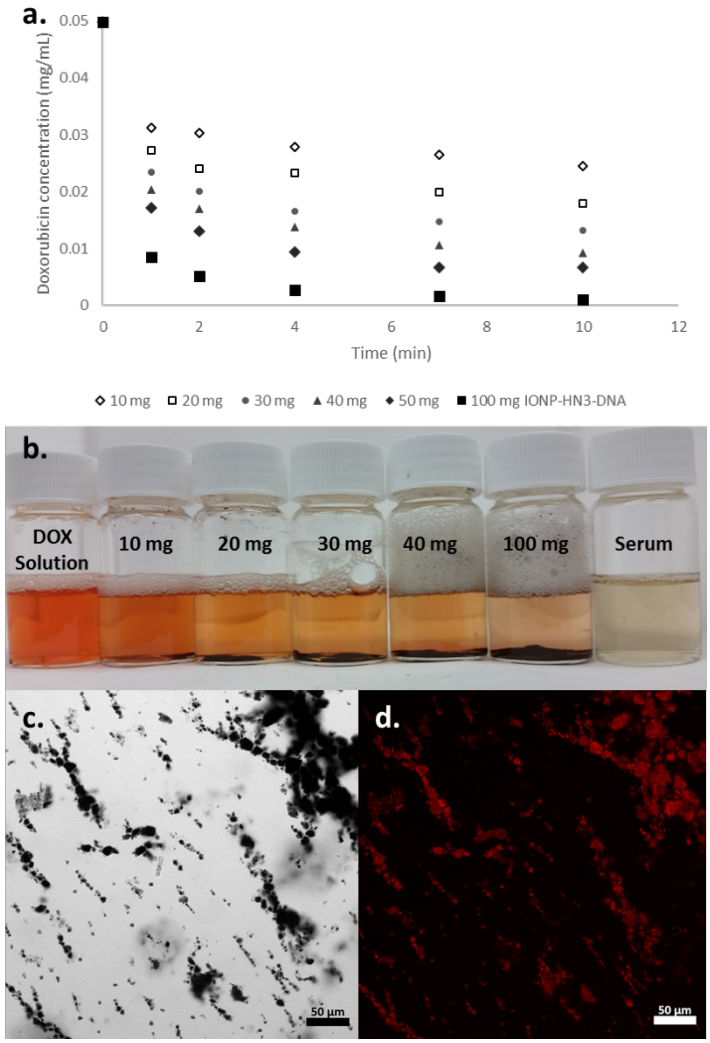


Figure 13: a. DOX capture as a function of the amount of IONP-HN3-DNA from a DOX serum solution (0.5 mg total DOX, 0.05 mg/mL); average of three experiments, data set with error bars in Supplementary Information. b. Resulting serum solutions from experiments summarized in (a). c. Brightfield image of IONP-HN3-DNA aggregates bound to DOX. d. Fluorescence from DOX bound to IONP-HN3-DNA.

A device (**Fig. 4a**) consisting of IONP-HN3-DNA magnetically adhered to the surface of cylindrical rare-earth magnets strung along a PTFE coated nitinol wire was evaluated using a closed loop flow model[3] (see Supplementary Information) and subsequently tested *in vivo* using a porcine model. The device was inserted into the inferior vena cava (IVC) and DOX

was injected over ten minutes into the left common iliac vein proximal to the device (**Fig. 4b**). As the drug flowed through the inferior vena cava, it made contact with the bound IONP-HN3-DNA and was captured. Blood aliquots were taken proximal to, adjacent to the midpoint of, and distal to the device using separate catheters. Peak drug concentration was observed at three minutes since the blood at the injection site had recirculated and live injection was still underway. At peak concentration, a 60% reduction in serum DOX concentration was observed half-way across the device, while a total reduction of 82% was observed at the end of the device (**Fig. 4c,d**).

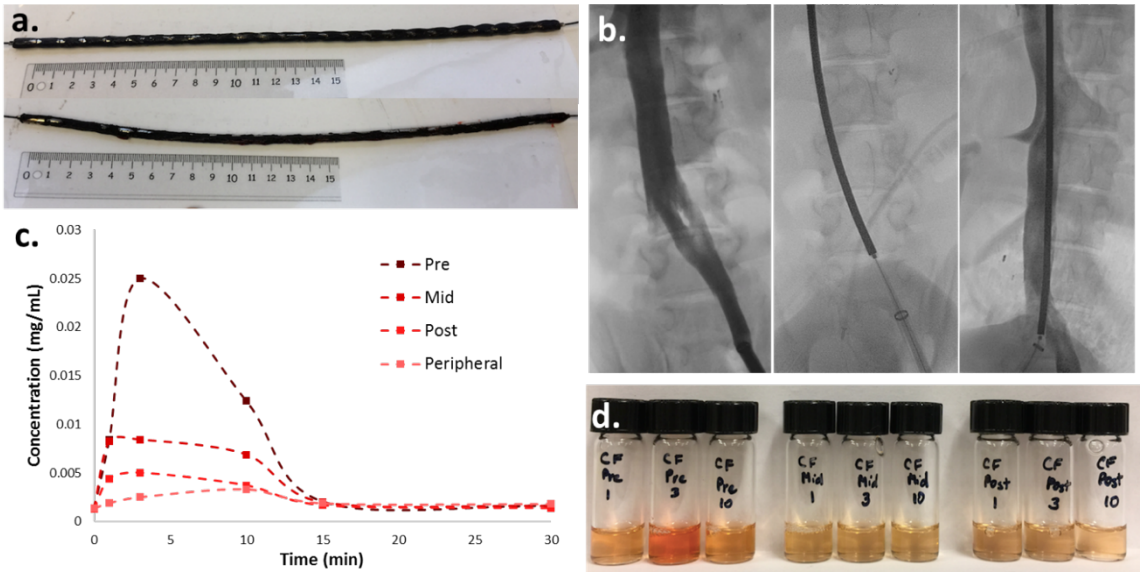


Figure 14: a. Device containing 25 magnets (1 cm x 0.5 cm) with IONP-HN3-DNA coating (above), and the same device after the in vivo experiment (below), demonstrating minimal loss of particles after removal of the device. b. Fluoroscopy images during in vivo porcine experiment demonstrating the inferior vena cava with opacified right renal veins. The device was placed within the inferior vena cava. The sampling catheters were placed immediately proximal to the device, prior to the renal vein, and distal to the device. c. DOX concentration measurements from pre-device, mid-device, post-device, and peripheral locations. d. Plasma solutions from the experiment described in (c).

We have demonstrated two viable synthetic pathways to genomic DNA-functionalized magnetic particles, both on multi-gram scale. To the best of our knowledge, this is the first report of a functional material synthesized with genomic DNA. Moreover, these novel methodologies for DNA surface functionalization are not limited to magnetic metal-oxides, but may also be exploited for other substrates. The synthesized materials captured three commonly used chemotherapy agents from relevant biological solutions (PBS, human serum, or porcine whole blood), at therapeutically relevant concentrations and timescales. This approach is the first to demonstrate such high efficacy and versatility. A proof of concept device was developed, which demonstrated efficient capture of doxorubicin *in vivo*. Similar devices could be readily developed that would reduce the off-target toxicity and damaging side-effects associated with the use of doxorubicin, cisplatin, and epirubicin during TACE or similar procedures. Ultimately, we believe our approach is general for all DNA-targeting chemotherapy drugs, and we hope that this work will provide a foundation for further work on DNA-based materials and drug capture approaches both for oncologic and non-oncologic applications.

**References:**

1.Cleeland, C. S. *et al.* Reducing the toxicity of cancer therapy: recognizing needs, taking action. *Nat. Rev. Clin. Oncol.* **9,** 1–8 (2012).

2.Tatonetti, N. P., Ye, P. P., Daneshjou, R. & Altman, R. B. Data-driven prediction of drug effects and interactions. *Sci Transl Med* **4,** 125ra31 (2012).

3.Patel, A. S. *et al.* Development and Validation of Endovascular Chemotherapy Filter Device for Removing High-Dose Doxorubicin: Preclinical Study. *J. Med. Device.* **8,** 0410081–0410088 (2014).

4.Chen, X. C. *et al.* Block Copolymer Membranes for Efficient Capture of a Chemotherapy Drug. *ACS Macro Lett.* 936–941 (2016).

5.Altekruse, S. F., McGlynn, K. A. & Reichman, M. E. Hepatocellular carcinoma incidence, mortality, and survival trends in the United States from 1975 to 2005. *J. Clin. Oncol.* **27,** 1485–1491 (2009).

6.Belghiti, J. & Kianmanesh, R. Surgical treatment of hepatocellular carcinoma. *HPB (Oxford).* **7,** 42–49 (2005).

7.Marelli, L. *et al.* Transarterial therapy for hepatocellular carcinoma: Which technique is more effective? A systematic review of cohort and randomized studies. *Cardiovasc. Intervent. Radiol.* **30,** 6–25 (2007).

8.Cheung-Ong, K., Giaever, G. & Nislow, C. DNA-Damaging Agents in Cancer Chemotherapy: Serendipity and Chemical Biology. *Chem. Biol.* **20,** 648–659 (2013).

9.Minotti, G., Menna, P., Salvatorelli, E., Cairo, G. & Gianni, L. Anthracyclines: molecular advances and pharmacologic developments in antitumor activity and cardiotoxicity. *Pharmacol. Rev.* **56,** 185–229 (2004).

10.Ryberg, M. *et al.* Epirubicin cardiotoxicity: An analysis of 469 patients with metastatic breast cancer. *J. Clin. Oncol.* **16,** 3502–3508 (1998).

11.Miller, R. P., Tadagavadi, R. K., Ramesh, G. & Reeves, W. B. Mechanisms of cisplatin nephrotoxicity. *Toxins (Basel).* **2,** 2490–2518 (2010).

12.Wang, D. & Lippard, S. J. Cellular processing of platinum anticancer drugs. *Nat. Rev. Drug Deliv.* **4,** 307–320 (2005).

13.Rahman, A. M., Yusuf, S. W. & Ewer, M. S. Anthracycline-induced cardiotoxicity and the cardiac-sparing effect of liposomal formulation. *Int. J. Nanomedicine* **2,** 567–583 (2007).

14.Buzdar, A. U., Marcus, C., Smith, T. L. & Blumenschein, G. R. Early and delayed clinical cardiotoxicity of doxorubicin. *Cancer* **55,** 2761–2765 (1985).

15.Yeh, E. T. H. & Bickford, C. L. Cardiovascular Complications of Cancer Therapy. *J. Am. Coll. Cardiol.* **53,** 2231–2247 (2009).

16.Tsochatzis, E. A., Germani, G. & Burroughs, A. K. Transarterial Chemoembolization, Transarterial Chemotherapy, and Intra-arterial Chemotherapy for Hepatocellular Carcinoma Treatment. *Semin. Oncol.* **37,** 89–93 (2010).

17.Hwu, W. J. *et al.* A clinical-pharmacological evaluation of percutaneous isolated hepatic infusion of doxorubicin in patients with unresectable liver tumors. *Oncol Res* **11,** 529–537 (1999).

18.Hurst, S. J. *et al.* Synthetically programmable DNA binding domains in aggregates of DNA-functionalized gold nanoparticles. *Small* **5,** 2156–2161 (2009).

19.Cohen, G., Deutsch, J., Fineberg, J. & Levine, A. Covalent attachment of hybridizable oligonucleotides to glass supports. *Nucleic Acids Res.* **25,** 911–912 (1997).

20.Beier, M. & Hoheisel, J. D. Versatile derivatisation of solid support media for covalent bonding on DNA-microchips. *Nucleic Acids Res.* **27,** 1970–1977 (1999).

21.Kumar, A., Larsson, O., Parodi, D. & Liang, Z. Silanized nucleic acids: a general platform for DNA immobilization. *Nucleic Acids Res.* **28,** E71 (2000).

22.Yao, G. *et al.* Clicking DNA to gold nanoparticles: poly-adenine-mediated formation of monovalent DNA-gold nanoparticle conjugates with nearly quantitative yield. *NPG Asia Mater.* **7,** e159 (2015).

23.Mirkin, C. A., Letsinger, R. L., Mucic, R. C. & Storhoff, J. J. A DNA-based method for rationally assembling nanoparticles into macroscopic materials. *Nature* **382,** 607–609 (1996).

24.Macfarlane, R. J. *et al.* Nanoparticle superlattice engineering with DNA. *Science* **334,** 204–8 (2011).

25.Lipshutz, R. J., Fodor, S. P., Gingeras, T. R. & Lockhart, D. J. High density synthetic oligonucleotide arrays. *Nat. Genet.* **21,** 20–4 (1999).

26.Smolensky, E. D., Peterson, K. L., Weitz, E. A., Lewandowski, C. & Pierre, C. Magnetoluminescent Light Switches − Dual Modality in DNA Detection Eric. *J. Am. Chem. Soc.* **135,** 8966–8972 (2013).

27.Siddik, Z. H. Cisplatin: mode of cytotoxic action and molecular basis of resistance. *Oncogene* **22,** 7265–79 (2003).

28.Polavarapu, A., Stillabower, J. A., Stubblefield, S. G. W., Taylor, W. M. & Baik, M. H. The mechanism of guanine alkylation by nitrogen mustards: A computational study. *J. Org. Chem.* **77,** 5914–5921 (2012).

29.Agudelo, D. *et al.* Probing the binding sites of antibiotic drugs doxorubicin and N-(trifluoroacetyl) doxorubicin with human and bovine serum albumins. *PLoS One* **7,** 1–13 (2012).

30.Agudelo, D., Bourassa, P., Bérubé, G. & Tajmir-Riahi, H. A. Intercalation of antitumor drug doxorubicin and its analogue by DNA duplex: Structural features and biological implications. *Int. J. Biol. Macromol.* **66,** 144–150 (2014).

**Acknowledgments:**

The authors gratefully acknowledge the financial support from the NIH (R01CA194533, Hetts; 5T32EB001631-13, Aboian). Confocal imaging was performed in the Biological Imaging Facility, with the support of the Caltech Beckman Institute and the Arnold and Mabel Beckman Foundation. The authors additionally acknowledge support from the Beckman Institute of the California Institute of Technology to the Molecular Materials Research Center. The authors wish to thank Dr. Andres Collazo for assistance with imaging, Mr. Daryl Yee for assistance with X-ray photoelectron spectroscopy, and Wesley Kuo for performing flow model experiments and for assisting with fluoroscopy image acquisition

during *in vivo* porcine experiments. We would like to thank UCSF Interventional Radiology laboratory members for assisting with *in vivo* porcine experiments including Carol Stillson, Dr. Maythem Saeed, Anqi Liang, Joshua Fisher, Jay Yu, and Dr. Caroline Jordan. We would also like to thank Sravani Kondapavulur for expert advice on the assembly of the magnetic device.

**Author contributions:**

C.M.B. designed nanostructured materials and synthesized materials. M.D.S. conceived experimental concepts. C.M.B. and M.D.S. performed *in vitro* experiments. S.W.H. conceived the notion of chemotherapeutic removal. R.H.G., S.W.H., and M.W.W. supervised the project. M.S.A conceived the use of genomic DNA for binding chemotherapeutics and carried out proof of concept experiments, and performed and designed *in vivo* experiments with magnetic device. T.M. supervised and performed *in vivo* experiments. All authors discussed the results.

**Supplementary Information:**

**Materials and Methods:**

*Instrumentation:* Fluorescence measurements were made using a 96-well plate on a Molecular Devices FlexStation 3 Multi-mode microplate reader. Scanning electron micrographs (SEM) as well as electron dispersive scattering (EDS) measurements were made on a Zeiss 1550VP Field Emission SEM equipped with an Oxford EDS module. Inductively coupled plasma-mass spectrometry (ICP-MS) was carried out on an HP 4500 ICP-MS equipped with a Cetac ASX-500 autosampler. Infrared measurements were made on a Nicolet iS50 Fourier Transform Infrared spectrometer equipped with a DuraScope ATR unit. C, H, N analyses were carried out using a PerkinElmer 2400 Series II CHN Elemental Analyzer.

*General Procedures:* Unless otherwise stated reactions were carried out on the bench. Magnetite ($Fe_3O_4$, 40 nm APS, 99%) was purchased from Nanostructured & Amorphous

Materials, Inc. Silane reagents were purchased from Gelest, Inc. Genomic DNA (isolated from Herring sperm), human serum (OptiClear), and cisplatin were purchased from Sigma Aldrich. Doxorubicin was purchased from LC Labs and epirubicin was purchased from Biotang Inc. Potassium tetrachloroplatinate was purchased from Pressure Chemicals. All reagents not otherwise mentioned were purchased from Sigma Aldrich, and were used without further purification.

Device construction: 25 cylindrical rare earth magnets (N52 grade, 5mm OD x 1mm ID x 5mm L, magnetized through the diameter) were strung along the length of a PTFE coated nitinol wire (Terumo Glidewire). IONP-HN3-DNA (1.0 g) was suspended in water and subsequently magnetically adhered to the surface of this device.

Flow Model experiments: A closed-circuit flow model was used to measure doxorubicin clearance in a setting the simulates suprahepatic inferior vena cava conditions.[1,2] In this model, the porcine blood is circulated through the polyvinyl chloride tubing at a rate of approximately 150 ml/min. The tubing size matches the average human hepatic vein measuring 1.2 cm as described previously.[3] Testing was performed with 200 ml porcine blood and samples were obtained from the tubing downstream from the device.

*In vivo* porcine experiments: *In vivo* device testing was performed in farm swine (n=1, 45-50 kg), which was under humane care. Experimentation was under compliance with UCSF IACUC protocols. The animal was monitored with blood pressure, pulse oximetry, heart rate, and electrocardiogram while under general anesthesia with isoflurane. Using fluoroscopic guidance, an 18Fr sheath was placed into the left external iliac vein for introduction of the device. A pre-device sampling catheter was introduced through the right external iliac vein with the tip terminating in the left common iliac vein near the bifurcation. An additional catheter was introduced via the right internal jugular vein with the tip distal to the device in the IVC (post-device). The mid-device catheter and peripheral catheters were introduced through the left internal jugular vein. Prior to the start of the experiments, patency of the

venous system was demonstrated using contrast injection (Omnipaque). Doxorubicin was injected over ten minutes at a rate of 2.5 ml/min into the left common iliac vein proximal to the magnetic device. The pre-device doxorubicin concentration was measured by sampling with a 5 Fr catheter downstream of the doxorubicin infusion. Blood aliquots were taken proximal to, adjacent to the midpoint of, and distal to the device using separate catheters. To clear the sampling catheters, 2 mL of blood was drawn immediately prior to taking the aliquot (3 mL). The blood samples were placed on ice until they were centrifuged to isolate the plasma fraction for analysis. A control experiment was also performed using the same procedures but with no device inserted.

*Particle Synthesis:*

**IONP-Pt**: 3.31 g Magnetite ($Fe_3O_4$) was dried *in vacuo* at 120° Celsius. Upon cooling, the sealed material was introduced into an inert atmosphere nitrogen glovebox. To the magnetite was added 23 mL anhydrous toluene along with 4 mL N-(2-aminoethyl)-3-aminopropyltrimethoxysilane. The reaction was mechanically stirred on the bench at 110° Celsius for 2 hours and subsequently dried *in vacuo* at 110° Celsius for 20 hours. The reaction mixture along with 1.0 g $K_2PtCl_4$, was stirred at 70° Celsius for 21 minutes and then washed three times with water. Following this, the mixture was diluted to a total volume of 450 mL with 18.2 MΩ water was treated with 1.3 g KCl and an additional 10 mL water.

**IONP-Pt-DNA**: IONP-Pt materials along with 5.1 g deoxyribonucleic acid from herring sperm were mechanically stirred in 450 mL 18.2 MΩ water at 37° Celsius for 20 hours. To ensure covalent attachment as opposed to being physically adsorbed, the particles were isolated from the reaction mixture, washed three times under vigorous mechanical stirring with 18.2 MΩ water (400 mL), frozen, and lyophilized to afford 3.08 g IONP-Pt-DNA.

**IONP-NH2**: 4.2 g Of magnetite ($Fe_3O_4$) was dried *in vacuo* at 120° Celsius. The $Fe_3O_4$ was allowed to cool to room temperature under vacuum. To the $Fe_3O_4$ was added 25 mL toluene

(freshly dried over magnesium sulfate) and 3.2 mL 4-aminobutyltriethoxysilane. The reaction was sealed and stirred mechanically for 2 hours at 120° Celsius. The reaction was removed from heat and the particles were isolated from the toluene solution. The reaction mixture was washed once with toluene and subsequently dried *in vacuo* at 120° Celsius for 1 hour and 45 minutes. 4.02 g of IONP-HN3 was isolated.

**IONP-HN3-DNA**: 3.4750 g IONP-HN3 was added to a vial along with 1.02 g tris(2-chloroethyl)amine hydrochloride and dimethylformamide (30 mL). The reaction was stirred mechanically for 1 hour at room temperature, at which point the particles were isolated from the dimethylformamide. The particles were then washed three times with dimethylformamide. The isolated particle as well as 3.35g deoxyribonucleic acid from herring sperm were transferred into a flask along with 400 mL 18.2 MΩ water. The reaction was mechanically stirred at 38° Celsius for 17 hours and 45 minutes. To ensure covalent attachment, the particles were then washed thoroughly under vigorous mechanical stirring three times with 18.2 MΩ water (400 mL) and magnetic separation. The particles were then frozen in liquid nitrogen and lyophilized to afford 3.79 g of IONP-HN3-DNA.

*Representative Binding Studies*:

**DOX:** To a scintillation vial was added 19 mL human serum. Drug was injected at a concentration of 1 mg/mL from a concentrated stock, to bring the total concentration to approximately .05 mg/mL. An initial time point is taken before drug capture. DNA particles (100±5 mg) is added to the serum mixture, which is constantly, mechanically stirred. 20 seconds before a time point is taken, a strong, rare earth, magnet is used to isolate the particles at which point a 100 μL aliquot is taken and placed in a 96 plate microplate well. The solutions are then measured by way of fluorescence on a microplate reader.

**Cisplatin**: Phosphate buffered saline solution (19 mL) was added to a scintillation vial. Cisplatin solution (1 mL, 1 mg/mL solution) was then injected, followed by 117±5 mg of IONP-HN3-DNA, and the mixture was mechanically stirred over the course of an hour. At predetermined time points the magnetic materials were temporarily isolated using an external

magnet so that 100 μL aliquots could be taken, which were diluted 200X in 2% nitric acid solution and subsequently analyzed by ICP-MS to determine the concentration of platinum remaining in solution.

**EPI:** Human serum (19 mL) was added to a scintillation vial. EPI solution in water (1 mL, 1 mg/mL solution) was then added. The particles (100±5 mg IONP-HN3-DNA) were then added and the solution was mechanically stirred over the course of 25 minutes. At predetermined time points, the magnetic materials were temporarily isolated using an external magnet and 100 μL aliquots were taken, which were subsequently diluted 100X in water and analyzed by fluorescence on a microplate reader in order to characterize the amount of EPI remaining in solution.

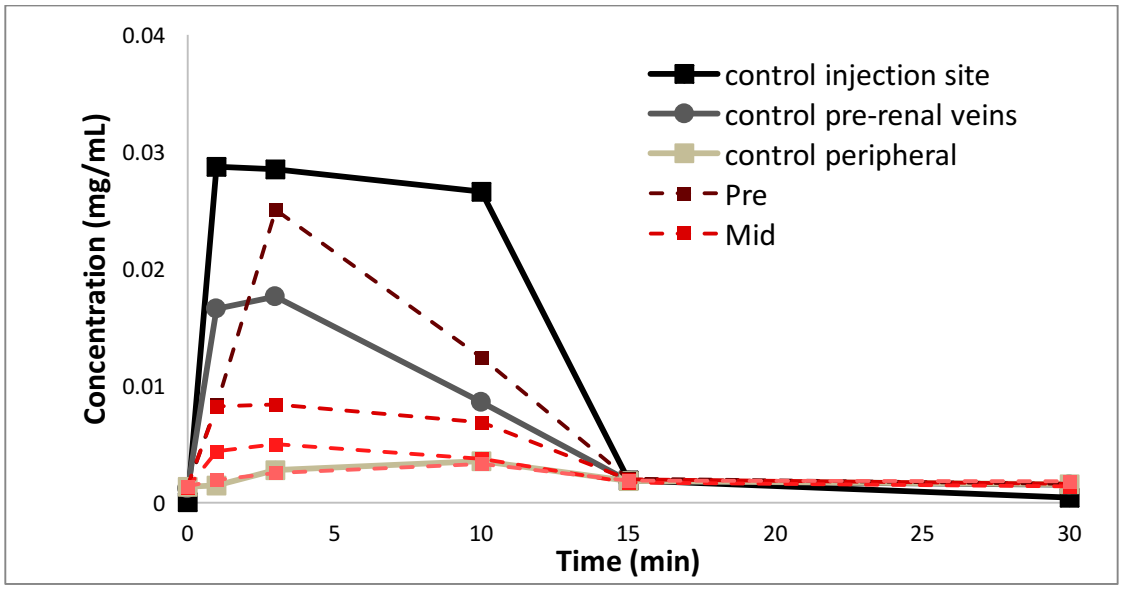


**Supplementary Figure 1.** ***In-vivo*** **capture data for both control (no device) and IONP-HN3-DNA coated device.**

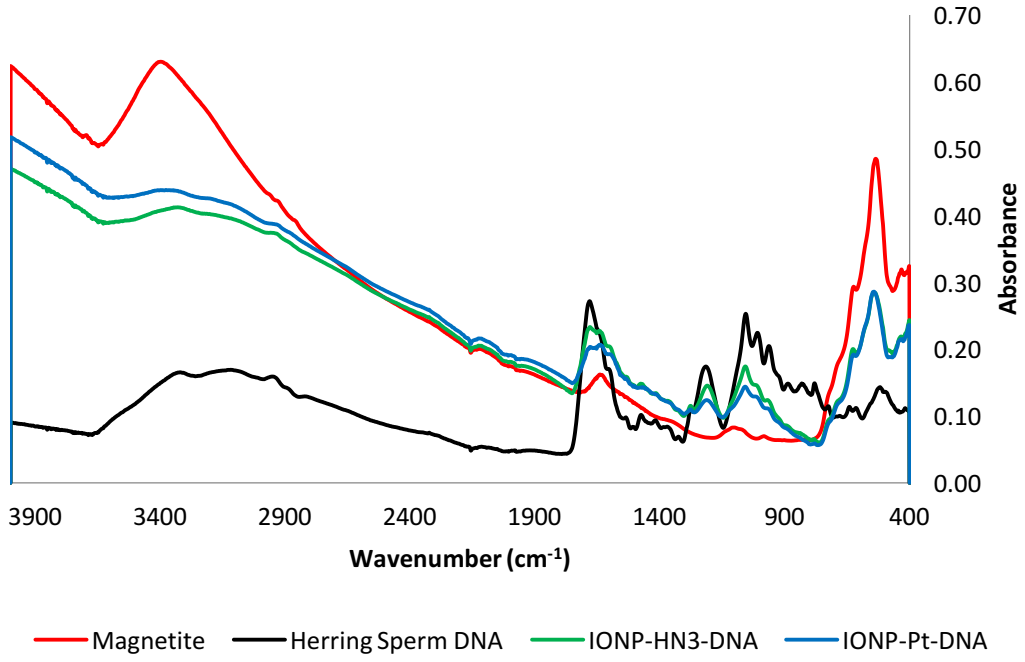


**Supplementary Figure 2. Full ATR-IR spectrum of magnetite, genomic DNA, and DNA-functionalized particles (IONP-HN3-DNA and IONP-Pt-DNA).**

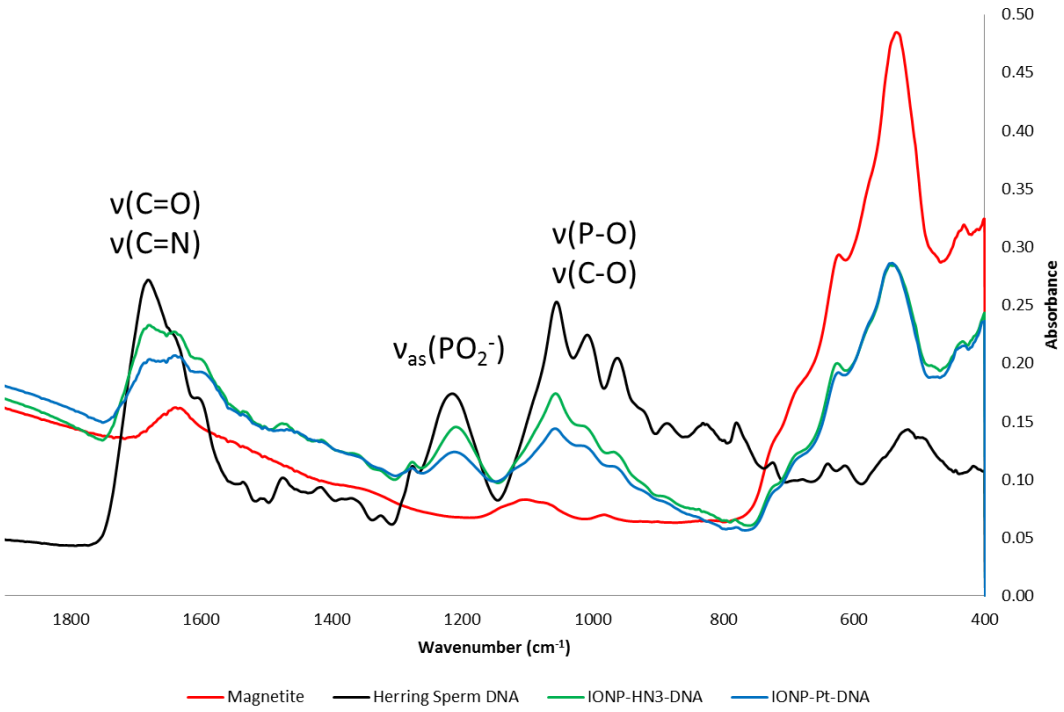


**Supplementary Figure 3. ATR-IR spectrum (1800-400 $cm^{-1}$) of magnetite, genomic DNA, and DNA-functionalized particles [IONP-HN3-DNA and IONP-Pt-DNA].[4]**

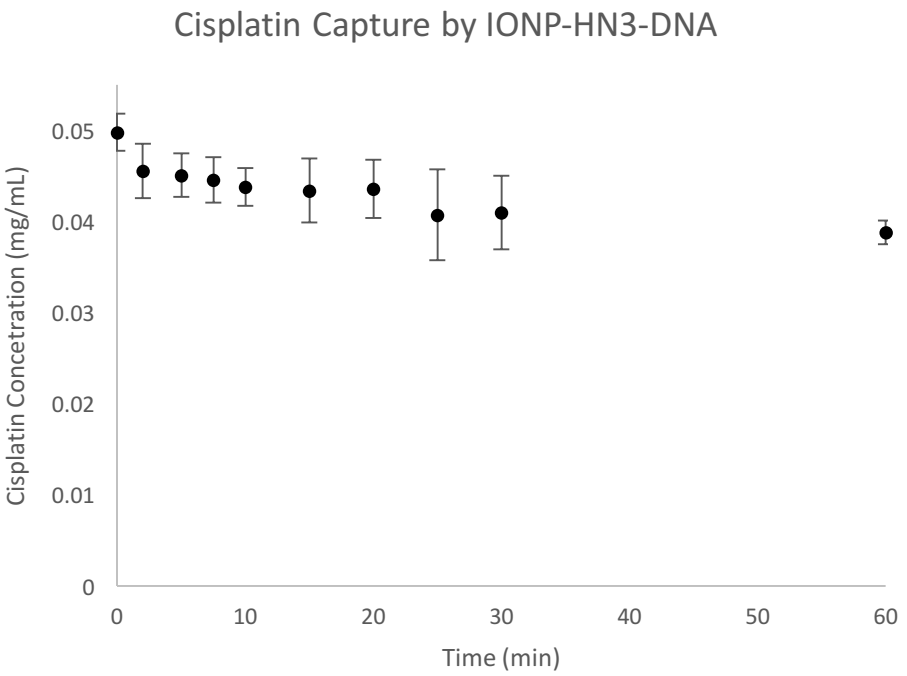


**Supplementary Figure 4. Reduction of cisplatin concentration over time due to capture by IONP-HN3-DNA particles, as characterized by ICP-MS. Cisplatin solution (20 mL, 0.05 mg/mL) with 100 mg IONP-HN3-DNA. Average of three runs (error bars = 1 standard deviation).**

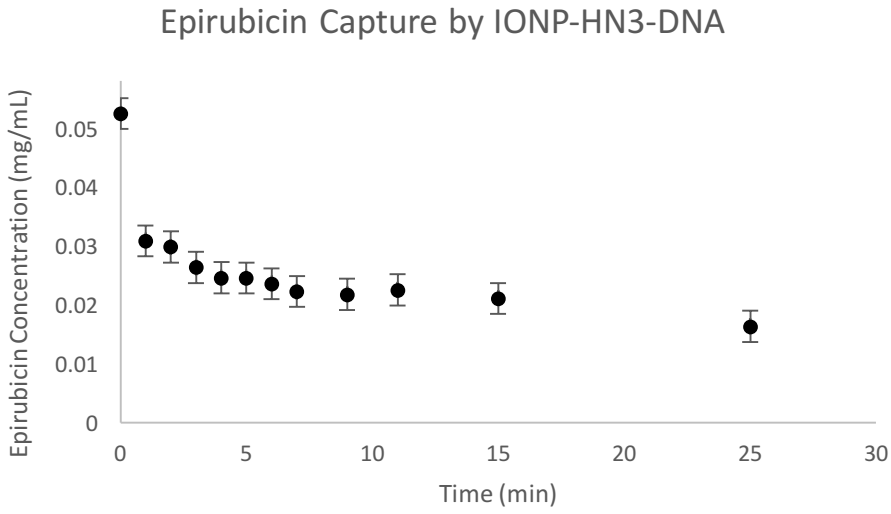


**Supplementary Figure 5. Reduction of EPI concentration over time due to capture by IONP-HN3-DNA as characterized by fluorescence measurements. EPI solution (20 mL, 0.05 mg/mL) with 100 mg IONP-HN3-DNA. Average of three runs (error bars = 1 standard deviation).**

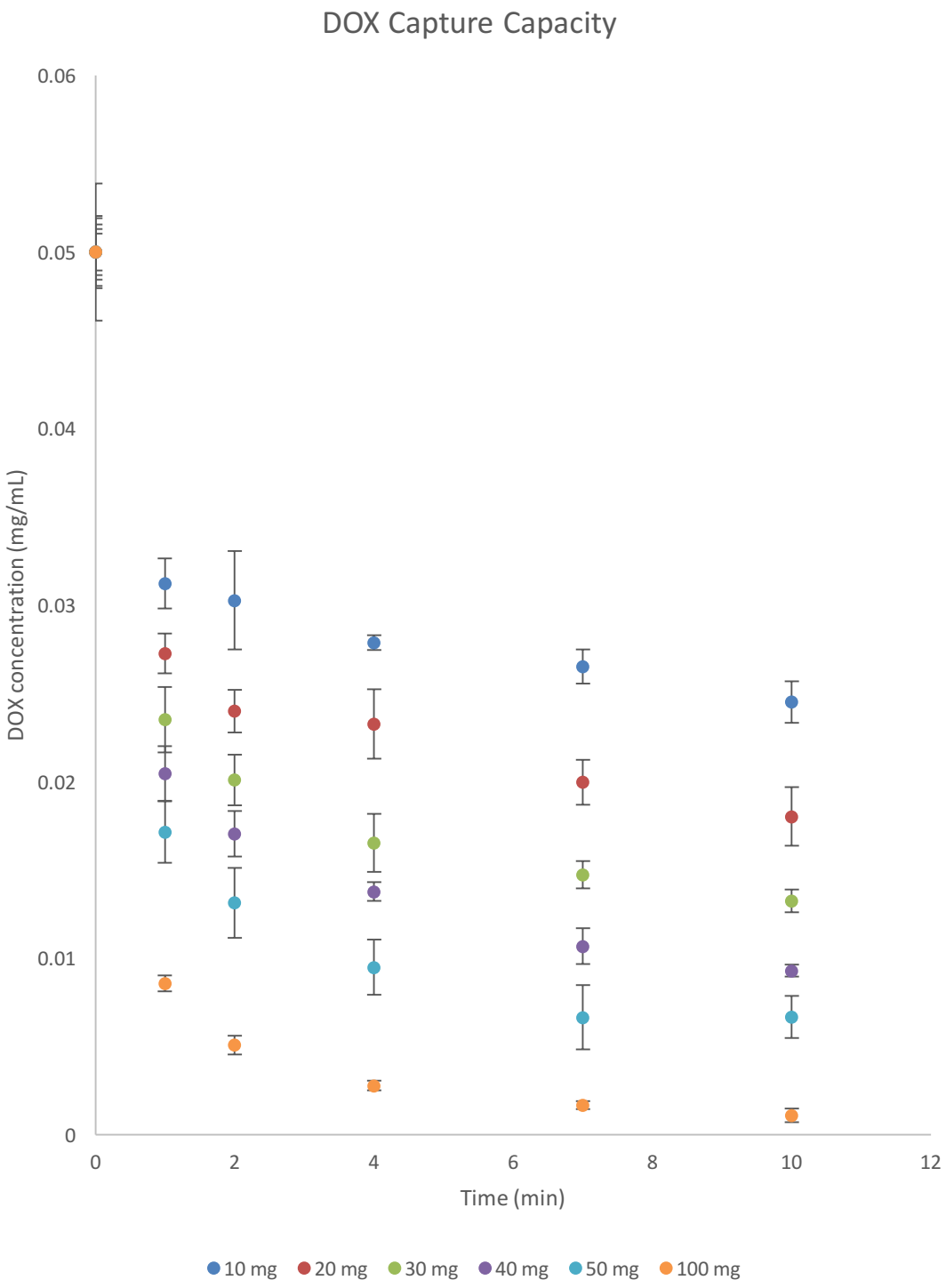


**Supplementary Figure 6. DOX capture as a function of particle loading. Average of three runs (error bars = 1 standard deviation).**

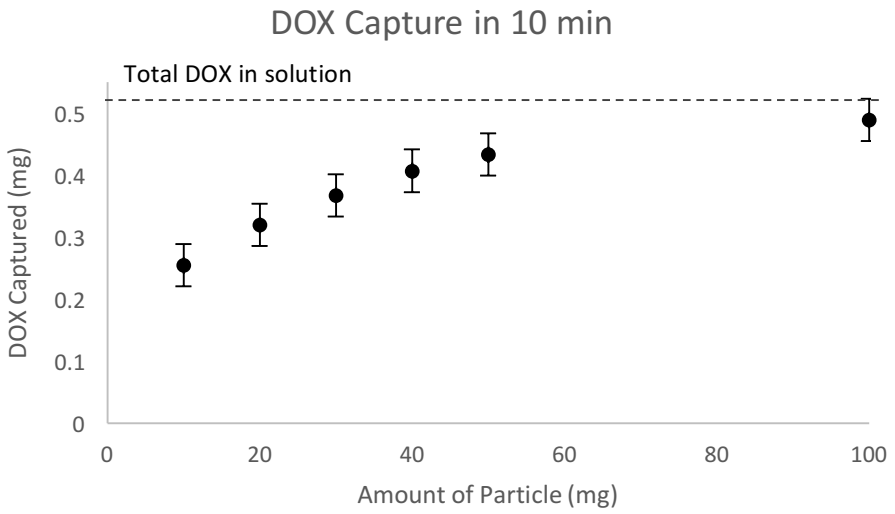


**Supplementary Figure 7. DOX capture in 10 minutes from human serum (10 mL, 0.05 mg/mL, 37 °C) as a function of amount of IONP-HN3-DNA added. Average of 3 runs, error bars = 1 standard deviation.**

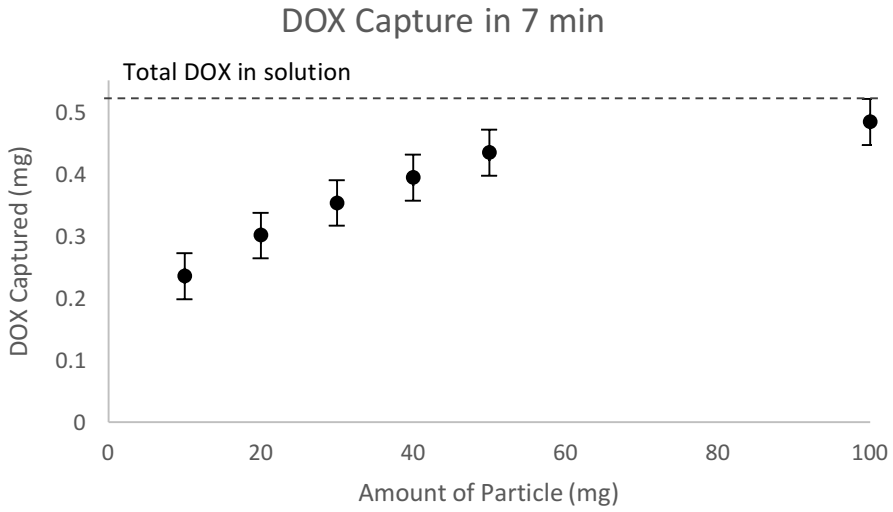


**Supplementary Figure 8. DOX capture in 7 minutes from human serum (10 mL, 0.05 mg/mL, 37 °C) as a function of amount of IONP-HN3-DNA added. Average of 3 runs, error bars = 1 standard deviation.**

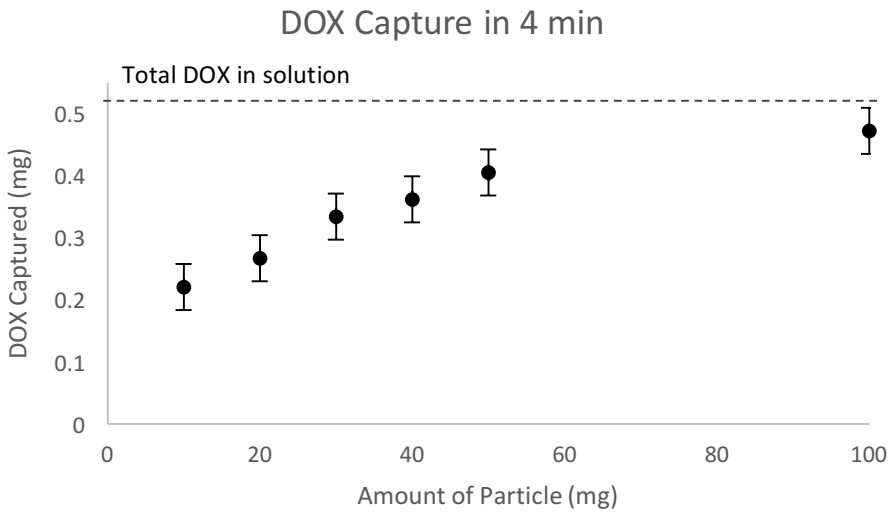


**Supplementary Figure 9. DOX capture in 4 minutes from human serum (10 mL, 0.05 mg/mL, 37 °C) as a function of amount of IONP-HN3-DNA added. Average of 3 runs, error bars = 1 standard deviation.**

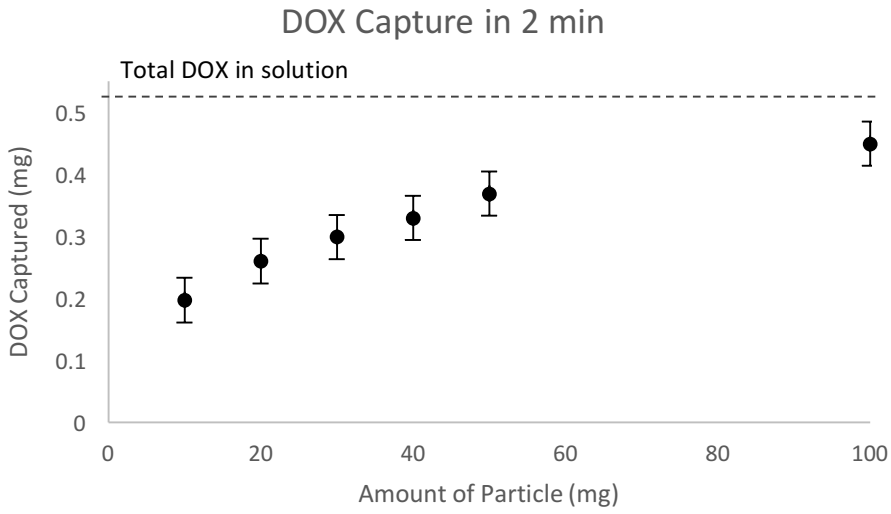


**Supplementary Figure 10. DOX capture in 2 minutes from human serum (10 mL, 0.05 mg/mL, 37 °C) as a function of amount of IONP-HN3-DNA added. Average of 3 runs, error bars = 1 standard deviation.**

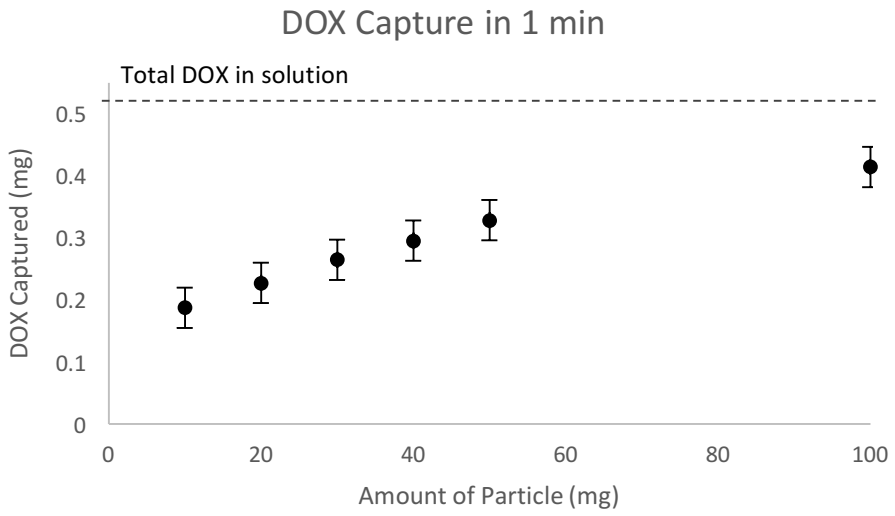


**Supplementary Figure 11. DOX capture in 1 minute from human serum (10 mL, 0.05 mg/mL, 37 °C) as a function of amount of IONP-HN3-DNA added. Average of 3 runs, error bars = 1 standard deviation.**

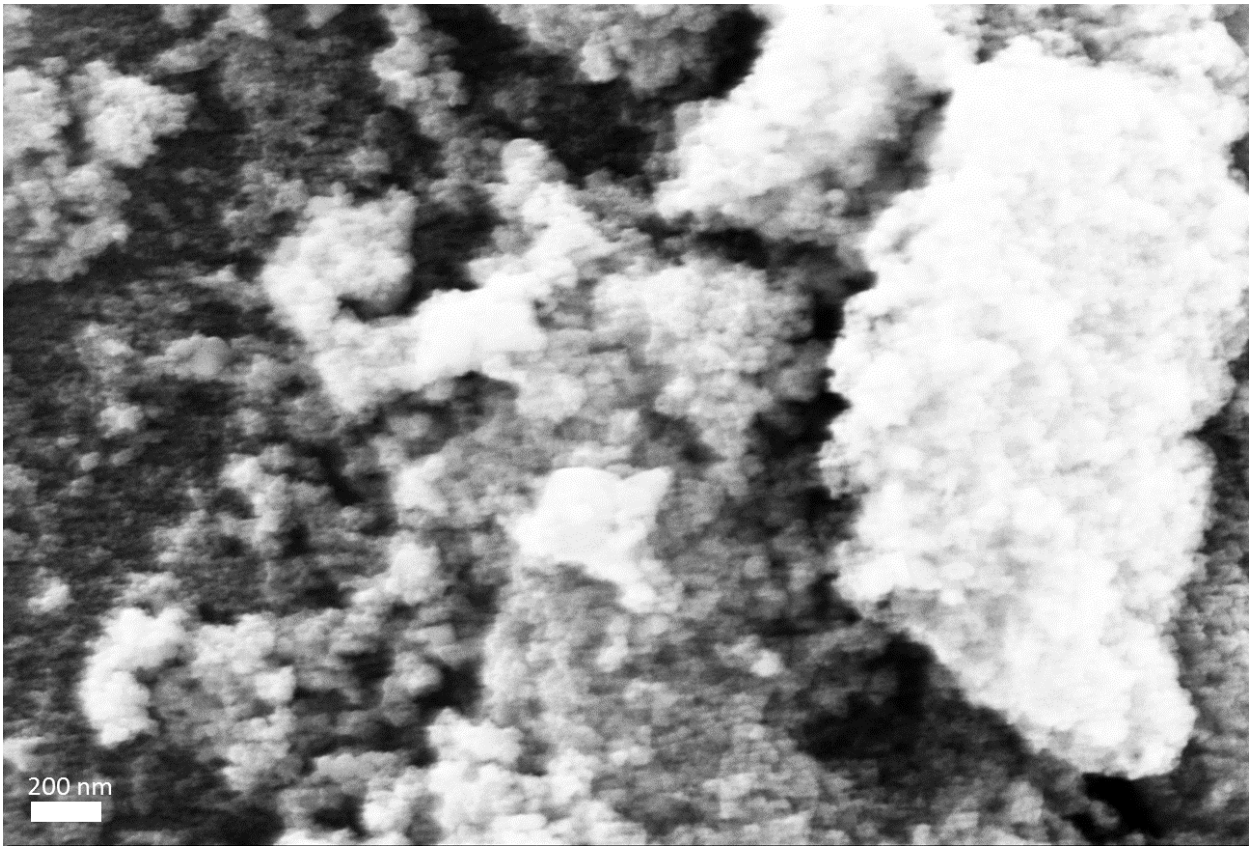


**Supplementary Figure 12. SEM image of $Fe_3O_4$ particles.**

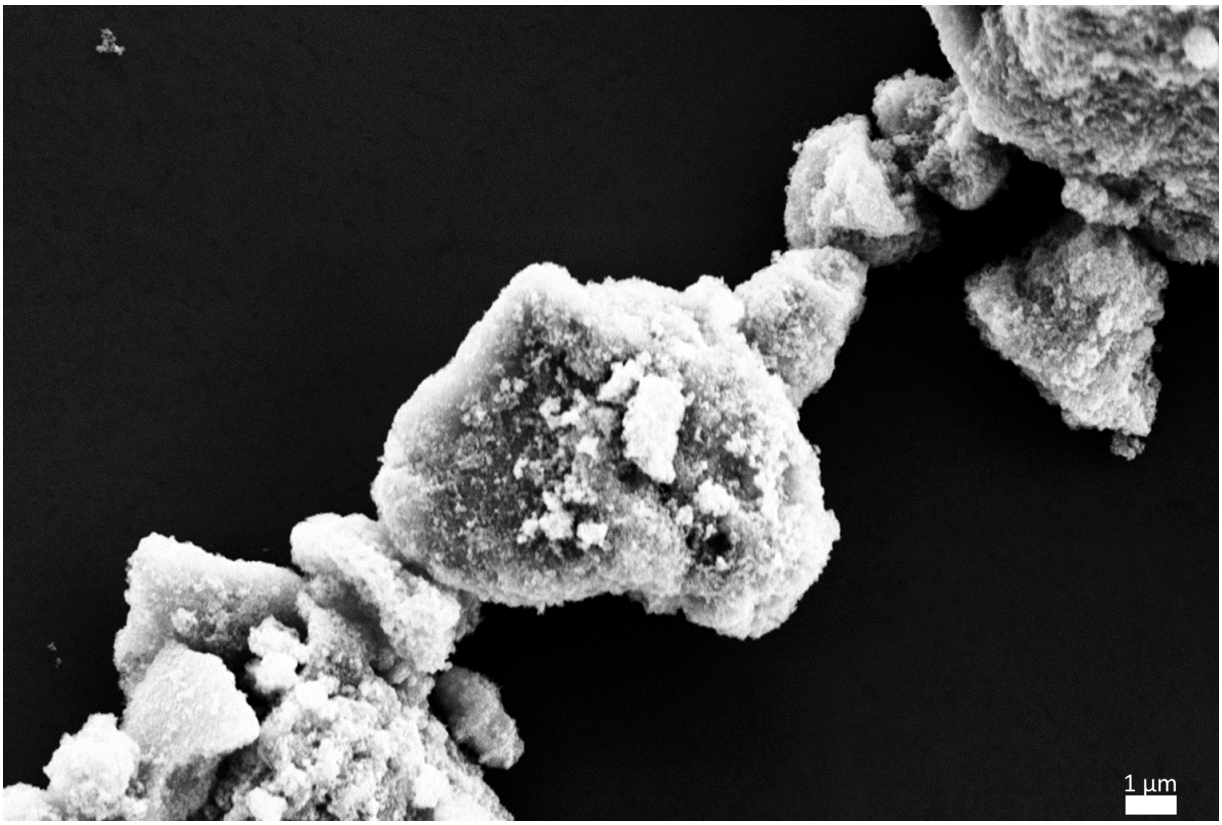


**Supplementary Figure 13. SEM image of $Fe_3O_4$ particle aggregates.**

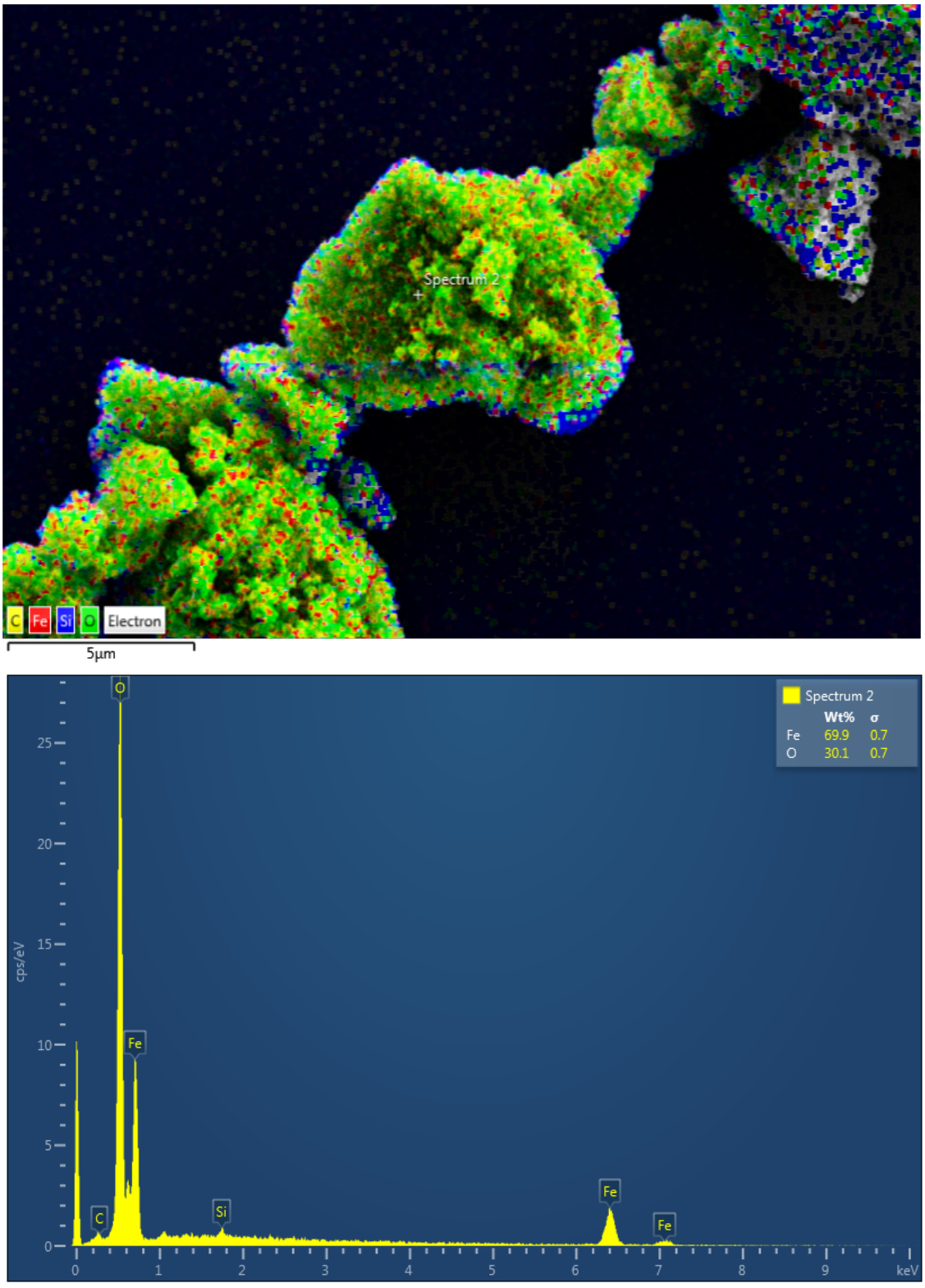


**Supplementary Figure 14. EDS map and spectrum of $Fe_3O_4$ particle aggregates.**

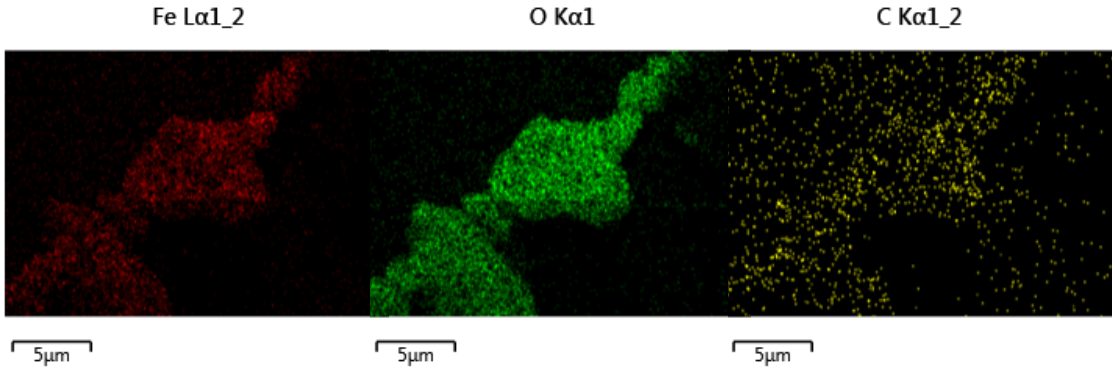


**Supplementary Figure 15. EDS element maps of $Fe_3O_4$ particle aggregates.**

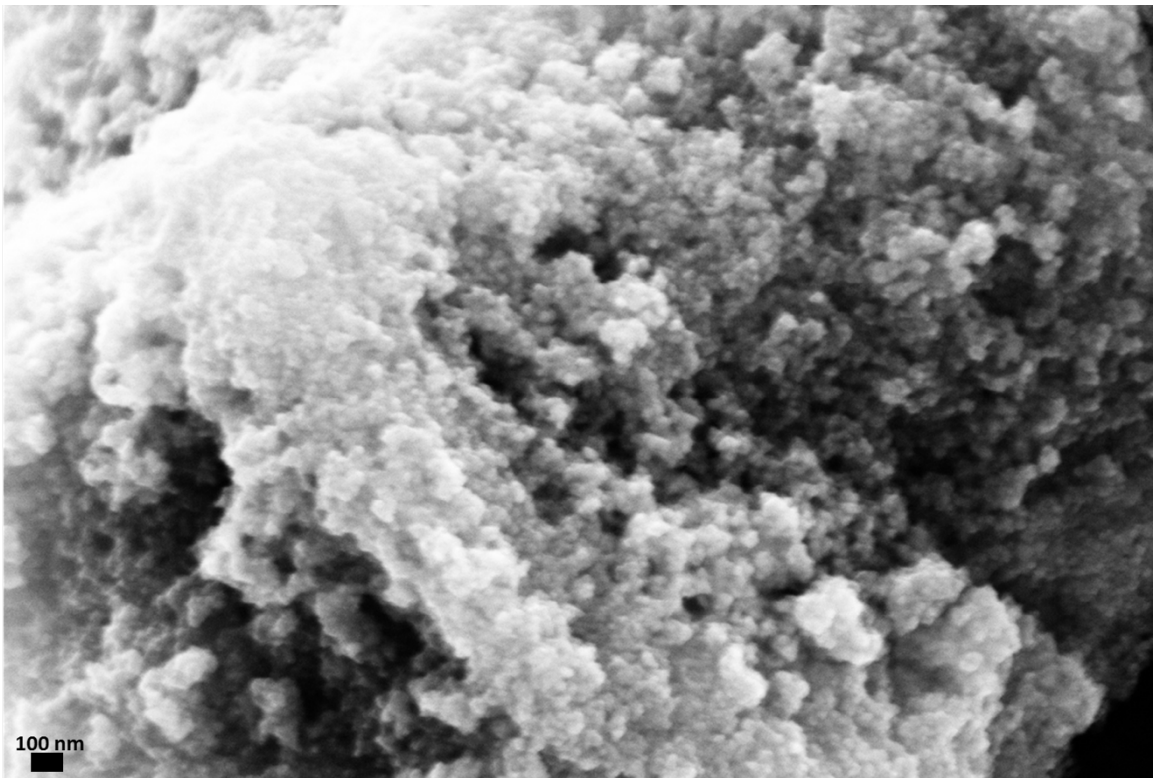


**Supplementary Figure 16. SEM image of IONP-HN3-DNA.**

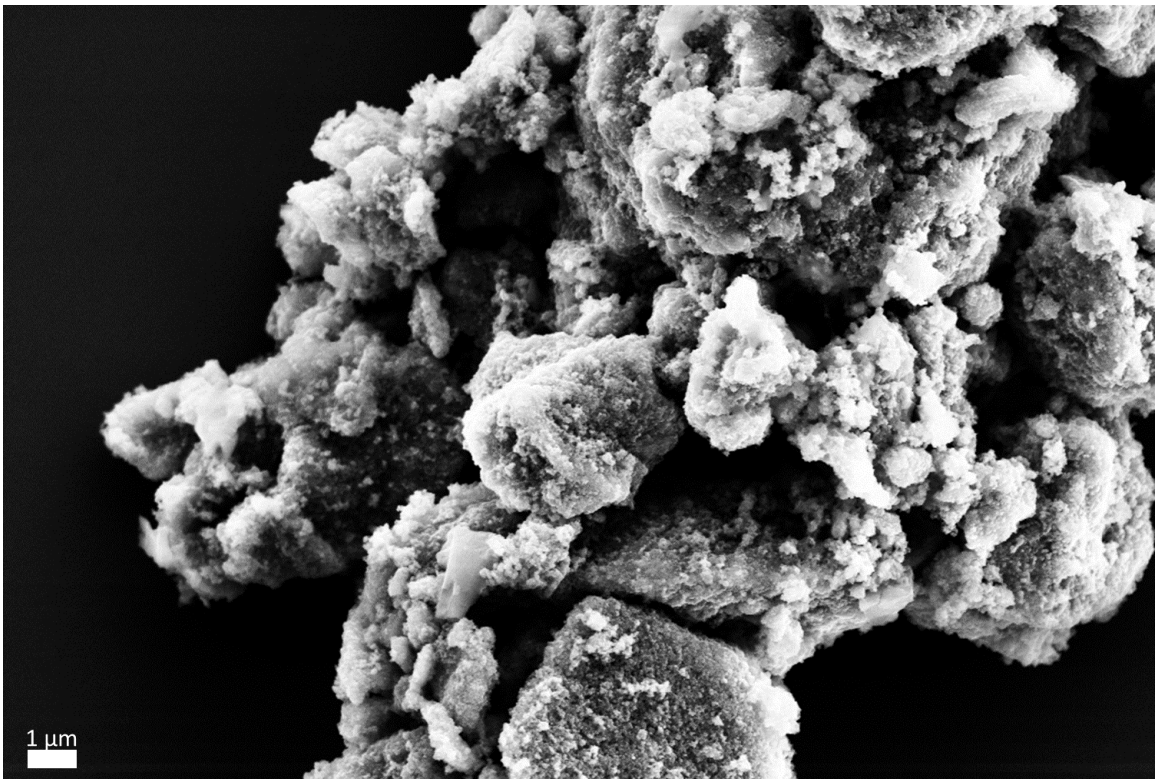


**Supplementary Figure 17. SEM image of IONP-HN3-DNA aggregates.**

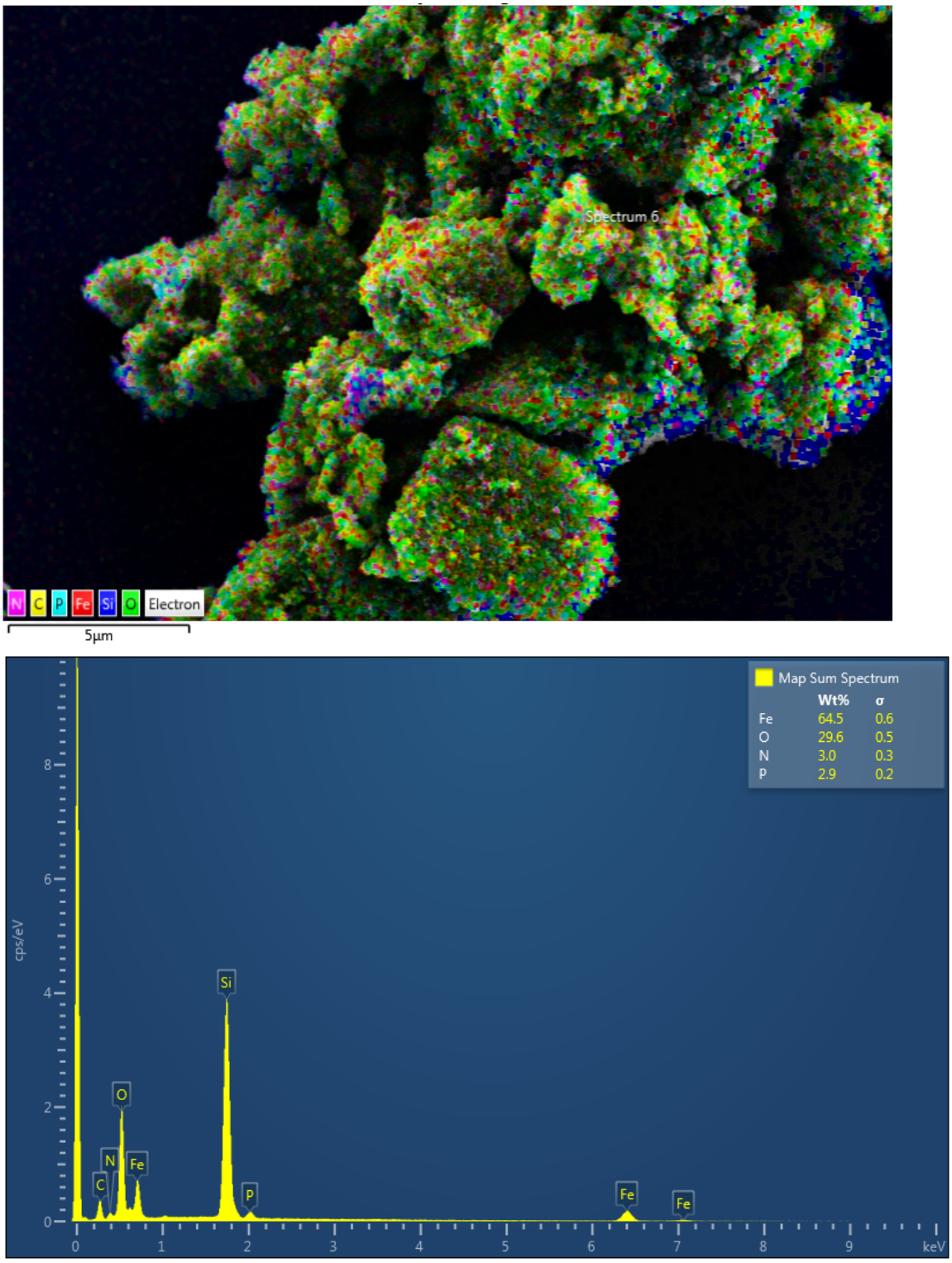


**Supplementary Figure 18. EDS spectrum and map of IONP-HN3-DNA aggregates.**

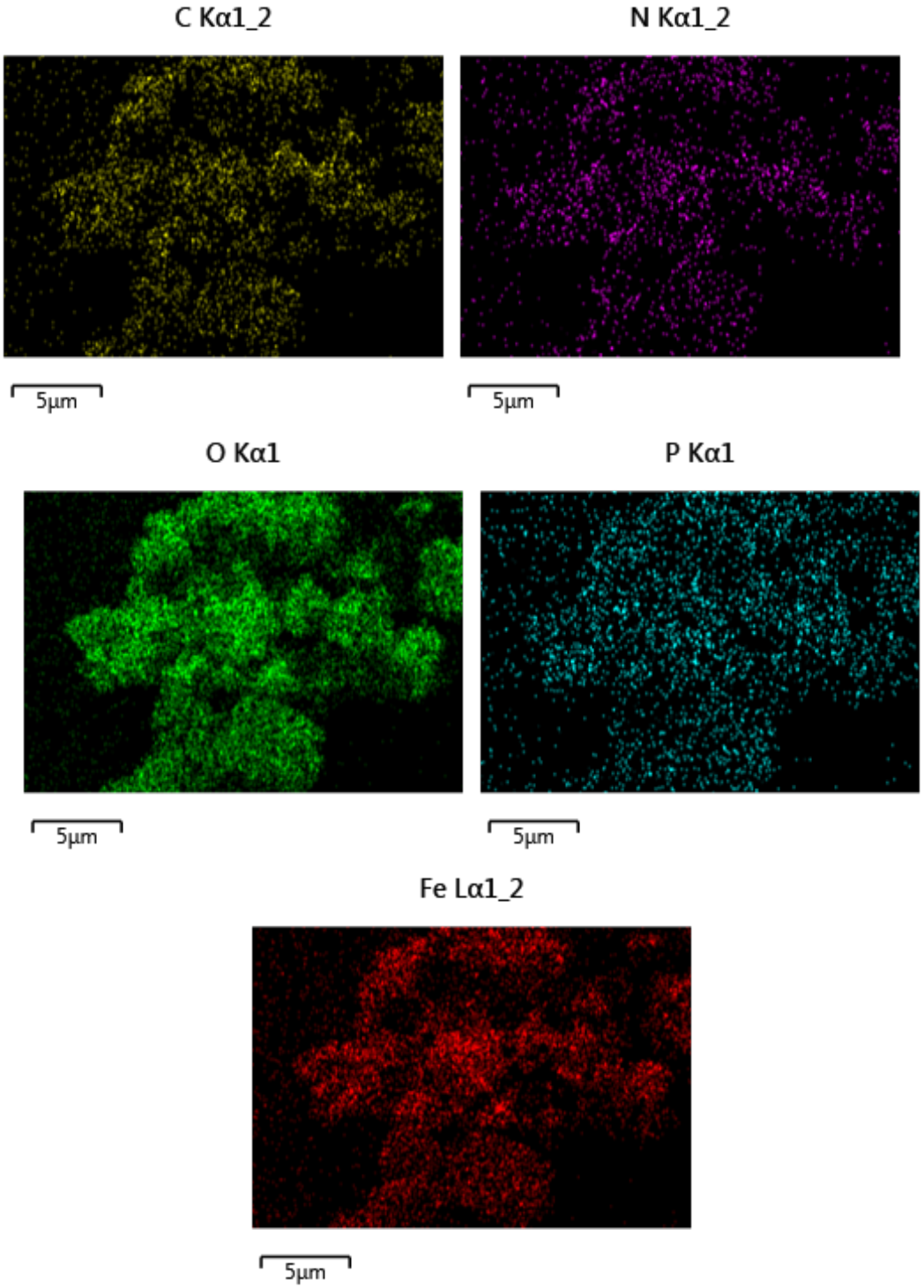


**Supplementary Figure 19. EDS element maps of IONP-HN3-DNA aggregates.**

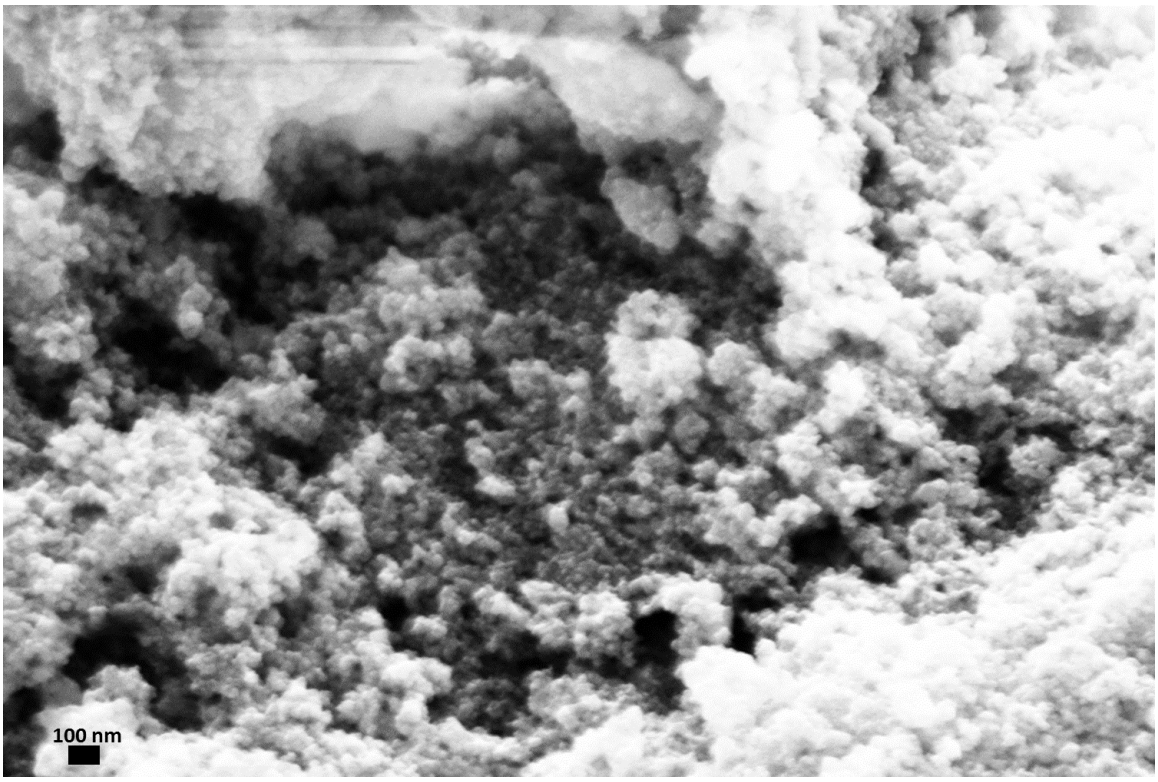


**Supplementary Figure 20. SEM image of IONP-Pt-DNA.**

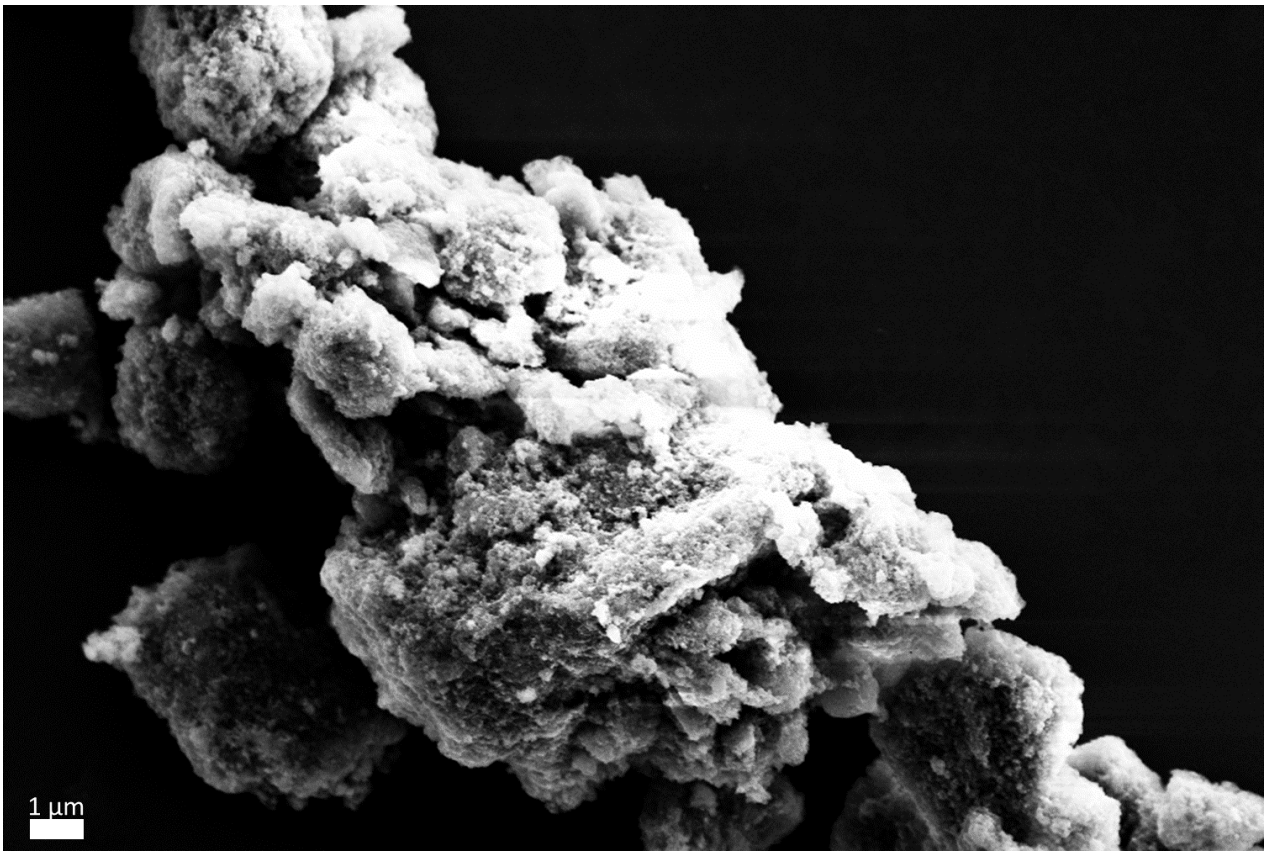


**Supplementary Figure 21. SEM image of IONP-Pt-DNA aggregates.**

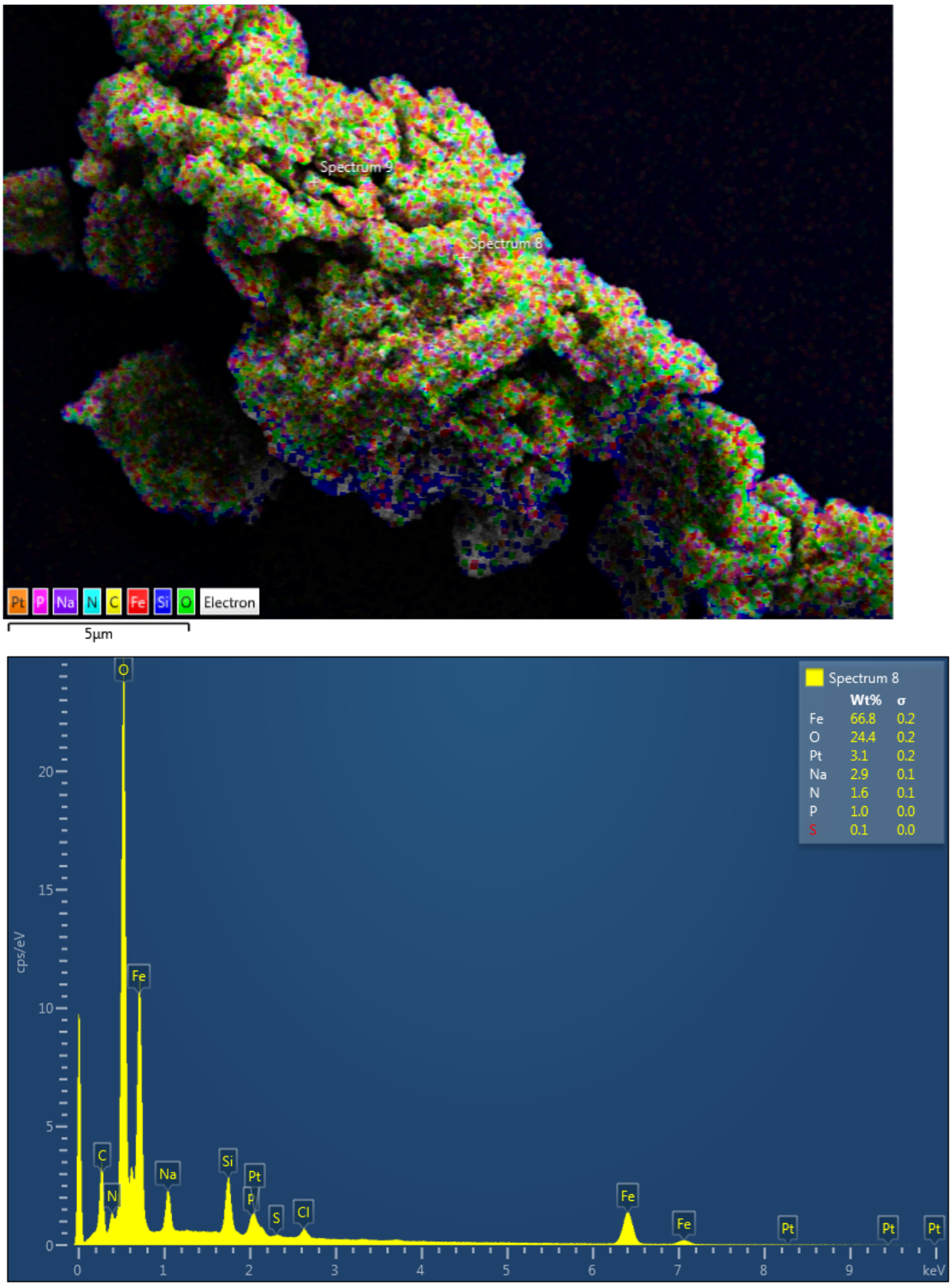


**Supplementary Figure 22. EDS map and spectrum of IONP-Pt-DNA aggregates.**

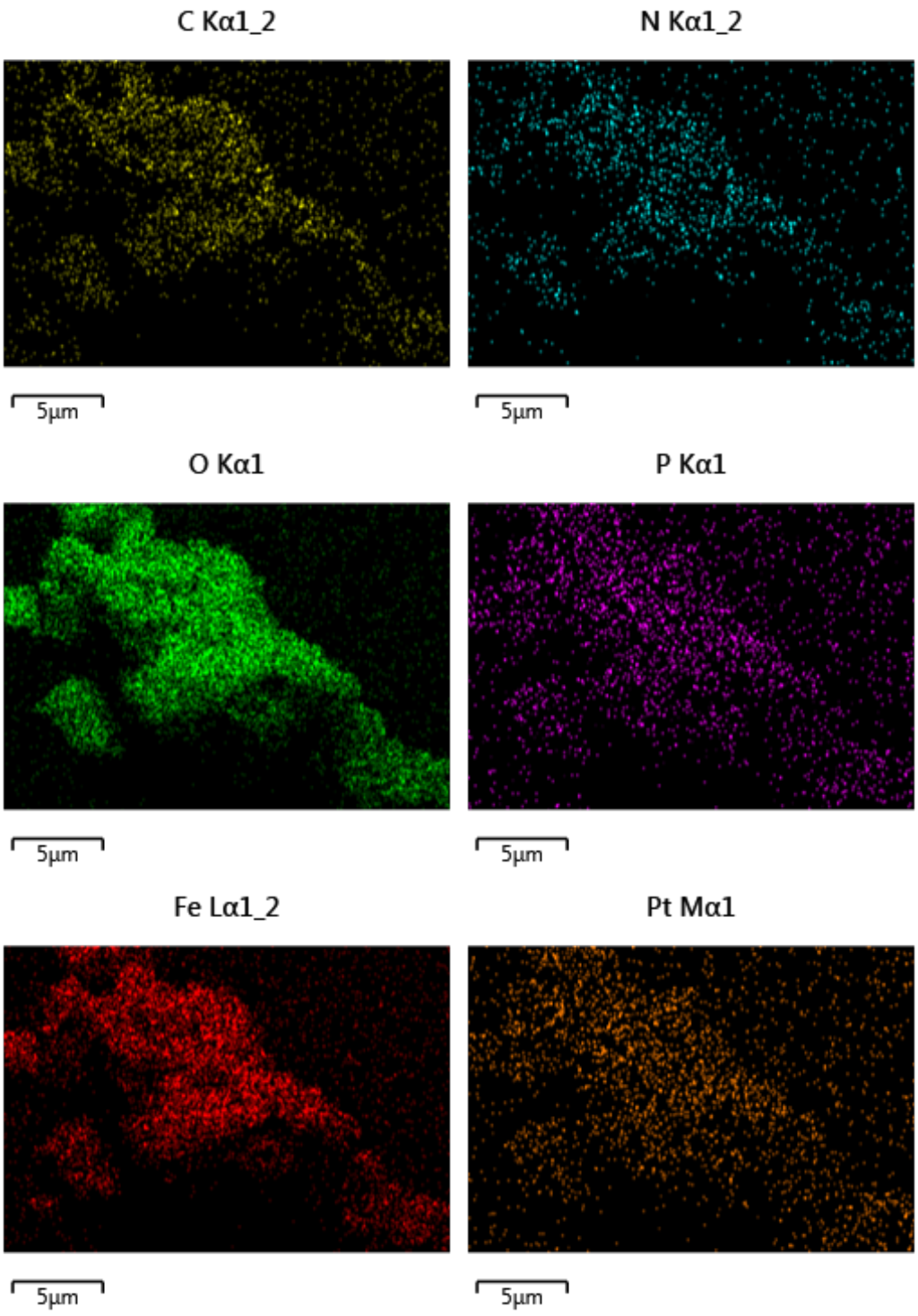


**Supplementary Figure 23. EDS element maps of IONP-Pt-DNA aggregates.**

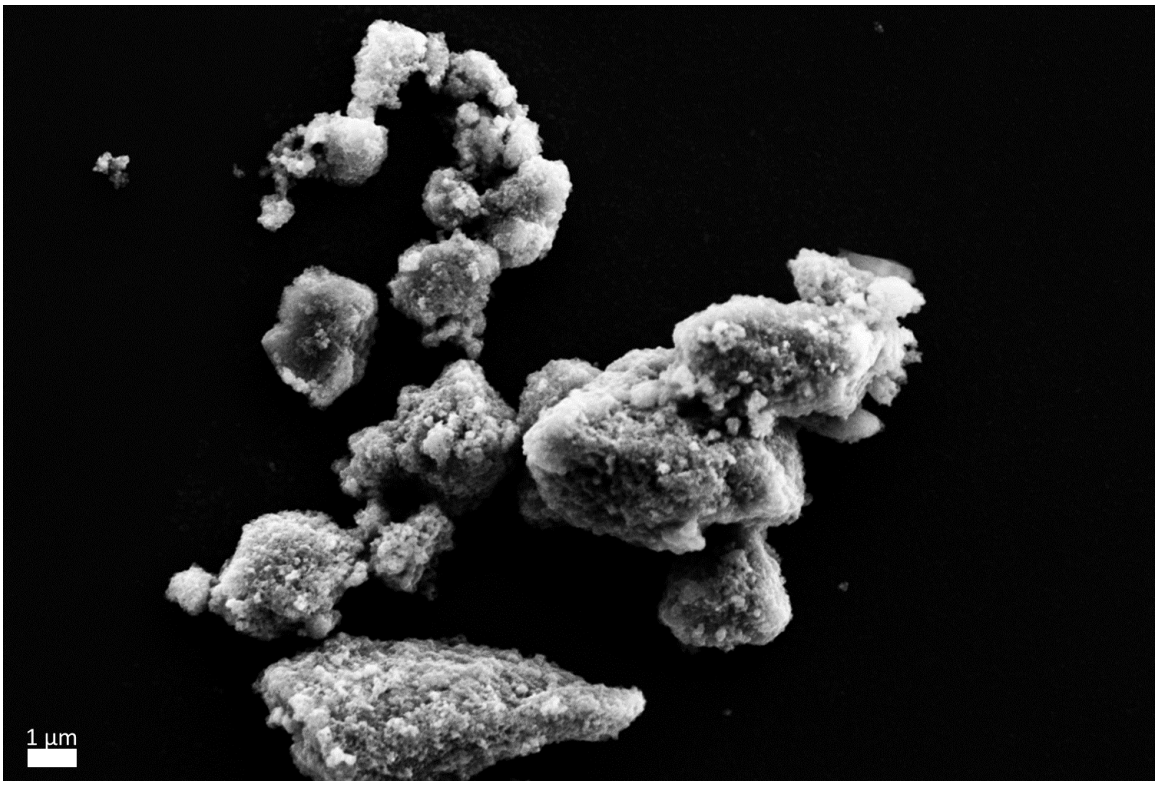


**Supplementary Figure 24. SEM image of IONP-Pt aggregates.**

A.

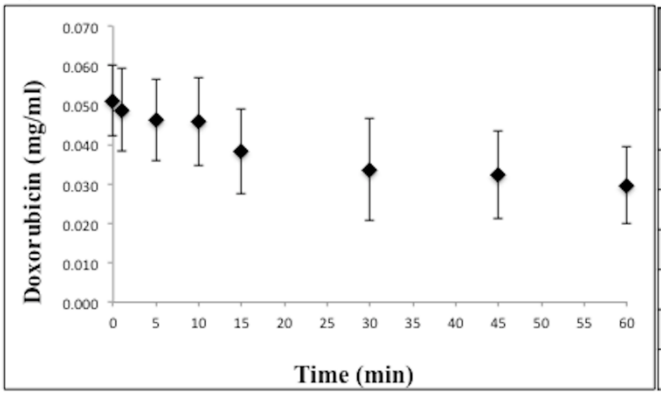


| Time (min) | Doxorubicin mg/ml | SD | % drop |
|---|---|---|---|
| 0 | 0.051 | 0.009 | |
| 1 | 0.049 | 0.010 | -5% |
| 5 | 0.046 | 0.010 | -5% |
| 10 | 0.046 | 0.011 | -10% |
| 15 | 0.038 | 0.011 | -25% |
| 30 | 0.034 | 0.013 | -34% |
| 45 | 0.032 | 0.011 | -37% |
| 60 | 0.030 | 0.010 | -42% |

B.

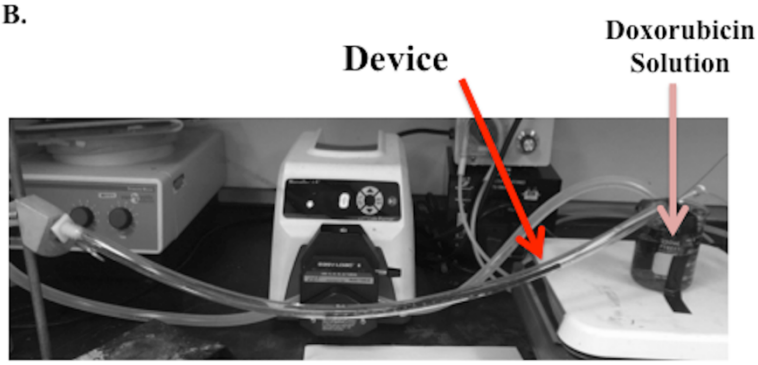


**Supplementary Figure 25. A. Doxorubicin clearance from porcine blood in closed loop flow model. B. Closed loop flow model design with 25 magnet device within the lumen of the flow model.**

| Sample ID | %C | %H | %N | Sample mass (mg) |
|---|---|---|---|---|
| Fe3O4 | 0.71 | 0.44 | 0.02 | 19.78 |
| | 0.44 | 0.37 | 0.02 | 9.267 |
| Average | 0.575 | 0.405 | 0.02 | 14.5235 |
| Standard Deviation | 0.19 | 0.05 | 0 | - |
| IONP-Pt-DNA | 5.27 | 1 | 2.15 | 16.98 |
| | 5.28 | 1.01 | 2.14 | 14.91 |
| Average | 5.275 | 1.005 | 2.145 | 15.945 |
| Standard Deviation | 0.007 | 0.007 | 0.007 | - |
| IONP-HN3-DNA | 6.6 | 0.99 | 2.64 | 9.933 |
| | 6.51 | 1.04 | 2.6 | 14.67 |
| Average | 6.555 | 1.015 | 2.62 | 12.3015 |
| Standard Deviation | 0.06 | 0.04 | 0.03 | - |
| Herring DNA | 33.81 | 4.61 | 14.5 | 3.666 |
| | 33.92 | 4.66 | 14.68 | 7.386 |
| Average | 33.865 | 4.635 | 14.59 | 5.526 |
| Standard Deviation | 0.08 | 0.04 | 0.13 | - |

**Supplementary Table 1. Elemental analysis data for all materials.**

**References:**


1. Patel, A., et al., *O-016 development and validation of an endovascular chemotherapy filter device for removing high-dose Doxorubicin from the blood: in vivo porcine study.* J Neurointerv Surg, 2014. 6 Suppl 1: p. A9.
2. Patel, A.S., et al., *Development and Validation of Endovascular Chemotherapy Filter Device for Removing High-Dose Doxorubicin: Preclinical Study.* J Med Device, 2014. 8(4): p. 0410081-410088.
3. Aboian, M.S., et al., *In vitro clearance of doxorubicin with a DNA-based filtration device designed for intravascular use with intra-arterial chemotherapy.* Biomed Microdevices, 2016. 18(6): p. 98.
4. Gnapareddy, B. *et al.* Chemical and Physical Characteristics of Doxorubicin Hydrochloride Drug-Doped Salmon DNA Thin Films. *Sci. Rep.* 5, 12722 (2015).

**Thank you for your attention!**